2021

Interclass GPCR heteromerization affects localization and trafficking

Rudy Toneatti
Virginia Commonwealth University

Interclass GPCR heteromerization affects localization and trafficking

A thesis submitted in partial fulfillment of the requirements for the degree of
Doctor of Philosophy at **Virginia Commonwealth University**

By

Rudy TONEATTI
Master of Science, University Pierre et Marie Curie, 2016

Director: Javier González-Maeso, PhD.
Department of Physiology and Biophysics

Virginia Commonwealth University
Richmond, Virginia
August 2021

ACKOWLEDGMENTS

I would like to thank Dr. Javier González-Maeso for welcoming me in the lab at the Biophysics and Physiology Department of the Virginia Commonwealth University School of Medicine.

I would like to offer my best wishes and sincere gratefulness to my committee members who reviewed my thesis, and for their patience: Interim Chair Dr. Clive M. Baumgarten, Dr. Kurt F. Hauser, Dr. Gretchen N. Neigh-McCandless, Dr. Ian Scott Ramsey.

To the Director of the Neuroscience program, Dr. John W. Bigbee, without whom I would probably been lost more than once. For his amazing teaching and guidance all along my studies.

To Dr. Louis de Felice, who accepted me and trusted me to start the PhD program.

To Pr. Diomedes Logothetis for his support during my first steps at the VCU.

I would also like to thank my lab mates and friends, Dr. José L. Moreno and Dr. Mario de la Fuente Revenga for their help and troubleshooting in many occasions. Dr. Justin Saunders for his unconditional support and for our hours of deep thinking and laughing. We ended our studies and the adventure together. Jong Shin for his help with the binding and his fortunate presence in the lab. Travis Cuddy and Doan On for sharing ideas and more. Dr. Juan López-Giménez who showed me some tricks. Dr. Supriya Gaitonde for her enjoyable presence in the lab and sustained encouragements. Dr. Urijta Shah with whom with shared a very nice project and loved to work with. And to our new crew, Dr. Somdata Saha for welcoming me back to the lab. I also wish the best to our present and incoming master and PhD students.

I am also very thankful to Julie Farnworth who trained me on the different flow cytometers and related software with passion and patience, and helped me manipulating data files for my analyses. Dr. Miguel Fribourg for the hours spent over the phone about colocalization considerations and the use of the BDS score in IDEAS. Dr. Henderson, Dr. Bernas and Frances White to have trained me on the confocal microscopes. Dr. Carl Mayer for his Python knowledge and sharing of FRET techniques. To all the collaborators who followed me and who I followed during these years of work and discoveries.

Finally, I am also very thankful for the financial support provided by the scholarship AMIE of the Région Île de France, by the Master BIP of the Université Pierre et Marie Curie during my master internship in the Maeso Lab, and by the VCU School of Medicine for all those three years.

For their help in providing resources for my experiments: we thank P. Rondard (University of Montpellier) for the donation of the Gαqi9 construct; S. Ferré (NIDA) for advice on experiments with TAT-linked peptides; and M. Dozmorov, for help in biostatistical analysis; the Microscopy Shared Resource and Flow Cytometry Core at VCU.

TABLE OF CONTENTS

LIST OF PUBLICATIONS

Research articles:

de la Fuente Revenga M, Zhu B, Guevara CA, Naler LB, Saunders JM, Zhou Z, Toneatti R, Sierra S, Wolstenholme JT, Beardsley PM, Huntley GW, Lu C, González-Maeso J. Prolonged epigenomic and synaptic plasticity alterations following single exposure to a psychedelic in mice. Cell Rep. 2021 Oct 19;37(3):109836

Sánchez-González A, Thougaard E, Tapias-Espinosa C, Cañete T, Sampedro-Viana D, Saunders JM, Toneatti R, Tobeña A, Gónzalez-Maeso J, Aznar S, Fernández-Teruel A. Increased thin-spine density in frontal cortex pyramidal neurons in a genetic rat model of schizophrenia-relevant features. Eur Neuropsychopharmacol. 2021 Mar;44:79-91

Shah UH, Toneatti R, Gaitonde SA, Shin JM, González-Maeso J. Mapping the interface of an heteromeric GPCR complex using genetically encoded photo-crosslinkers in living cells Cell Chem Biol. 2020 Oct 15;27(10):1308-1317.

Toneatti R, Shin JM, Shah UH, Saunders JM, Mayer CR, Janssen W, Conway DE, Bensson DL, González-Maeso J. Interclass GPCR heteromerization affects localization and trafficking, Science Signaling 2020 Oct 20;13(654)

de la Fuente Revenga M, Ibi D, Cuddy T, Toneatti R, Kurita M, Ijaz MK, Miles MF, Wolstenholme JT, González-Maeso J. Chronic clozapine treatment restrains via HDAC2 the performance of mGlu2/3 agonism in a rodent model of antipsychotic activity. *Neuropsychopharmacology* 44:443-454 (2019)

de la Fuente Revenga M, Ibi D, Saunders JM, Cuddy T, Ijaz MK, Toneatti R, Kurita M, Holloway T, Shen L, Seto J, Dozmorov MG, González-Maeso J. HDAC2-dependent antipsychotic-like effects of chronic treatment with the HDAC inhibitor SAHA in mice. *Neuroscience* 388:102-117 (2018)

Book chapter:

Salvador Sierra, Rudy Toneatti, Javier González-Maeso,

Chapter 8 - Class A GPCR oligomerization: Reasons of controversy,

Editors: Beata Jastrzebska, Paul S.-H. Park,

GPCRs. Structure, Function, and Drug Discovery

Academic Press, 2020, Pages 121-140.

LIST OF FIGURES AND TABLES

LIST OF ABBREVIATIONS

5-HIAA: 5-hydroxy indole acetic acid

5-HT: 5-hydroxytryptamin

7TMR: Seven transmembrane receptors

AAP: Atypical antipsychotic

AP-2: Adapter protein-2 complex

β_2AR: β_2-adrenergic receptor

BBB: Blood brain barrier

BDS: Bright detail similarity

BLOC-1: Biogenesis of Lysosome-related Organelles Complex-1

BRET: Bioluminescence resonance energy transfer

cAMP: Cyclic adenosine monophosphate

CPN: Caudate-putamen nucleus

CSF: Cerebrospinal fluid

CoIP: Coimmunoprecipitation

DAG: Diacylglycerol

DAMGO: [D-Ala^2, NMe-Phe^4, Gly-ol^5]-enkephalin

DPDPE: [D-Pen^{2,5}]Enkephalin, [D-Pen^2,D-Pen^5]Enkephalin

DOI: (±)-2,5-Dimethoxy-4-iodoamphetamine

DMT: Dimethyltryptamine

DxR: Dopamine receptors x

ECD: Extracellular domain

EE: Early endosome

EEA: Early endosome antigen

EEAT: Excitatory amino acid transporter

ER: Endoplasmic reticulum

ERK: Extracellular signal-regulated protein kinase

δOR: δ-opioid receptor

FRET: Förster resonance energy transfer

GEF: Guanosine nucleotide exchange factor

GA: Golgi apparatus

$GABA_BR$: gamma-aminobutyric acid receptor type B

GAP: GTPase activating proteins

GDP: Guanosine diphosphate

GIRK: G protein-activated inwardly rectifying K^+ channel

GTP: Guanosine triphosphate

GPCR: G protein-coupled receptor

GRK: G protein-coupled receptor kinases

HAL: Hallucinogenic/Psychedelic compound

ICD: Intracellular domain

iGluR: Ionotropic glutamate receptor

ISH: *in situ* hybridization

IP: Inositol phosphate

IP3: Inositol triphosphate

κOR: κ-opioid receptor

LE: Late endosome

LSD: Lysergic acid diethylamide

mGluR: Metabotropic glutamate receptor

MAPK: Mitogen-activated protein kinase

MAO: Monoamine oxidase

MVB: Multi-vesicular body

μOR: μ-opioid receptor

NAc: Nucleus accumbens

NAM: Negative allosteric modulator

NHAL: Non hallucinogenic/ non Psychedelic compound

PAM: Positive allosteric modulator

PFC: Prefrontal cortex

PI3K: Phosphatidylinositol 3 kinase

PIP2: Phosphatidyl inositol-bisphosphate

PKA: Protein kinase A

PKC: Protein kinase C

PLA: Proximity ligation assay

PLC: Phospholipase C

PSD: Post synaptic density/PSD-95

RE: Recycling endosome

RTK: Receptor tyrosine kinase

RRI: Receptor-receptor interaction

SE: Sorting endosome

SERT: Serotonin reuptake transporter

SNARE: Soluble NSF attachment protein receptor

TM: Transmembrane (domain)

VGLUT-1: Vesicular glutamate transporter

STATEMENT OF CONTRIBUTIONS

Figure 6 J has been generated by **Dr. M. Fribourg**.

Figure 5 A, B and C, and Figure A1 have been generated by a Python software manipulated by **Dr. Carl R. Mayer** who trained me to use it.

Figure 10 C and D, and Figure A3 have been generated by **Dr. Deanna L. Benson** and **William G. Janssen**.

Dr. Urjita H. Shah helped me with the calcium mobilization assay on the Flexstation.

Jong M Shin helped my for cell lines characterization binding assays.

This story is dedicated to my Father (February 1933 – October 2020)

Information is any difference that makes a difference

Gregory Bateson

I am among those who think that science has great beauty. A scientist in his laboratory is not only a technician: he is also a child placed before natural phenomena which impress him like a fairy tale. We should not allow it to be believed that all scientific progress can be reduced to mechanisms, machines, gearings, even though such machinery has its own beauty.

Marie Curie

The wonder of nature does not become smaller because one cannot measure it by the standards of human moral and human aims.

Albert Einstein

My life seemed to be a series of events and accidents. Yet when I look back, I see a pattern.

Benoît B. Mandelbrot

ABSTRACT

Class A serotonin (5-hydroxytryptamine) 2A (5-HT_{2A}R) and class C metabotropic glutamate 2 receptors (mGluR2) are seven transmembrane receptors (7TMRs or G protein-coupled receptors – GPCRs) involved in multiple neuropsychiatric disorders including schizophrenia. Previous findings from our laboratory reported that 5-HT_{2A}R and mGluR2 are dysregulated in the prefrontal cortex of patients suffering from this psychiatric condition, although 5-HT_{2A}R's expression was recovered in antipsychotic-medicated patients. Genome-wide association studies on schizophrenia reported that endosomal trafficking that regulates cell surface abundance of another 7TMR implicated in this disease (dopamine D2 receptor) can be altered. Ligand-activated receptors, including the 7TMR superfamily, are dynamic entities whose signaling depends on trafficking, and trafficking on signaling. Impairments in the spatial and temporal regulation of 7TMRs result in homeostasis perturbations and later in diseases. Like other cell surface proteins expressed in mammals, such as enzyme-associated receptors and ligand-gated ion channels, 7TMRs form homo- or hetero-oligomers, conferring novel and unique functional properties to the complex. Our previous findings suggested that 5-HT_{2A}R and mGluR2 are assembled in a functional GPCR heteromeric complex in both heterologous expression systems and in mouse and human brain frontal cortex. However, evidence that GPCR heteromerization can directly affect receptor subcellular organization and localization is missing, especially across classes. Here, we showed in mammalian HEK293 cells that 5-HT_{2A}R affected the localization and trafficking of mGluR2 through a mechanism that required their physical assembly. In the absence of agonists, 5-HT_{2A}R was primarily localized within intracellular compartments. Intriguingly, the plasma membrane-localized mGluR2 was redistributed in internal compartments when coexpressed with 5-HT_{2A}R. Agonists for either 5-HT_{2A}R or mGluR2 differentially affected trafficking through Rab5- or Rab7-positive endosomes in cells expressing the receptors alone, or together. In addition, overnight blockade of 5-HT_{2A}R with antipsychotic clozapine, but not with M100907, decreased mGluR2 density through a mechanism that involved 5-HT_{2A}R-mGluR2 heteromerization. Using TAT-tagged interfering peptides and a chimeric construct unable to heteromerize with 5-HT_{2A}R, we showed that heteromerization was necessary for the 5-HT_{2A}R-mediated co-trafficking of mGluR2. Furthermore, using bimolecular fluorescence complementation (BiFC), we tracked the maturation of the 5-HT_{2A}R-mGluR2 complex in the endoplasmic reticulum and the Golgi apparatus. In accordance with our findings in HEK293 cells, mGluR2/Rab5 colocalization was diminished in neuronal cortical primary culture of 5-HT_{2A}R-/- mice as compared to controls. Additionally, mGluR2 was mostly localized near the plasmalemma in brain sections of 5-HT_{2A}R-/- mice frontal cortex glutamatergic excitatory postsynaptic compartments. Together, our data suggest that GPCR heteromerization may itself represent a mechanism of receptor trafficking and sorting.

Introduction

7TMRs superfamily

With more than 800 members (a number that varies across studies) counting for about 2-3% of the total human protein-encoding transcripts[1–3], guanine nucleotide binding protein (G protein)-coupled receptors (GPCRs), or more accurately, heptahelical or seven transmembrane receptors (7TMRs), constitute the largest superfamily of spanning membrane proteins in the Metazoa and the mammalian genome. Mammals express about 400 non-odorant 7TMRs[4]. As a matter of comparison, the second largest family of receptors, the receptors-enzyme tyrosine kinase (RTK) family counts about 58 receptor-types in 20 subfamilies[5]. Because they represent fundamental interfaces between a tremendous diversity of extracellular stimuli*, triggering inner molecular cascades, cellular responses and genes transcription, 7TMRs provide highly valuable targets for clinical pharmacology. About 34% of FDA approved drugs target 107 unique 7TMRs, of which 27% treat neuropsychiatric disorders[6,7]. Often termed metabotropic receptors, as opposed to ionotropic receptors, whose activation and subsequent cell reaction is faster than the former, they process and transduce signals throughout structural and biochemical steps much slower than receptor channels. A cell response is always a combination and a cooperation between fast and slow transmitters. The classical/canonical mode of signal transduction through 7TMRs cognate G proteins is widely accepted, although recent findings proposed G protein independent signaling[8–10]. For a concern of accuracy over widely acceptance, this report will use the term 7TMRs.

7TMRs and G protein signaling likely appeared before Plants, Fungi and Animals, and diverged from their common ancestor about 1.2 billion years ago[11]. Primitive structures of 7TMRs existed in unicellular eukaryotes that resemble Metazoa cells[12]. The glutamate-receptor-like receptor is one of the oldest. The serotonin receptors subfamily is also one of the oldest in class A/rhodopsin-

* Stimuli can be exogenous chemical ligands such as drugs, vitamins, odorants, tastants, and viruses, and physical stimuli such as photons. Endogenous ligands can be biogenic amines, nucleotides, hormones, large and small peptides, cations and lipids, small molecule neurotransmitters, chemokines, and more.

like 7TMRs, which appeared between 700 and 800 million years ago[13]. This evolutionary success gives an idea of the robustness of such biostructures, having evolved and diversified under selective pressure, to finally regulate almost all aspects of living organisms' physiology. 7TMRs share a minimal and unique common attribute that is the seven transmembrane α-helices domain connected by three extracellular (EC1, EC2, EC3) and three intracellular (IC1, IC2, IC3) alternated loops, in between an extracellular N-terminus and an intracellular C-terminus, often ended by a so-called helix 8.

Classification of 7TMRs

All characterized 7TMRs, as well as the orphan 7TMRs, are classified and categorized within the International Union of Basic and Clinical Pharmacology (IUPHAR) database†, which recognizes 6 classes, widely used among studies. Several other classifications are often based on structural homology, but not only. 7TMRs are organized into 5 or 6 major nomenclatures according to their sequence similarity and functional properties (A to F)[14], as well as structural and ligand-binding features (1 to 5)[15]. Also referenced phylogenetically as GRAFS[16], acronym for Glutamate, Rhodopsin, Adhesion, Frizzled/Taste2, Secretin, the rhodopsin-like or class A/1 is the most represented subfamily in the human genome. The class A includes, with light-activated rhodopsin and highly numerous olfactory receptors, monoaminergic norepinephrine, dopamine and serotonin neurotransmitters/modulators transducers. Their homology of sequence indicates that they also share palmitoylated cysteine at their C-terminal tail, as well as a triplet of glutamic/aspartic acids - arginine/tyrosine termed E/DRY motif on their helix III[17]. This motif is the target of a strong ionic interaction that is involved in receptor activation as shown for the 5-HT_{2A} receptor, thought to be a generalizable activation system within the class A[18]. Another shared feature of class A receptors is that they harbor a long N-terminus with conserved cysteines[17]. Class B/2 are secretin-like 7TMRs among which corticotrophin-releasing factor (CRFR1, CRFR2),

† www.guidetopharmacology.org/GRAC/GPCRListForward?class=A

parathyroid hormone (PTHR1, PTHR2) and glucagon-like peptide receptors (GLPR) among others may be mentioned. Class C/3 regroups metabotropic glutamate (mGluR) and gamma-aminobutyric acid type B receptors ($GABA_BR$), which bind respectively the main excitatory/inhibitory neurotransmitters in the central nervous system (CNS), along with the sweet and umami taste receptors (T1R1/2+3) and the calcium sensing receptors (CaSR). Classes D and E constitute two minor families not represented in vertebrates, like cAMP receptor involved in protozoan chemotaxis signaling, and class F includes frizzled/smoothened receptors[19]. Further analogies between those nomenclatures remains unlikely since the criteria used are not conform.

Signal transduction

External ligands or stimuli are typically treated in two ways. Ionotropic receptors convey fast information flux, whereas metabotropic receptors transmit signals slowly, engaging a series of chemical and/or physical modifications from ligand binding to cell response. The signal transduction can be simply represented as an information crossing a regulated field. Information, the ligand, is treated, sorted and processed by the transmitter and its cognate G proteins, together with intracellular signaling molecules. A series of phosphorylations takes place within cascades, where the signal can be amplified and/or transmitted to the different target components. Because cell's phospholipid bilayer membrane must maintain the system closed and tightly regulated, communications operate uniquely through transmitters and channels, or both, and by endo/exocitic vesicular trafficking. Nonetheless, it is likely that other modes exist (gasotransmitters[20]).

Receptor activation starts with ligand binding that initiates conformational changes within the seven transmembrane domains that resonate to receptor extremities, and convey signal transduction through heterotrimeric αβγ G proteins' subunits. The inactive state, reflecting basal activity, remains stable during low ligand concentration. Upon binding of its ligand, receptor changes its conformation that activates its cognate G protein. The activation/deactivation process

should not be envisioned as an on/off switch, with two distinct conformations. Receptors are in constant and continuous vibration, oscillating between a multitude of different conformations, toward active or inactive state, and get stabilized by the ligand[21]. It is considered as a multi-active state model[22].

The specificity of the GPCR-mediated signal transduction was initially thought to solely lay in the dissociation of the trimeric G protein's αβγ subunits upon ligand binding. The α subunit catalyzes GDP to GTP to exchange and split from the tripartite GTPase to signal downstream effectors and second messengers, while βγ is involved in regulating ions channels switching, as well as other effector proteins. The GTPase family of G proteins is also well diversified, the four main G proteins being $G\alpha_s$, $G\alpha_{i/o}$, $G\alpha_{q/11}$ and $G\alpha_{12/13}$. The first two respectively stimulate or reduce adenylyl cyclase activity, resulting in the augmentation or the reduction of cyclic adenosine monophosphate (cAMP) internal concentration. The cAMP-dependent protein kinase A (PKA) signal is amplified or dampened accordingly, which modulates specific cell responses. A typical example is the human class A $G\alpha_s$-coupled β_2 adrenergic receptor ($\beta_{2A}R$), which triggers cardiac myocytes contraction after binding of adrenaline in tissues involved in sympathetic neurotransmission[26]. Class C mGluR2/3 glutamatergic receptors are linked to the $G\alpha_{i/o}$ pathway that inhibits cAMP production and reduces glutamatergic tone in presynaptic terminals where it acts as an autoreceptor. The class A 5-HT_{2A} receptor provides an example of $G\alpha_{q/11}$ coupling. Agonist binding stabilizes the receptor in its active conformation that triggers the phospholipase C (PLC) DAG/IP3/PKC pathway. For example, in 5-HT_{2A}R-expressing neurons, the $G\alpha_q$ activates PLC-β which catalyzes the hydrolysis of phosphatidyl inositol-bisphosphate (PI(4,5)P2) into two second messengers, diacylglycerol (DAG) and inositol triphosphate (IP3). DAG remains attached to the membrane and recruits the protein kinase C (PKC), while IP3 diffuses in the cytoplasm to trigger calcium release from the endoplasmic reticulum storage. While diffused into the cytoplasm, Ca^{2+} can operate several cellular events such as activation of PKC (feedback), stimulation of ionic channels and

enzymes recruitment that together modulate synaptic transmission. The PKC is also involved in triggering cellular responses, such as neuronal plasticity, cell survival, and transcription factors activation. Several studies recently showed that the canonical linear model was not sufficient to describe unexpected results while tracking G protein activation. This led to separate G protein-dependent and -independent signaling[8–10,23–26].

To prevent response overload, and/or to return to basal state*, i.e.* low ligand concentration, a termination mechanism shuts down the signaling components by acting directly on the receptor, typically involving two major pathways: the receptor phosphorylation by G protein-coupled receptor kinases (GRK), and the subsequent recruitment of β-arrestins (1 or 2). GRK are recruited by Gβγ once released upon ligand-dependent receptor activation and split from the α subunit, so that receptor phosphorylation happens relatively fast after ligand binding. β-arrestins are thought to specifically bind GRK-phosphorylated receptors while competing with the G proteins in the vicinity. Arrestins are responsible for the recruitment of the endocytic machinery that involves dynamin and the formation of clathrin-coated vesicles. Successive intracellular mechanisms such as Rab-dependent desensitization (receptor endocytosis) and recycling from endosomes further affect receptor's fate and cell's responsiveness.

7TMRs structure and oligomerization

Class A 7TMRs or rhodopsin-like receptors share the minimal features that defines the superfamily, a seven transmembrane (TM) spanning helices domain, or heptahelical domain, connected by three intracellular loops (IL1-3) and three extracellular loops (EL1-3). This class of receptors has an extracellular cavity within their TM domain dedicated to the binding of the orthosteric ligand. They have also in common few conserved motifs[27]. They are devoid of the large extracellular bilobal domain (ECD) characteristic of the class C 7TMRs, the Venus Fly Trap (VTF) domain. The typical receptors of this family, the $GABA_B$ and the metabotropic glutamate receptors (mGluRs), share this VFT domain dedicated to the binding of the orthosteric ligand, as well as

holding a cysteine disulfide bridge necessary for the receptors obligatory dimerization. A cysteine rich domain is also partially involved in the dimeric interface, and proposed to relay ligand-induced conformal adjustment[28]. The lack of covalent bond between protomers have led some reports to justify that class A dimers are not stable enough to remain bound supported by weak interactions[29]. Class A receptor dimers are indeed less stable than class C[30,31]. This does not rule out that they are functional. The rapid conversion between monomers and dimers and their resulting ratio may regulate receptor function[30].

Since the first biochemical findings showing that a peptide derived from a β_2 adrenergic receptor (β_2-AR) transmembrane (TM) domain prevented both receptor complex formation and agonist-promoted stimulation of adenylyl cyclase activity[32], the class A 7TMRs never ceased to attract attention for their ability to associate as dimers or higher oligomers[33,34]. Despite certain limitations and caveats of most biophysical and biochemical approaches and technologies, including coimmunoprecipitation (CoIP), crosslinking, bioluminescence and Förster resonance energy transfer (BRET/FRET), SNAP- or CLIP-tag[35,36], bimolecular fluorescence complementation (BiFC) and other protein complementation assays (PCA), these studies generally provide evidence related to the fundamental role of class A 7TMR homo/heteromerization in the control and regulation of both agonist-induced receptor-G protein coupling[37,38] and trafficking[39–43]. Similarly, contemporary advanced techniques such as single molecule imaging in intact cells indicate that certain class A 7TMRs form stable homomers[41,44–46], while others, using similar approaches, have shown either transient interactions[30,47,48], or negligible to absence of class A dimerization[49–51]. Accordingly, many questions still remain open about the role of receptor complex formation in 7TMR's dynamics and behavior.

Between 2000 and 2004, a series of articles published in the Journal of Biological Chemistry (JBC) by several laboratories either directly implied the oligomeric association as a mean for 7TMRs to undergo internalization after ligand binding or assumed that receptor oligomerization could

influence both trafficking and signaling. These results directly followed pioneer discoveries about both class A and class C 7TMRs with the case of β_2-AR and $GABA_BR$, respectively (see below). Among those studies, the scope has been extended to several other subtypes, β_2-AR heterodimerization with β_1-AR[52–54], β_2-AR with β_3-AR[55], oligomerization of other adrenergic subtypes alpha, such as α_{1a}- and α_{1b}-AR[56], but also across subtypes[57]. Likewise, an early study demonstrated that the δ-opioid receptor dimerize, suggesting that such receptor-receptor-interaction (RRI) was particularly important for their desensitization and subsequent internalization[58,59]. Dimerization was also found to play a critical role in the agonist-independent desensitization and internalization of the human platelet-activating factor receptor (hPAFR)[60]. These novel ideas also emerged within the opioid receptor subfamily following a series of impactful discoveries, such as the oligomerization of the μ- and the δ-opioid receptors[61], where again, the scope extended the idea that those associations, this time among different protomer subtypes, would create novel functional properties that was not previously observed by classical pharmacological characterization. In the same journal, another study implicated heteromerization of somatostatin and μ-opioid receptors as a principal component of the cross-phosphorylation and the desensitization of both receptors[62].

Although few studies directly implicated the 7TMRs homo/heteromerization in both endocytosis and biosynthesis processes, several of them though clearly suggested that such interactions can modulate function and trafficking. Opioid receptors were the first class A 7TMR to be thoroughly studied following the discoveries of dimerization and oligomerization within the subfamily. The μ- and the δ-opioid receptors have been demonstrated to heterodimerize using epitope tagged constructs submitted to subsequent immunoprecipitation. Moreover, whereas DAMGO (μ selective agonist) did now affect desensitization of the receptors expressed together, treatment with DPDPE (δ selective agonist) induced a resistance to desensitization and internalization of the two receptors. Opioid receptors are well studied for their capacity to be internalized and

desensitized after ligand binding. The fact that this process was affected by the coexpression and the putative interaction between μ and δ suggested that heteromerization can also affect basic components of class A receptors function such as internalization and desensitization[61], as well as binding affinities of the ligands[63]. These two studies published the same year demonstrated that oligomerization is an important feature of the opioid receptor subfamily. Heterodimerization also was demonstrated to create novel functions for the δ- and the κ-opioid receptors[64]. Although the three opioid transmitters share a relatively high homology of sequence (about 65% identical amino acids), the diversity of RRIs demonstrates a great variety of novel functions that affect most aspects of receptor signaling and trafficking. Together these pioneer studies provided the first indirect evidence that one protomer is able to affect both signaling and trafficking of another protomer within the class they belong to.

Within the class C, aside from similar conclusions about the novel properties provided by receptor homo/heteromerization, it has been shown that such associations are necessary for the proper cell surface addressing of the protomers together, as a single entity. The classical case illustrated by the class C $GABA_BR$ remains remarkable as it is considered a paradigm. This obligate dimer is composed by the $GABA_BR1$ protomer that is unable to trigger G protein-activated inwardly rectifying K^+ channels (GIRKs) signals alone, when overexpressed in mammalian cells: it requires heterodimerization with $GABA_BR2$, a subsequently described protomer that shares 35% homology with the subtype R1[65]. The reason behind this resides in the early association of the two subunits; while crossing the endoplasmic reticulum during the protomers biosynthesis, R2 masks a retention motif lodged at the R1 C-terminus[66,67], allowing the full heteromer to exit the ER, otherwise retained in the organelle as single units. Here, heterodimerization is necessary for the cell surface addressing of a functional $GABA_BR$. These findings also indicated that the $GABA_B$ receptor is an obligate dimer. More recently, a group demonstrated that $GABA_BR2$ competes with a gatekeeper protein termed PRAF2, which results in passing prerequisite quality controls prior to ER exit[68]. It

highlights that 7TMRs can hold the role of chaperonin-like proteins, although finely regulated by resident chaperone molecules[69–71]. Similarly, the class A β_2-AR homodimerizes in the ER to allow upward trafficking to the plasma membrane. Using two different mutation approaches, it was revealed that retention/export motifs mutants act as dominant negative on WT β_2-AR species, precluding their ER export and migration to the cell surface: first, by generating a chimera where the C-terminus tail of the β_2-AR is interchanged with that of $GABA_BR1$, containing the above-mentioned retention motif; second, by mutating an ER export signal from the D_1R sequence in order to generate an unrecognizable binding site for specific resident proteins involved in the ER exit of D_1R. The structure/function role of such coupling has also been illustrated by the required dimerization of metabotropic glutamate receptor 2 to enable ligand-induced G protein activation, while monomeric 7TM domain appears sufficient for its coupling[72], supporting the idea that dimers are the minimal signaling units, constituting a 2:1 ratio with the G protein they are associated to[70]. Although truncated mGluR2 lacking their ECD can homodimerize using only the 7TM interface, the stability of this formation is assured by the cysteine 121 located in the VFT that provides a covalent intersubunit disulfide bound. Isolation of truncated receptors (purified 7TM domains) in lipid nanodiscs producing two different fractions enriched with two or one receptor, mGluR2 was able to signal with the latter fraction using positive allosteric modulator (PAM), which binds the ECD, but not the VFT. However, truncated mGluR2 lacking the VFT domain were unable to activate the G protein in presence of the orthosteric ligand glutamate, supporting the fact that only full length dimeric species can activate $G\alpha_i$ protein signaling as assessed by GTPγS assay, while monomeric species are sufficient to the coupling to the G protein[73].

The accurate description of the interactions between residues that hold weak forces and stabilize oligomeric interfaces is an essential component of the pharmacological properties of 7TMRs, besides providing important information for the development of therapeutics and 3D models, which simulate dynamic structures and interactions at the atomic level. Advances in structural biology

technologies have allowed to elucidate and validate the precise transmembrane domains and often the residues involved in the conformations responsible for the activation/deactivation of oligomeric receptors. Across studies, TM domains I, IV and V typically appear to be the implicated interfaces in the formation of transient and/or stable class A 7TMRs oligomers[74].

How TM domains associate is well illustrated by the class C metabotropic glutamate receptors, which exhibit the most stable RRI within the superfamily. It was first proposed that the mGlu5 receptor is a naturally occurring dimer linked by a disulfide bound at the extracellular domain, and that concept could be generalizable to all mGluRs[75]. The prototypic class A dimerization held by the μ-opioid receptor has been challenged, suggesting that the dimer populations are scarce and negligible at physiological concentrations[51]. Nevertheless, a great majority of theoretical approaches remain in favor of receptor oligomerization that provides an array of supplementary functions: antagonistic assemblies to cross-modulate protomer signaling, chaperones and guides through the biosynthesis pathway, subcellular co-trafficking and co-desensitization: dynamic or stable, kiss-and-fly or covalent[76,77].

In a review focused on class A 7TMRs homo/heterodimerization, several studies are listed according to the technique used and the involvement of the TM interaction to stabilize the dimeric formation, seven of nine class A receptor homo/heterodimers involve at least the TM IV and/or TM V. In a second chart similar findings are proposed[78]. The diversity of the TM interaction is provided by the highly flexible linkers and loops that allow fast conformational modifications and relatively large movements of the TM domain[78,79]. TM I and II were also mentioned for the muscarinic receptor 3 (M3), suggesting that each combination of the transmembrane interfaces is specific to a mode of functioning, either active or inactive states[74]. At the time of this report, a study elucidated the active and inactive conformation used by the mGluR2 dimer to activate $G\alpha_i$ protein using cryoEM technology, showing asymmetric positioning of the TM helices both during activation and at basal inactive state, involving TM III/IV, and TM VI/VI respectively[80].

As illustrated by the muscarinic acetylcholine receptor 2 (M_2R) case, which has been found as monomeric, but also in dimeric and tetrameric forms by three different studies using different techniques and systems, class A 7TMRs could associate in various homomeric ratios[74,81–83]. Although discrepancies for the same target receptor may be interpreted as a lack of reproducibility, feeding the debate on class A 7TMRs oligomerization, it might instead indicate that each study has revealed a different state of this receptor at a different time and under different conditions, as has been noted,

"*Until recently, these were often considered to be mutually exclusive scenarios, but the co-existence and potential interchange between such forms, based in part simply upon mass action, has resulted in a more textured view.*"[84]

Receptor oligomers can be formed by different mechanisms, by weak forces at the plasma membrane, or covalently during biosynthesis. The origin of the coupling must have a physiological significance[85–87]. Homo or heterodimerization most likely occurs within the same 7TMRs classes due to more compatible structural homology of their TM domain[15,70], the natural interface of receptor coupling. Nevertheless, interclass receptor associations are progressively more reported[86]. A remarkable association has yet been suggested for the 5-HT_2R and the CRFR1[88]. In this proposed model, 5-HT_2R cell surface expression and signaling is increased by agonist-stimulated CRFR1 trafficking. The accuracy in detecting the physical interaction at the interface of TM dimerization starts to provide more granular visualization on how oligomers associate and function[89]. The proof provided by visual evidence is also a criteria in favor of 7TMRs oligomerization[90]. Finally, the theory of moonlighting proteins, as a powerful and economic natural feature of proteins to organize, associate and function, support the idea that (receptor) oligomerization is not a rare and fortuitous event, but rather a common mechanism found everywhere that enables complexity and diversity[91–93].

Serotonin

Serotonin is the first neurotransmitter/trophic factor to appear in both Protozoan and Metazoan[94], probably inherited from unicellular eukaryotic precursors, which likely firstly evolved in mitochondria a billion years ago[95]. Plants produce a large amount of serotonin for both trophic factor that regulates growth together with auxin and antioxidants to preserve cell from damages provoked by excessive production of molecular oxygen[96]. Serotonin-based analogs and alkaloids such as ibogaine, mescaline, dimethyltryptamine (DMT) and psilocybin (in the Fungi) are produced by plants and fungi to resolve the problem of oxidation and protect them from radical oxygen, which is intrinsic to their photosynthetic abilities[95]. Serotonin is a biogenic amine synthetized from indole precursor tryptophan primarily after its hydroxylation into 5-hydroxytryptophan by the tryptophan hydroxylase enzyme. Its product subsequently undergoes a decarboxylation by a decarboxylase enzyme in presence of the cofactor pyridoxal phosphate which produces 5-hydroxytryptamin (5-HT). Serotonin does not cross the blood brain barrier (BBB) but L-tryptophan does, being the rate-limiting precursor for the synthesis of serotonin. After being released presynaptically in the extracellular milieu (synaptic cleft), serotonin is either metabolized by monoamine oxidase (MAO) into 5-hydroxy indole acetic acid (5-HIAA), or recycled by serotonin reuptake transporter (SERT) or autoreceptors. 5-HIAA is an interesting metabolite that could be used as a marker because of its suggested abnormal levels in psychiatric disorders (often found as decreased), reflecting serotonin levels in the brain[97]. Altered blood, serum or cerebrospinal fluid (CSF) levels of both serotonin and its metabolites have been associated with impulsive and aggressive behaviors in general[98–102] and in suicide[103–106] and autism[107–111] in particular, although these findings are still under debate[112].

Serotonin can be found in all human body tissues and fluids. In the CNS, it modulates a large number of cerebral, cognitive, hormonal and emotional functions. Mood, appetite and sleep, aggressive and sexual behaviors, locomotion, learning and memory consolidation are all regulated

by serotoninergic neurons. Additionally, it regulates pulmonary and cardiovascular physiology, hemostasis, and endocrine functions. As a trophic factor, it is involved in neural development, homeostasis and plasticity. Serotonin is synthesized in dorsal raphe nuclei located in the primitive brainstem, but about 95% is found in blood platelets, insuring aggregation and vasoconstriction of blood vessels, and in enterochromaffin cells within the digestive apparatus[113]. The remaining synthesized neurotransmitters are delivered throughout the entire brain using outputs originating from the caudal raphe to innervate the spinal cord, while medial and dorsal raphe nuclei project toward almost all brain areas[113,114] (for a map of the main serotonin projections in the brain and the spinal cord, see figure 7 in ref[96]). Within the forebrain, the frontal cortex, together with the corpus striatum, the lateral region of the hypothalamus and the amygdala are innervated by projections issuing from the dorsal division of the nucleus centralis superior[96]. An exhaustive listing of the areas innervated by the dorsal raphe is not relevant for this report, but the extent to which serotonin influences the overall brain activity by its ubiquitous presence demonstrates its pleiotropic role over all other monoamines[115]. All effects and regulatory processes controlled or modulated by serotonin necessitate its interaction with serotonin receptors.

Serotonin receptors

The serotonin receptors appear to be among the oldest neurotransmitter receptor system within the rhodopsin-like 7TMR subfamily[11,116]. All subtypes are expressed in the CNS by nineteen genes (14 metabotropic receptors and 5 ionotropic receptor subunits) coding for seven different receptor types composed by nineteen different subtypes. Except for the 5-HT_3 receptor (constituted by 5 subunits 5-$HT_{3(A,B,C,D,E)}$) forming a pentameric structure) which are a cys-loop ligand-gated ion channels activating inward K^+/Na^+ currents[117,118], all other receptors are metabotropic and classified in three categories according to their G protein signaling. The 5-$HT_{1A,}$ 5-$HT_{1B,}$ 5-$HT_{1D,}$ 5-$HT_{1E,}$ 5-HT_{1F} and the 5-HT_{5A}, 5-HT_{5B} receptors are inhibiting cAMP accumulation after release of the $G\alpha_{i/o}$ subunit following receptor activation. The 5-HT_{1C}R has been revealed to be the 5-HT_{2C}R

receptor. Conversely, the 5-HT_4, 5-HT_6 and 5-HT_7 are $G\alpha_s$-coupled and stimulate cAMP production in cells. The subtype 2 regroups the 5-HT_{2A}, 5-HT_{2B} and 5-HT_{2C} mostly coupled to production of IP3 and DAG after hydrolysis of PIP2 following activation of the $G\alpha_{q/11}$ pathway, also stimulating PLC and PKC.

5-HT_{2A} receptor

The class A 5-HT_{2A} receptor, encoded by the *HTR2A* gene, is a subtype of the 5-hydroxytryptamine receptors type 2 and shares this subgroup with 5-HT_{2B} and 5-HT_{2C} receptors. These subgroup 2 receptors share 45-60% of sequence homology and are coupled to their canonical $G\alpha_{q/11}$ signaling pathway[119]. Although found outside the CNS, a study provided evidence that serotonin-induced activation of 5-HT_{2A}R in cultured rat renal cells produced about 50% inhibition of forskolin-stimulated cAMP accumulation, a signal that was reversed by application of the antagonist ketanserin, indicating that this mainly $G\alpha_{q/11}$ coupled receptor can activate $G\alpha_{i/o}$ signaling pathway, at least in this peculiar primary culture[120].

The 5-HT_{2A}R is by far one of the most studied 7TMR and consequently, one of the most known serotonin receptor[121]. This is in part due to its atypical and unique pharmacology, as well as its wide distribution in the CNS and substantial involvement in neuropsychiatric disorders.

5-HT_{2A} receptor distribution

A recent study analyzed the human biodistribution of the 5-HT_{2A}R by positron emission tomography (PET) with two specific radioligands and showed a wide expression in numerous organs and tissues[122]. In the brain, it is well characterized and widely distributed in Rodents[123] and non-human Primates[124], and although mostly present in postsynaptic neurons[125–127], its presynaptic activity has been demonstrated[124,126–128]. It is also present on astrocytes[127,129]. In rat and human, [^{3}H]ketanserin radioligand binding co-distributes and overlaps with mRNA histochemistry demonstrating dense labelling of the major parts of the cerebral cortex regions, though denser in laminae I, IV and Va, the piriform and the entorhinal cortexes, as well as the

claustrum[119]. Using another 5-HT_{2A}R radioligand antagonist, [^{3}H]MDL100,907, radiolabeling signals coupled to *in situ* hybridization (ISH) showed a matching overlap of both transcripts and protein in the rat brain, confirming most of the cortical regions previously described in Mammals and in Rodents, with a preference for the layer V of prefrontal cortex pyramidal neurons[130]. Lesser densities are found in the basal ganglia, in particular the caudate-putamen nucleus (CPN) and the nucleus accumbens (NAc). The cerebellum seems exempt of signal across many studies and often used as a control or reference area[119,131,132], however some findings involved serotonin receptor localization and dysfunction in this area in humans and in rats[133,134]. Caution must be taken about the specificity of the radioligands used to label expressed receptors prior to the development of [^{3}H]MDL100,907[114,135] and [^{11}C]-Cimbi-36[136], accounting for their technical limitations and caveats[114].

In situ hybridization enabled to localize 5-HT_{2A}R mRNA in diverse cell types of the rat brain, mostly pyramidal neurons of the neocortex and the hippocampus, as well as interneurons of the piriform cortex[132]. The lamina IVc of the human striate cortex also showed positive signal. Immunoreactivity in the rat brain displays dense staining in the apical dendrites of pyramidal shaped neurons of the neocortex, as well as both parvalbumin positive and negative interneuron bodies[137].

The cellular and subcellular distribution of this receptor remains difficult to ascertain. Despite numerous examples of its localization both at the plasma membrane and within neuron somas, there is to date no definitive accordance on its spatial distribution either in heterologous cell systems or in native tissues. It is however accepted that 5-HT_{2A}R acts both intracellularly and as a prototypical plasma membranous 7TMR depending on the brain regions and/or the neuronal/peripheral function involved (see discussion below). Therefore, the localization of the 5-HT_{2A}R may affect both its trafficking and signaling properties, and vise-versa.

5-HT$_{2A}$ receptor pharmacology

5-HT$_{2A}$ receptor is the target of endogenous neuromodulator serotonin (5-HT). It is also targeted by atypical antipsychotics (AAP) such as clozapine, olanzapine, quetiapine, paliperidone, aripripazole and risperidone, but also M100907, altanserin, mianserin, and ketanserin, acting as inverse agonists or neutral antagonists. It is also bound by agonists and partial agonists among a wide range of hallucinogenic compounds (HAL) which effects are psychedelic, phenethylamine-like, *e.g.* DOI, DOB, and indolamine-like, *e.g.* mescaline, dimethytryptamine (DMT), psilocybin, lysergic acid diethylamide (LSD), acting as partial agonists[138–140]. Remarkably, some compounds are not hallucinogenic (NHAL) (*e.g.* lisuride, ergotamine) despite high molecular similarity with HALs. 5-HT$_{2A}$R thus exhibits a singular pharmacology[141], being the primary target of pro- and antipsychotic drugs[114,140,142,143]. Such psychedelic compounds elicit response in humans that profoundly affects behavior and consciousness[139,144]. In peak phases, this singular response is often compared to delusions and hallucinations that resemble acute positive symptoms of the schizophrenia spectrum disorder[145,146]. However, while psilocybin provokes psychosis-like behavior in healthy volunteers via 5-HT$_{2A}$R activation[138], other agonists, including psilocybin, are currently considered as potential treatment for depression and other psychiatric conditions[147–155]. This is indeed of particular interest for psychiatric disorders and related pharmacology, because HALs are employed to model psychosis in Rodents and in Humans[138,156]. Activation of 5-HT$_{2A}$R is not sufficient to elicit hallucinogenic response, but it is necessary[140,143,157].

5-HT$_{2A}$ receptor signaling and trafficking

Serotonin regulates essential functions in the CNS such as mood appetite and sleep, along with peripheral vasoconstriction and organs development. The 5-HT$_{2A}$R transduction model describes the G$\alpha_{q/11}$-coupled signaling pathway upon ligand binding, stimulating PKC through PLC recruitment, to finally mobilize calcium release from the ER[158]. The trafficking of the 5-HT$_{2A}$R has been described as atypical. Internalized by either agonists or antagonists, this is a specificity

hardly found in other classes and other types of 7TMR[159,160]. The 5-HT_{2A}R is also thought to activate pathways differentially and promote agonist-directed trafficking of receptor stimulus[161]. Latter termed “biased agonism”, this functional selectivity has been shown to differentially signal downstream upon activation by either psychedelic or non-psychedelic agents. While canonical signaling through $G\alpha_{q/11}$ would be responsible for non-hallucinogenic-mediated downstream activation, hallucinogens require in addition to signal through pertussis toxin-sensitive $G\alpha_{i/o}$ pathways[140,162]. Similar to this concept of signaling, it has also been shown that the 5-HT_{2A}R is at the center of a biased phosphorylation which provides additional trafficking and internalization selectivity through the β-arrestin dependent pathway[163]. While ERK-dependent phosphorylation by HAL such as LSD and DOI is abolished by pretreatment with pertussis toxin, ergotamine and lisuride NHAL signaling remained unaffected, comforting the idea that two G protein-activated pathways are required to elicit hallucination-like behavior *in vivo,* using the Head-Twitch Response as a proxy of hallucinogenic intoxication response in mice[164]) or the ERK signaling readout in pyramidal neurons, as well as in *in vitro* heterologous systems[114].

5-HT_{2A} receptor oligomerization

The 5-HT_{2A}R has been shown to form homo/heterodimers[165–170] and oligomers with other 7TMRs[171–175]. Several lines of evidence have shown that 5-HT_{1A} and 5-HT_{2A} receptors, which are co-expressed in cortical pyramidal neurons, form an antagonistic receptor heteromer by modulating NMDAR currents[114]. 5-HT_{2A}R and D_2R have been shown to associate as a functional receptor heteromer eliciting a signaling crosstalk signaling in cells[172,176].

Physiopathology of the 5-HT_{2A} receptor

5-HT_{2A} receptor is involved in the pathophysiology of schizophrenia-like phenotypes, depression and suicide, to name a few[131,177–187]. It has been linked along with other subtypes to physiopathology of psychiatric and cognitive disorders, such as mood disorders and depression, suicide and schizophrenia, associative learning, where preferentially affecting areas regrouped in

the neocortex, in which the prefrontal cortex (PFC) seems to play an important role[124,125,143,183,187,188]. The list of disorders implicating the 5-HT_{2A}R is long, and it is clear that the receptor regulate many diverse systems and functions in the body and the brain; it comprises Alzheimer disease, autism, Parkinson disease, obsessive compulsive disorder, addiction, suicide, cardiovascular lung and skin disorders, as well as diabetes and inflammation, to name a few. What is unclear though, is how dysregulated is the receptor in many neuropsychiatric disorders. Discrepancies about the level of 5-HT_{2A} protein and mRNA, often is post-mortem human brains, is still a matter of debate[185,189].

Glutamate

Neurotransmission in the mammalian brain is usually depicted as a synchrony between excitatory and inhibitory electrochemical signals. L-glutamate is known to be the main excitatory[190,191] and the most abundant[192] non-essential amino acid in the mammalian CNS, while GABA relays inhibitory neurotransmission. Glutamate concentration is high in the CNS, partly because it is not solely used for excitatory neurotransmission, thus holding other metabolic activities in glia and neurons[193]. Both glutamate and GABA are synthesized from glutamine precursor. Glutamine is synthetized from glutamate by ATP-dependent glutamine synthetase in astrocytes. Glutamine is exported to the neuron by glycine/glutamine transporters. In the neuron, it is then converted into glutamate by the phosphate-activated glutaminase[194]. Glutamate is decarboxylated by the glutamic acid decarboxylase in presence of cofactor pyridoxal phosphate and converted into GABA. After vesicular glutamate transporter 1 (VGLUT-1)-mediated packaging of glutamate in synaptic vesicles, it is released to bind both post synaptic ionotropic and post/presynaptic metabotropic glutamate receptors/autoreceptors respectively. This results in modulation of Ca^{2+} release, acting as a second messenger required for the activation of signaling cascades. It is removed from the synaptic cleft back to the astrocytes through transmembranous excitatory amino acid transporter (EEAT), thus completing the glutamate-GABA/glutamine cycle. It also suggests

the existence of different pools of glutamate-containing neural cells, providing the resources to tightly regulate glutamine, glutamate and GABA homeostasis in the brain. Glutamate concentration is maximal intracellularly, and extracellular increase of glutamate produce neuron's excitotoxicity[195–197].

Glutamate receptors

As mentioned above, there are two types of glutamate receptors expressed in the CNS. Ionotropic glutamate receptors (iGluRs) are fast-acting ligand-gated ion channels that are non-selective cations channels, thus mainly exchanging Na^+ and K^+, together with lesser concentration of Ca^{2+} (in the case of NMDAR). They are termed according to their main activating ligand: NMDA (*N*-methyl-D-aspartate), AMPA (α-amino-3-hydroxyl-5-methyl-4-isoxazole-propionate), and kainate (kainic acid) receptors. As cation channel, their carry out excitatory post synaptic currents resulting in cell depolarization and in optimal cases, creation of an action potential. As their related metabotropic cousins, iGluRs can be both pre- and post-synaptic, complexifying the simplistic black and white view on presynaptic mGluRs and postsynaptic iGluRs[198]. Slow modulation of glutamate release is accomplished by metabotropic glutamate receptors (mGluRs). Indeed, the role of mGluRs differs from that of fast-acting ion channels, because they can be sensitive to both orthosteric and allosteric pharmacological compounds and drugs, thus changing the excitability of the postsynaptic neurons. Additionally, their G protein coupling triggers intracellular messengers that affect neuron homeostasis, function and transmission.

To date, the class C 7TMRs mGluRs are categorized into 3 different groups according to their G protein coupling and sequence homology[199,200]. Splicing variants are common in this subfamily (subscript letters). Group I contains $G\alpha_q/\alpha_s$-mediated signaling subtypes, $mGlu1_{(a, b, c, d, e, f)}$, taste-mGluR1 and $mGlu5_{(a, b)}$ receptors. Group II and III are mainly inhibitory-mediated signaling, coupled to $G\alpha_i$ protein, decreasing adenylyl cyclase activity, stimulating K^+ inward ion channels and altering Ca^{2+} currents, thus negatively affecting neurons firing and excitability by an overall

reduction of glutamate neurotransmission. Group III is composed by mGlu4 and taste-mGlu4 (a shortened, less sensitive version of mGluR4[201]) receptors, the retinal $mGlu6_{(a, b, c)}$ and the presynaptic $mGlu7_{(a, b, c, d, e)}$ and $mGlu8_{(a, b, c)}$ receptors. mGlu2 and $mGlu3_{(A2, A4, A2A3)}$ receptors form the Group II, sharing homology of structure and $G\alpha_q$ protein signaling and pharmacological characteristics. They all bear a large extracellular domain responsible for the binding of orthosteric ligands, the VFT.

mGlu2, mGlu3 receptors distribution

Group II mGluRs are encoded by the *GRM2* and the *GRM3* genes. The homology of sequence between the two genes approximates 67%, with 70% among the conserved regions between mGluR1, 2, 3, and 4, especially at the c-terminus and at the VFT domain. Besides, they do not share any similarly with the other 7TMR classes[202]. *In situ* hybridization studies indicate a wide distribution of mGluR2 in discrete cell types in the rat CNS. It is high in the olfactory bulb and the cerebral cortex. Immunohistochemistry studies with a specific mGluR2/3 antibody showed expression of both receptors in many regions of the mouse brain with variable expression patterns and intensities. This suggests that a wide array of subregions where both receptors are coexpressed and possibly interact[203]. Additionally, the cell types are distinguishable among regions but both pre- and post-synaptic neurons are positive for either mRNAs or protein expression of mGluR2/3, as well as substantial glial expression[203]. In the cerebral cortex, layer I to IV were highly stained, as well as deeper regions in the layer V and VI of medium and pyramidal neurons[203]. Other important reactive regions were the piriform, frontal and entorhinal cortexes, subregions of the hippocampus, the thalamus, and main nuclei of the basal ganglia such as nucleus accumbens and caudate putamen. A study using autoradiography coupled to electrophysiology with the selective mGluR2/3 radioagonist [^{3}H]LY459477 in WT, $mGluR2^{-/-}$ and $mGluR3^{-/-}$ mice, to specifically address distribution of each receptor, matched most of the regions cited above in CD-1 mice[204]. In the basal ganglia, no signal could be found outside the substantia

nigra, though both caudate-putamen and nucleus accumbens shell were mGluR2 positive, in accordance with monoclonal antibody immunoreactivity in both mouse and rat, which also detected mGluR2 in the ventral tegmental area (VTA)[205]. mGluR3 was also found in the same subcortical regions with high immunolabeling ultrastructure resolution[206]. The claustrum was also positive for mGluR2 and mGluR3 radioactivity with different amounts, although the above study using immunohistochemistry technique reported a weak signal[205]. This study[204] was also able to differentiate regions expressing either mGluR2, such as prefrontal cortex, and mGluR3, such as dorsolateral and entorhinal cortexes.

Whereas electron microscopy study found mGluR2/3 staining in many glial processes, vesicles of putative excitatory synapses, presynaptic terminals near synaptic clefts of the layer I cerebral cortex, signal was also high in postsynaptic small spine synapses. Glial staining was detected in all layers, although the authors commented on the difficulty to delineate accurately the processes that seemed positive[203]. Conversely, no glial cell expressing mGluR2 were found with monoclonal immunostaining technique at the EM resolution[205]. Subsequently, other EM studies demonstrated the presence of mGluR2/3 in astrocytic bodies that ensheathed glutamatergic-like synapses, and confirmed the localization of both receptors indistinctly in pre- and post-synaptic processes such as axons, dendrites and spines of the dorsolateral prefrontal cortex of non-human Primates[207]. In the same region of the same animal model, it was specified the relative amount and presence of both mGluR2 and mGluR3. Because this region is critical for many neurodegenerative and psychiatric disorders, the localization of group II mGluRs invests a substantial importance. mGluR2 is mostly reported as a presynaptic terminals autoreceptor[200,208–210], and, to a lesser extent, on a variety of spines, but mostly as an extrasynaptic receptor. It was also clearly present in astrocytes although previously thought to be absent in glia[205]; mGluR3 seemed to be the prominent glial receptor[211]. mGluR3 was mostly present on astrocytes and postsynaptic spines, where it was shown to negatively modulate cAMP production[212]. These findings suggested, in the

context of delayed neurons firing in the layer II of the dorsolateral prefrontal cortex, that mGluR2 and mGluR3 have distinct functional roles in distinct regions of the tripartite synapse, although it was previously assumed that they could share similar brain functions, where mGluR2 was assumed to reduce neurons sensitivity together with other $G\alpha_i$-coupled mGluRs[200,213,214], while mGluR3 would act as a potent mechanism of reuptake glutamate following vesicular release in the extracellular field of excitatory glutamatergic terminals[197].

Most of these regions also express the 5-HT_{2A}R, in particular the layer Va of the prefrontal cortex that showed dual labelling of [^{3}H]LY459477 and either [^{125}I]DOI or [^{3}H]M100907 (in mGluR3 KO mice)[204], indicating that 5-HT_{2A}R and mGluR2 co-distributed in critical regions involved in neuropsychiatric disorders, as previously reported[130]. Both receptors are expressed and detected in thalamic regions, the prefrontal cortex, hippocampal subregions such as the entorhinal cortex, as well as the dorsal and ventral striatum and the amygdala[204].

mGlu2, mGlu3 receptors pharmacology

Group II mGluRs can be sensitive to the same agonists as of their ionotropic cousins. Glutamate is obviously one of them, but also quisqualate, which initially served as a selective agonist for mGluR2 and mGluR3 with differential cellular electrophysiology in cloned expressed receptors[200,202]. As of today, and to our knowledge, agonists sufficiently selective to distinguish mGluR2 from mGluR3 are still not available. This is due to the sequence proximity at the extracellular orthosteric binding site. Pharmacological design has however progressed in the selectivity of this Group II agonists, and a compound, partial agonist at mGluR2 and antagonist at mGluR3 has been developed and tested[215]. Another compound, N-acetylaspartylglutamate (NAAG), the most abundant peptide in the mammalian brain, elicited high mGluR3 selectivity but not at other mGluRs, including mGluR2, implicated in synaptic plasticity and neuroprotection against excitotoxicity[216,217]. Although selective, it remains an endogenous mGlu3 receptor agonist. Other agents could possibly be used in some cases, but the constraints over group II mGluRs

pharmacology limit studies that would be able to distinguish the exact role held by each receptor. This issue can be somewhat overcome by the recent availability of positive and negative allosteric modulators, (PAM or ago-PAM and NAM respectively[218–220]).

The development of highly selective orthosteric mGluR2/3 agonists such as LY379268, LY354740, LY2140023 (the LY404039 prodrug) and LY404039 enabled to refine the function of each receptor in experiments *in vitro*, but also in clinical trials to treat neuropsychiatric disorders such as schizophrenia and anxiety, stress and neurodegeneration, and even cancer and pain management, to name a few[221–235]. Additionally, the affinity of such drugs can differ from one brain area to another, or across different neuronal cell types[236]. LY379268, LY2140023 (the LY404039 prodrug) and LY404039 suppress the behavioral and physiological effects of psychotomimetic drugs and serotonergic hallucinogenic drugs, both enhancers of glutamate release, and show their efficacy in the treatment of schizophrenia[211]. The metabotropic glutamate receptors, including mGluR2 and mGluR3 are considered new targets for their antipsychotic activity and, despite undergone a hold in clinical application, their effects on the positive, negative and cognitive symptoms of schizophrenia continue to raise hopes[170,218,226,234,237–240].

mGlu2, mGlu3 receptors signaling

Because of their similarity in residues sequence, cognate G protein and pharmacology, it has long been assumed that they also share function and similar roles in the brain, despite being localized in different amounts in different localizations and cellular types. The overall decrease of glutamatergic excitability follows the reduction of presynaptic vesicle release caused by the inhibition of Ca^{2+} inward currents. Moreover, ligand-induced dissociation of the $G\alpha_i$ protein βγ subunit can signal through a wide array of second messengers, typically the mitogen-activated protein kinase (MAPK) and the extracellular signal-regulated protein kinases (ERK) pathways, mediated by the phosphatidylinositol 3 kinase (PI3K)[241]. This is a fundamental signaling route involved in critical cellular responses such as cell proliferation and transcription factors regulation.

The loss of function remains a pertinent strategy to decipher to study the role of a protein or a gene. As mGluR2 and mGluR3 being very close on many aspects, the use of knock-out animal models, or even double knock-outs, has provided important information about the precise functions of each receptor in the rodent brain. It offers a unique way to study such features, coping with the issue of non-selective agonists within the mGluRs group II. To that end, several studies have attempted to discern the specific role of mGluR2 over mGluR3 in pain[242], cognition, arousal and anxiety[239,243], and the circadian system[244]. With regards to circadian rhythm and sleep disruption, it is a comorbid symptom of schizophrenia, affecting 30-80% of patients[245]. When mice were depleted of both mGluR2 and mGluR3, their sleep was perturbed, reduced and fragmented, implicating group II mGluRs in sleep regulation[244]. It also suggests a possible link between the implication of both receptors in schizophrenia and such perturbations of fundamental physiology[246]. The above-mentioned mGluR2 agonists are used in clinical trial to test a new kind of antipsychotics or anxiolytic medications, among other targeted neuropsychiatric disorders. They were suggested to show reduced heavy side effects associated with atypical antipsychotics or benzodiazepines. Although there is to date no correlation between the *GRM2* gene and schizophrenia, *GRM3* abnormalities however have been detected multiple times in genome of patients suffering from this syndrome.

mGlu2 receptor oligomerization

As mentioned above, class C 7TMRs are obligate dimers though their function in signaling G protein is mitigate by their stoichiometry. They also form heterodimer within their class and across subtypes, including mGluR2/mGluR3 heterodimers[240,247–249].

Pathophysiology of the mGlu2 receptor

Some authors have associated schizophrenic phenotype with mutations within mGlu receptor genes *GRM2* and *GRM3*[211]. Altered dimerization of type 3 has been implicated in schizophrenia[250]. Structural and functional interactions have been reported for the mGluR2-5-HT_{2A}

heterocomplex[183,251–254]. Both receptors, but especially mGluR2 has been the center of intense researches for its potential antipsychotic activity with potentially less side effects.

Summary

Given the number of matched regions expressing either 5-HT_{2A}R, mGluR2 and mGluR3, there is a high probability that a single neuron expresses these receptors or receives input from one and expresses the second. Because their synaptic localization is also pre- and postsynaptic, as well as glial, (*i.e.* all membranes and soma of the tripartite synapse), it increases the probability for a functional role of the interaction formed by 5-HT_{2A}R and mGluR2 or by mGluR2 and mGluR3 (or by 5-HT_{2A}R and mGluR3 even if they do not seem to interact directly[183]). Together this information provides evidence and leads in the involvement of 5-HT_{2A} and mGlu2 receptors, in participating in brain functions and their alterations. They co-distribute and colocalize, their antagonistic signaling is physiologically relevant and different from each other canonical signaling[255–257]. Moreover, the absence of one affects the behavioral effect of the other. All those criteria are consistent to the required properties necessitated by a receptor heteromer[86].

5-HT_{2A}-mGlu2 receptor heterocomplex

Those two receptors have been reported to play independently and then likely as a heterocomplex, significant roles in psychiatric disorders and especially schizophrenia[183]. As previously mentioned, the PFC represents the area of interest demonstrated by previous electrophysiological studies that suggested an antagonistic crosstalk[125]. *In situ* hybridization experiments reported that both receptors are co-transcribed in pyramidal neurons of mouse cortex and human PFC, where they co-immunoprecipitate and show close molecular and functional interactions revealed by B/FRET analyses coupled to functional assays, excluding 5-HT_{2A}/mGluR3 assembling[183,252]. Electron microscopy by immunogold particles colocalization confirmed close proximity in ultrastructural resolution of pre- and post-synaptic elements[252]. Additionally, this interclass association modulates $G\alpha_q$ and $G\alpha_i$ pathways in an antagonistic and specific manner and support evidences

of heteromeric structures with physiological relevance[67,69,70,251,254]. The structure interface responsible for their heteromerization has been established by a mutation study of the TM4 of the glutamate receptor[252]. In follow up experiments, these findings have been corroborated using photocrosslinking assay, where the covalent linkage between the unnatural amino acids in the TM regions occurs within a distance of 2-4 Å[89].

7TMR trafficking and biosynthesis

7TMRs are synthesized throughout the maturation pathway from ribosomal translation processes at the edge of the endoplasmic reticulum where they are folded and glycosylated, undergoing quality control checkpoints[258]. The Golgi apparatus constitutes the exit pathway as an active post-translational element, finalizing 7TMR biosynthesis. This export process is highly regulated by cargo and scaffold proteins[70,258]. 7TMRs are described as actual signaling units when reaching the plasma membrane, but increasing evidence suggest signaling can occur from endosomes[259]. It is also of particular interest that 7TMR signaling may occur during their trafficking stages[260]. Although it is not the case for all of them, as β-arrestin-independent mechanisms have been described[158,261–263], most 7TMRs undergo ligand-induced endocytosis through β-arrestin/dynamin/clathrin-coated-pits interactions, a 7TMR core process. Among 7TMR subcellular trafficking regulators, the Ras-family small-GTPases Rab proteins are ubiquitous[258,263]. In particular, Rab5 regulates endocytic/early endosomal processes, Rab4 and Rab11 control rapid and slow recycling from recycling endosomes, Rab7 is a regulator of the late endosomes and the lysosomal degradation pathway taken by ubiquitylated proteins. Localized throughout specific intracellular stages, they can therefore serve as exploratory molecules to characterize GPCRs trafficking pathways.

Rab proteins

Navigating through the ultra-dense network of actin fibers and microtubules necessitates the guidance of proteins and cargoes to their appropriate destinations. These two last words suggest

specific recognition and trajectories taken by the cargoes. This is accomplished by a set of proteins counting around 60 subtypes: Rab proteins are small monomeric G proteins constituting the largest group of the Ras-like protein superfamily and hold a common GTPase activity. They orchestrate trafficking events between donor and target membranes. Each Rab protein is a resident of the organelle membrane they regulate, providing an identity to the subcellular compartment[264]. Organelles are also defined by specific scaffold proteins that anchor them to the cytoskeleton, but also by the lipid composition of their membrane layers. Rab1 interacts with the Golgi apparatus and the ER protein complexes each dedicated to their organelles functioning, to activate the environing SNAREs, and to “read” compartments scaffolds to facilitate transport in between the ER and the Golgi apparatus[264].

The duration the GTPase activation cycle is regulated by guanine nucleotide exchange factor (GEFs), who sustains the GDP/GTP exchange, and terminated by hydrolysis of GTP carried out by GTPase activating proteins (GAPs). Rab proteins partner with Arf family to interact with the cell cytoskeleton and in particular with the motor proteins that mediate the transportation of cargoes along the microtubule/actin networks, in both directions[265,266]. For instance, Rab7a promotes the trafficking of cargoes by recruiting the dynein/dynactin motor protein complex to the late endosomes, to direct the enriched vesicles toward the perinuclear areas[267]. Similarly, Rab5 binds to the early endosome antigen 1 protein (EEA1) to recruit the early endosome target, with concomitant association to PI3P. Rab5 also recruit membrane effectors that allow interaction with SNAREs for further engage membrane fusion[268,269].

Rab proteins, besides providing identity and mobility to their respective organelles, can interact with specific GEFs and GAPs of the next Rab protein, thus creating “Rab cascades” that will orient and organize transitions between compartments. In particular, it has been proposed that Rab7 is present on early Rab5 endosomes. Rab7 buds then grows on the Rab5 early endosome membrane and likely interacts with converter proteins. These proteins would turn off the recycling

properties of the sorting early endosomes (which are defined by Rab4 and Rab11), and convert it to a late endosome[270]. Rab5 is displaced and Rab7 is activated. Because effector protein GEF can recognize an increase in Rab5 and PIP3, this gives selectivity to the process. It is also coincident with the membrane recruitment, therefore allowing Rab5 displacement toward Rab7 at a specific time in a specific localtion[271]. This example demonstrates a mechanism that synchronizes protein trafficking in time and space.

Considered as master regulators[272], Rab proteins regulate vesicle sorting, docking, budding, tethering and membrane fusion. They define the secretory and the endocytic routes by interacting with specific components along these pathways. They also specify the microdomain occupied by the organelle they control, underneath the plasma membrane. Rab proteins also regulate the trafficking of 7TMRs, and it has been demonstrated that the basic four Rab proteins (4, 5, 7 and 11) direct and orient internalization and recycling of several 7TMRs[273]. Following β-arrestin-dependent desensitization after being internalize, 7TMRs follow multiple routes in accordance with their interacting Rab protein, effector, or β-arrestin type. Indeed, it has been shown that 7TMRs can follow two different arrestin-mediated pathways[274]. Following ligand-induced internalization, β_2AR has been shown to traffic through Rab5 endosomes[275]. Overstimulation of Rab5 by expressing a dominant positive mutant affect β_2AR trafficking through early endosomes. Conversely, dominant negative Rab5 impairs early trafficking of the receptor. This was also the case for the D_2R, which is regulated by dynamin following phosphorylation by GRK2[276]. Interestingly, the class A angiotensin receptor 1A ($AT_{1A}R$) has been shown to use both β-arrestin-dependent and -independent pathways without being regulated by Rab5, although it is bound by the receptor. This suggests that Rab5 mediates different endocytic mechanisms[277].

Endosomes

Endosomes are dynamic cytoplasmic vesicles acting as trafficking regulators and sorting platform. Their importance has generated much attention as targets for novel therapeutics[278,279]. They

provide the necessary space and means to regulate the trafficking, and identify not only the nature of the entrant and recycled particles, endocytosed receptors and lipids, but also a platform for receptor signaling, whether they come from the plasma membrane or from the secretory pathway. They appear poorly studied despite their critical role in protein trafficking, as well as in receptor signaling[280].

Usually categorized as early (EE), sorting (SE), recycling (RE), or late endosomes (LE), they adopt different shapes structured around the cytoskeleton with specific cellular functions. They can be ramified to tubular extensions (EE, multi-vesicular body MVB) or simply remain spherical-like, mostly depending on their function and associated motility, sustained over the microtubular network[281]. The pH gradient between the cytoplasm and the lumen of intracellular vesicles provides the differential ionic concentration that serves to dissociate the ligand from its receptor, the former often directed to degradation whereas the latter can either been rerouted to the plasma membrane or follows the same fate as its ligand[282]. The role of each endosome also depends on their localization underneath the plasma membrane, constituting functional microdomains. Their identity is determined by the combination of regulatory proteins and lipids that are unique to each specialized endosome[283].

A pH gradient spans through the cytoplasm from the plasma membrane to deeper compartments. The higher pH is found right under the plasma membrane, where early endosomes control the endocytic trafficking of newly endocytosed elements[284] (recycling endosomes have a slightly higher pH). They are thought to constitute the first and only entry point of endocytosed proteins/lipids independently of the internalization mode, such as clathrin-mediated and lipid raft-mediated endocytosis or pinocytosis, as well as the first recycling platform[283,285]. To that end, their structure consists in several cisternal areas associated with budding vesicles and thin tubular emanations (for a stunning visualization by electron microscopy of the EE structure see ref[283]). A complex association and interplay of specific resident proteins participate to endosomal transport,

morphology, sequestration, docking, etc.[283]. Among them, Rab5 and its effectors appears to be the main regulators that take on several functions such as spatial organization, docking affectation from either trans-Golgi or plasma membrane. Membrane budding, fission and interaction with the cytoskeletal components are also among Rab5 attributes (see above)[268,286,287].

The model describing the compartmentalization of endosomes has been proposed by early studies that investigated fluorescent markers routing and chased their cellular destination and trafficking in a timely manner, usually depicting a common network of specialized vesicles as a general trafficking model[288]. Although it was assumed that integral proteins, ion channels and receptors underwent at least two types of internalization processes, degradation or recycling, the putative motion of different membrane-based vesicles was described as a bulk flow process, without specificity[288]. This model has been refined to the point that there is no longer such a bulk flow of membranes that fusion and interact, but rather a complex interplay orchestrated by specialized proteins and adaptors along endosomal-mediated tubular networks[289], sorting motifs attached to internalized cargoes that orient their route according to the cell needs[290].

EE provide both fast and slow recycling pathways[285], though evidence suggested that LE can also recycle cargoes. Lumen pH is lower in LE, which link endocytosed cargoes to degradation pathway through EE sorting[284,291]. Within the EE or the LE, cargoes routed to the recycling pathway should avoid inclusion in intermediate degradative vesicles (intraluminal vesicles) to be able to reach back to the plasma membrane, either by the slow or the fast recycling routes[290]. Thus, LE, also identified to MVB, function as sorting dispatchers[290].

A major shift in envisioning receptor signaling was provided by findings in regard to intracellular signaling, and more precisely, on signaling from endosomes. Receptor endocytosis has been studied as a termination mechanism to regulate available receptor density at the cell surface and mitigate cell responsiveness following agonist stimulation. Receptor desensitization and resensitization are not general mechanisms that all 7TMRs undergo. Although β-arrestin-

dependent internalization of clathrin-coated pits and adapter protein-2 complex (AP-2), in response to GRK-mediated receptor phosphorylation, plays a major role in 7TMR internalization, besides being the most well characterized system, some receptor types are recycled, some are not and get degradated[292]. Recycling endosomes employs several Rab proteins (Rab5, 4, and 11) while late endosomes are often related to degradation pathways and mostly regulated by Rab7 (and Rab9). The early or sorting endosome is the first encountered container of most internalized proteins and lipids[285].

Together, this information suggests that the endosomal network is finely regulated by resident and adaptor proteins, and that, together with the architecture of the specified endosomes, produces subcellular microdomains composed by the vesicles tubular extensions over the actin/microtubule skeleton[293]. Each microdomain, regulated by a specific Rab protein, serves as orientation platforms to either degrade or recycle cargoes that are either endocytosed or synthetized.

Schizophrenia

Schizophrenia, or schizophrenia spectrum disorder (or syndrome), is a serious multifactorial mental illness affecting up to 0.65% of the USA population and 20 million people worldwide[294] (up to 0.75%), with chronic, and in great majority, life-lasting social, emotional and cognitive alterations. Clinical symptoms are often grouped as so-called negative, positive, and cognitive[295,296]. Studies and definitions converge to acknowledge that a combination of genetic susceptibilities and harmful environmental factors participate to its etiology, which remains unknown. Nonetheless, despite a raise in the prevalence of brain disorders and consequent increase economic and social burden[297–300], where schizophrenia costs are disproportionately high[301], pharmacological companies have halted avenues of research for claimed financial reasons[302–308], creating a gap between a steady clinical and fundamental research and the availability of commercialized medications.

The classical hypothesis of dopaminergic hyperactivity gained attention since the antipsychotic activity of several commercialized dopamine receptor (DR) antagonists (typical) would correct some of the positive symptoms, especially delusions and hallucinations. The dopamine hypothesis suggests that there is an imbalance of the dopaminergic tone in the prefrontal cortex that can be rectified by treatment with D_2R antagonists, such as chlorpromazine, pioneer molecule to treat positive symptoms[309]. Compared to the first generation antipsychotics (the typical D_2R/D_3R antagonists), atypical antipsychotics (AAP) have more affinity for the 5-$HT_{2A}R$. Similarly, such pharmacological evidence fashioned the serotonin hypothesis, also based on the resemblance between serotonin receptor agonists that produce psychosis-like effects on humans. These molecules exhibit substantial off target occupancy and are considered as "*dirty drugs with rich pharmacology*"[310], carrying at the same time, important side effects. They are yet prescribed as first line compounds to treat schizophrenia's positive symptoms, with moderate improvements of negative and cognitive ones. A third of subjects do not respond to AAP[311,312]. Although the classical theories on the onset and the etiology of the disorder remain up to date, the scope has yet evolved toward other signaling pathways such as glutamate and GABA; the implication of a combination of neurotransmitter systems rather than a single defective gene or pathway could shed light on the disorder origin and mechansims[309,313,314]. Indeed, recent findings propose that a heterogeneous genetic network causes distinct clinical syndromes[315], as conveyed by years of research on the implication of several genes that regulate and express 7TMRs, receptor trafficking and neurotransmission, synaptic and structural plasticity[316–320].

The variability of symptoms combined to the diversity of phenotypes resulting from clinical and genetic observations conflict with a single disease paradigm, thus single medication are unlikely to treat the full spectrum that characterize the disorder[321]. The absence of a uniform syndrome renders difficult the delivery of accurate, specific and reproducible diagnostics[322–325], which also rely on definitions and clinical practices[326]. For instance, some criteria can overlap with those of

bipolar disorder[327] that may affect drug indication and assistance to patients[328,329], who eventually cope with long term/life lasting treatments, if they find access to them[295,296].

It is nowadays a common concern as to challenge the single disease paradigm[297,330], *i.e.* embrace several theories about the disorder to provide novel and more efficient medications. This was the case for atypical antipsychotics, who have affinity for both 5-HT_{2A}R and D_2R, and together increase the beneficial effects on the disorder process and evolution, rather than just on symptoms[311,331–333]. The glutamatergic system has also gained in importance with the findings related to altered NMDAR-mediated glutamatergic neurotransmission, signaling and trafficking. NMDAR dysfunction on GABAergic neurons implicate a hyperglutamatergic stimulation responsible for cognitive impairments and other deleterious effects found in schizophrenia. Agonizing the mGluR/2/3 pathway potentially rectifies the glutamatergic overstimulation by reducing the presynaptic release of glutamate on excitatory neurons, as a compensatory mechanism[233]. Those agonists have been found to relieve all 3 symptoms type in patient with schizophrenia[334]. It was believed that such molecules held a novel and promising mechanism of action that could be beneficial to patients[226,233].

Hypothesis

Investigations in post-mortem schizophrenic prefrontal cortexes suggested that 5-HT_{2A}R specific binding is increased yet rectified in treated subjects with AAPs. However, mGluR2 remained downregulated in both untreated and treated schizophrenic subjects. We thus hypothesize that biosynthesis and endocytosis of interacting 5-HT_{2A}R and mGluR2 may play a role in their common and linked dysregulation. Trafficking and signaling being entangled, endocytosis and biosynthesis of 7TMR complexes control their cellular localization in time and space. Conversely, trafficking failure implies signaling impairments, which eventually result in a host of pathologies. The objective of the following study is to elucidate in *in vitro* and *ex vivo* models, the maturation and

the ligand-dependent trafficking mechanisms regulating the 5-HT_{2A}R-mGluR2 signaling complex to further explicit the effect of their imbalance in schizophrenia.

Aims

Aim 1: **5-HT_{2A}R modulates mGluR2 post-endocytic sorting.** Hypothesis: Pharmacological modulation of 5-HT_{2A}R affects mGluR2 sorting and function through Rab-mediated trafficking pathways.

Aim 2: Effects of 5-HT_{2A}R antagonists/inverse agonists (antipsychotic) and hallucinogenic agonists (propsychotic) on 5-HT_{2A}R-mediated trafficking of mGluR2. Hypotheses: 5-HT_{2A}R and mGluR2 heterocomplex is affected by clozapine, as well as mGluR2 trafficking. Psychedelic agents promote Rab5-dependent pathway of mGluR2, while non-psychedelic agents do not.

Aim 3: 5-HT_{2A}R and mGluR2 are assembled as a GPCR complex in the biosynthetic pathway. Hypothesis: 5-HT_{2A}R and mGluR2 structurally associate in the biosynthetic pathway. BiFC of 5-HT_{2A}R and mGluR2 would be detected in both the endoplasmic reticulum and the Golgi apparatus.

Materials and Methods

Drugs

(±)-2,5-Dimethoxy-4-iodoamphetamine hydrochloride (DOI), 5-hydroxytrytamine hydrochloride (5-HT; serotonin), Lysergic acid diethylamide (LSD), Ergotamine, GDP, and GTPγS were purchased from Sigma-Aldrich. (1R,4R,5S,6R)-4-Amino-2-oxabicyclo[3.1.0]hexane-4,6-dicarboxylic acid (LY379268), (2S)-2-amino-2-[(1S,2S)-2-carboxycycloprop-1-yl]-3-(xanth-9-yl) propanoic acid (LY341495), clozapine, (*R*)-(+)-α-(2,3-dimethoxyphenyl)-1-[2-(4-fluorophenyl)ethyl]-4-piperinemethanol (M100907; MDL 100,907; volinanserin), 3-[2-[4-(4-fluorobenzoyl)-1-piperidinyl]ethyl]-2,3-dihydro-2-thioxo-4(1H)-quinazolinone hydrochloride (altanserin), L-glutamic acid, 3-hydroxynaphthalene-2-carboxylic acid (3,4-dihydroxybenzylidene)hydrazide (dynasore), [8β(*S*)]-9,10-didehydro-*N*-[1-(hydroxymethyl)propyl]-1,6-dimethylergoline-8-carboxamide maleate (methysergide) and Lisuride were purchased from Tocris Bioscience. [^{3}H]Ketanserin and [^{35}S]GTPγS were obtained from PerkinElmer Life and Analytical Sciences. [^{3}H]LY341495 was purchased from American Radiolabeled Chemicals. All other chemicals were obtained from standard vendors.

Plasmid Construction

All PCR assays were performed with PfuUltra Hotstart Polymerase (Stratagene) in a Mastercycler Ep Gradient Auto thermal cycler (Eppendorf). Cycling conditions were 30 cycles of 94°C for 30 s, 55°C for 30 s, and 72°C for 1 min/kb of amplicon, with an initial denaturation/activation step at 94°C for 2 min and a final extension step of 72°C for 7 min. All the constructs were confirmed by DNA sequencing. The following constructs have been previously described[183,251,252]: human 5-HT_{2A}R N-terminally tagged with the c-Myc epitope (pcDNA3.1-c-Myc-5-HT_{2A}R), human 5-HT_{2A}R N-terminally tagged with the c-Myc epitope and C-terminally tagged with enhanced cyan fluorescent protein (pcDNA3.1-c-Myc-5-HT_{2A}R-eCFP), human 5-HT_{2A}R N-terminally tagged with the c-Myc epitope and C-terminally tagged with mCitrine (pcDNA3.1-c-Myc-5-HT_{2A}R-mCitrine), human 5-HT_{2A}R N-terminally tagged with the c-Myc epitope and C-terminally tagged with mCherry

(pcDNA3.1-c-Myc-5-HT_{2A}R-mCherry), human 5-HT_{2A}R N-terminally tagged with the c-Myc epitope and C-terminally tagged with eYFP (pcDNA3.1-c-Myc 5-HT_{2A}R-eYFP), human mGluR2 C-terminally tagged with eYFP (pcDNA3.1-mGluR2-eYFP), human mGluR2 C-terminally tagged with eCFP (pcDNA3.1-mGluR2-eCFP), human mGluR3 C-terminally tagged with eYFP (pcDNA3.1-mGluR3-eYFP), human mGluR2 with substitution of residues A677$^{4.40}$, A681$^{4.44}$ and A685$^{4.48}$ in mGluR2 for S686$^{4.40}$, F690$^{4.44}$ and G694$^{4.48}$ in mGluR3 C-terminally tagged with eYFP (pcDNA3.1-mGluR2ΔTM4; formerly named pcDNA3.1-mGluR2ΔTM4N). The construct 5-HT_{2A}R-eCFP was subcloned into the vector pcDNA5/FRT/TO (Invitrogen) for the subsequent generation of Flp-In T-REx HEK293 cells, as we have previously reported[335]. For BiFC studies, constructs were generated by subcloning the sequence encoding the N-terminal 172-amino acid fragment (mCi-N172) or the C-terminal 67 amino acid fragment of mCitrine (mCi-C76), as we have previously described [see [40]]. The constructs pcDNA3.1-mCi-N172, pcDNA3.1-mCi-C67, pcDNA3.1-mGluR2-mCi-N172 and pcDNA3.1-mGluR2-mCi-C67 have been previously described[251]. The form of 5-HT_{2A}R C-terminally tagged with eCFP was digested with NheI and BamHI and subcloned into the same restriction sites of pcDNA3.1-mCi-N172 and pcDNA3.1-mCi-C67 to generate pcDNA3.1-5-HT_{2A}R-mCi-N172 and pcDNA3.1-5-HT_{2A}R-mCi-C67. The chimeric Gα protein $G\alpha_{qi9}$ has been previously reported[336]. FRET calibration was performed on parental HEK293 cells transfected with either pcDNA3.1-eCFP, pcDNA3.1-eYFP, or the tandem plasmid pcDNA3.1-eCFP-eYFP.

Transient Transfection of HEK293 cells

Human embryonic kidney (HEK293) cells (ATCC: CRL-1573) were maintained in Dulbecco's modified Eagle's medium (DMEM) supplemented with 10% (v/v) dialyzed fetal bovine serum (dFBS) and 1% penicillin/streptomycin (Gibco) in a 5% CO_2 humidified atmosphere. Transfection was performed using polyethylenimine (PEI) linear MW 2,500 (Polysciences), following standard protocols.

Generation of Stable Flp-In T-REx HEK293 cell lines

Generation Flp-In T-REx HEK293 cells expressing c-Myc-5-HT_{2A}R-eCFP in an inducible manner was preformed following standard protocols[337]. Briefly, Flp-In T-REx HEK293 cells were transfected with a mixture containing either c-Myc-5-HT_{2A}R-eCFP cDNA in the pcDNA5/FRT/TO vector and pOG44 vector (1:9) using Lipofectamine 2000 reagent (Invitrogen), according to the manufacturer's instructions. When cotransfected with the pcDNA5/FRT/TO plasmid into the Flp-In mammalian host cell line, the Flp recombinase expressed from pOG44 mediates integration of the pcDNA5/FRT/TO vector containing the gene of interest into the genome through Flp recombination target (FRT) sites. Clones resistant to blasticidin (5.0 µg/ml; InvivoGen) and hygromycin (2.2 µg/ml; InvivoGen) and expressing the Tet repressor (tetR) along with the inserted c-Myc-5-HT_{2A}R-eCFP at the FRT site were screened for eCFP expression by standard fluorescence microscopy protocols.

Double stable cell lines expressing mGluR2-eYFP, mGluR3-eYFP or mGluR2ΔTM4 constitutively and 5-HT_{2A}R-eCFP in an inducible manner were generated from the Flp-In T-REx HEK293 cells described above. Cells were transfected using Lipofectamine 2000 reagent (Invitrogen) with the vectors containing mGluR2-eYFP, mGluR3-eYFP or mGluR2ΔTM4. Following transfection, cells were selected for resistance to Geneticin (1 mg/ml; Invitrogen), and the resistant clones were screened for receptor expression by standard fluorescence microscopy. Flp-In T-REx HEK293 cells stably expressing µ-opioid receptor tagged with eYFP and able to express c-Myc-5-HT_{2A}R-eCFP in an inducible manner have previously been described[335]. To induce expression of 5-HT_{2A}R-eCFP, cells were treated with doxycycline (DOX) (1.0 µg/ml; 24 – 48 h). Dialyzed FBS was used for cell growth to avoid activation of 5-HT_{2A}R by 5-HT that is routinely present in serum.

Mice

5-HT_{2A}R knockout (*Htr2a*$^{-/-}$) mice of 129S6/Sv background have previously been described[140]. For experiments involving *5-HT$_{2A}$R*$^{-/-}$ mice, wild-type (*5-HT$_{2A}$R*$^{+/+}$) littermates on a 129S6/Sv background were used as controls. Animals were housed at 12 h light/dark cycle at 23°C with food

and water ad libitum. The Institutional Animal Use and Care Committee at Virginia Commonwealth University School of Medicine approved all the experimental procedures.

Cortical primary cultures

Fetuses (E17-18.5) from pregnant mothers were removed using aseptic techniques. Cortical primary cultures were performed as previously reported[140]. Cells were maintained for 7 days in vitro before use in experiments.

Immunocytochemistry

In HEK293 cells or mouse cortical primary cultures, immunocytochemical assays were performed as previously reported with minor modifications[183,251,252]. Briefly, cells were fixed with 4% paraformaldehyde (Sigma) supplemented with 100 µM $CaCl_2$ and 100 µM $MgCl_2$ for 10 min at room temperature, rinsed with PBS, and washed twice with PBS supplemented with 20 mM glycine. Coverslips were incubated with 0.2% Triton X-100 for 10 min at room temperature and incubated in the dark for 60 min with PBS containing 5% donkey or goat serum (according to the secondary antibody). Primary antibody was added (40 µl on each coverslip) and incubated overnight at 4°C. Primary antibodies used were rabbit anti-c-Myc (Cell Signaling Technology catalog no. 2272; diluted at 1:250), mouse anti-mGluR2 (Abcam catalog no. 15672; diluted at 6.5 µg/ml), goat anti-Rab5 (SICGEN catalog no. ab1024; diluted at 6.5 µg/ml [HEK293 cells] or 5.0 µg/ml [primary neurons]), rabbit anti-Rab7 (Cell Signaling Technology catalog no. 9367; diluted at 1:100), or rabbit anti-GFP (Invitrogen catalog no. A11122; diluted at 1:500) After washing with PBS, cells were incubated for 60 min at room temperature in the dark with the secondary antibodies Alexa Fluor 488-conjugated goat anti-rabbit (Invitrogen catalog no. A11011; dilution 1:1000), Alexa Fluor 568 conjugated goat anti-rabbit (Invitrogen catalog no. A11004; dilution 1:1000), Alexa Fluor 568-conjugated donkey anti-goat (Invitrogen catalog no. A11057; dilution 1:1000), or Dylight 650-conjugated donkey anti-mouse (Thermofisher catalog no. SA5-10169 [primary neurons]). For the maturation pathway: ER-Tracker Red (ER-Tr) dying protocol fits mostly manufacturer's recommendations (Thermofisher). Concentration was adjusted to 0.5µM of dye in

pre-heated HBSS (Gibco), cells were incubated for 20 minutes in the same conditions as above then fixed with 3% PFA during 2 minutes. For Golgi experiments, fixed cells were permeabilized in a 0.2% Triton X-100/PBS solution then disposed in a PBS/3%FBS/1%BSA blocking solution. Coverslips were then incubated for 60 minutes with 5µg/mL mouse anti-58K primary antibody (Abcam), followed by 50 minutes in 0.5µg/mL conjugated AlexaFluor568 goat anti-mouse IgG secondary antibody (Invitrogen). Nuclei were stained (5 min) with Hoechst 33342 (ThermoScientific). After washing (PBS, 6 × 5 min), the coverslips were mounted on glass slides with Prolong Diamond Antifade Mountant (ThermoFisher).

Confocal microscopy

Fixed cells and living cells were visualized on a Carl Zeiss Axio Observer LSM 710 laser scanning confocal microscope (LSCM) with a Plan-Apochromat 63×/1.40 Oil DIC M27 or 40× Cal objective. Hoechst 33342 was excited by a 405 nm blue diode, and eCFP with a 440 nm laser-pulse. Additionally, 488 nm and 514 nm multi-line Argon lasers were used to excite Alexa Fluor 488, mCitrine and eYFP, respectively, whereas a 561 nm green diode laser was used to excite mCherry and Alexa Fluor 568. Finally, DyLight 650 was excited with a 633 nm HeNe laser line. Emission signals were acquired in the same order using the following Main Beam Splitter/Dichroic Beam Splitter (MBS/DBS) and emission filters (EF) sets: InVis 405/Mirror EF: 410-482nm, InVis 445/Mirror EF: 435-480 nm, 488/Mirror EF: 494-523 nm, 458/514/Mirror EF: 523-543 nm, and 458/561/633/Mirror EF: 591-661 (mCherry) 573-620 (AF568) 654-700 (DyLight650). Pinhole was kept constant and adjusted at 1 airy unit. Living cells (cell cloning) were visualized on a Carl Zeiss Cell Axio Observer Z1 spinning disc confocal microscope (SDCM) with an embedded Yokogawa CSU-X1 spinning disc and a C-Apochromat 63×/1.20 W Korr UV-Vis-IR objective. Illumination sources were a 458 nm and 514 nm (multi-Ar) laser for eCFP and eYFP, respectively. Emission filters (SD mirror + bypass filters BP) were RTFT457/514/647 + BP485/30 (eCFP) and

RQFF405/488/568/647 + BP525/50 (eYFP). During image acquisition, cells were maintained at 37°C and 5% CO2 atmosphere by an incubation system.

Immunoblot Assays

Western blot experiments were performed as previously reported[252], using rabbit anti-c-Myc (Cell Signaling, catalog no. 2272; diluted at 1:400) and rabbit anti-β-actin (Abcam catalog no. 8227; diluted at 0.33 μg/ml).

TAT-fused transmembrane domain interference peptides

Peptides derived from human mGluR2 TM4 and TM1 were custom synthesized (Genemed Synthesis, Inc.). TAT (trans-activating transcriptional activator from human immunodeficiency virus; YGRKKRRQRRR) was fused to the N-terminus of the human mGluR2 TM4 (YGRKKRRQRRRSPASQVAICLALISGQLLIVVAWLVVE) and TM1 (AWAVGPVTIACLGALA-TLFVLGVFVRHYGRKKRRQRRR) to obtain the correct orientation for the inserted peptide because TAT binds to phosphatidylinosityol-(4,5)-biphosphate found on the inner surface of the membrane[338]. TAT-labelled 38-mer peptide was used as an internal control (YGRKKRRQRRR-VIAPLYTSCVNWQIF-VISMYRGARVAI). Stock solutions of the TAT-tagged peptides (5.2 mM) were prepared in DMSO supplemented with glacial acetic acid (1.93%). For FRET assays, cells were incubated with TAT-tagged peptides (10 μM, final concentration) for 60 min (DMSO's final concentration = 0.18%). For studies involving receptor agonists, TAT-tagged peptides were added 5 minutes before DOI or LY379269, or vehicle administration. For studies involving overnight treatment with clozapine, TAT-tagged peptides were added both 5 minutes before clozapine or vehicle administration and 65 minutes before cell fixation.

Proximity Ligation Assay

Heteromers of c-Myc-5-HT_{2A}R-eCFP and mGluR2-eYFP were detected using the Duolink In Situ PLA Detection Reagents Red technology kit (Sigma-Aldrich). Briefly, coverslips with fixed cells were incubated with 0.1% Triton X-100 for 10 min at room temperature then in blocking solution

according to manufacturer's instructions. Cells were incubated overnight at 4°C with a mixture of the primary antibodies (rabbit anti-c-Myc [Cell Signaling Technology, catalog no. 2272; 1:250], and mouse anti-mGluR2 [Abcam, catalog no. 15672; 1:200]). Samples were incubated with Duolink In Situ PLA Probe Anti-Rabbit PLUS Affinity purified Donkey anti-Rabbit IgG and Duolink In Situ PLA Probe Anti-Mouse MINUS Affinity purified Donkey anti-Mouse IgG. Samples were processed for ligation and amplification and were mounted onto glass slides with Prolong Diamond Mountant. Z-stack images were acquired in a Carl Zeiss Axio Observer LSM 710 laser scanning confocal microscope with a Plan-Apochromat 63×/1.40 Oil DIC M27 objective (to obtain a representative image) or 40× Cal objective (for quantification purposes). For each field of view, a stack of three channels (one per staining) was obtained. Images were processed with Fiji software version 2.0.0 (National Institutes of Health, Bethesda, MD). To quantify PLA signal, PLA-red channel remained hidden during cell identification process. Automated counting involved selection and cropping of each region of interest, Z-Stack projection of the PLA channel, subtraction of background with a rolling ball radius of 20 pixels and finding maxima with a noise tolerance value of 6000–10000 depending on the experiment and the background.

Radioligand binding assays

[^{3}H]Ketanserin, [^{3}H]LY341495 and [^{35}S]GTPγS binding assays were performed as previously reported[183,251,252]. The stoichiometry of 5-HT$_{2A}$R density (as assessed by [^{3}H]ketanserin binding) and mGluR2 density (as assessed by [^{3}H]LY341495 binding) is similar to that previously observed in native tissue, such as mouse frontal cortex and postmortem human frontal cortex[183,251,252] and in cross-talk positive clones[254].

[Ca^{2+}]$_i$ Mobilization assays

Two days before the assay, cells were plated onto poly-D-lysine coated 96-well plates (Greiner Bio-One GmbH) and, 48 hours later, treated with doxycycline (1 µM) for 40 h. Cells were washed with DPBS and loaded with 3 µM Fura 2-AM (Molecular Probes) in imaging solution (5 mM KCl,

0.4 mM KH_2PO_4, 138 mM NaCl, 0.3 mM Na_2HPO_4, 2 mM $CaCl_2$, 1 mM $MgCl_2$, 6 mM glucose, 20 mM HEPES, pH 7.4) supplemented with pluronic acid (20% solution in DMSO). After incubation for 30 min at 37°C, cells were washed twice with washing buffer before being placed on the FlexStation 3 microplate reader (Molecular Devices). The Fura-2 signal was acquired at 510 nm by switching the excitation wavelength between 340/380 nm. Intracellular calcium concentration was expressed as a 340/380 nm ratio, and values were normalized to the basal 340/380 nm ratio recorded during 30 seconds before perfusion of the drug using Softmax Pro (Molecular Devices). To allow efficient coupling of $G\alpha_{i/o}$-coupled mGluRs to the PLC pathway, cells were also transfected with the chimeric $G\alpha$ protein $G\alpha_{qi9}$[336]. Concentrations of LY379268 were selected based on our previous findings[251]. Thus, activation of the canonical $G\alpha_{i/o}$ protein-dependent pathway was tested in the presence of LY379268 (0.1 μM), but trans-activation of the $G\alpha_{q/11}$ protein-dependent pathway was tested in the presence of LY379268 (10 μM and 100 μM).

Flow cytometry and immunofluorescence

Cells were treated with for 60 min with either DOI (1 μM), LY379268 (10 μM), or vehicle, or (overnight) with clozapine (10 μM) M100907 (10 μM) or vehicle. Cells were trypsinized, washed with PBS, filtered through filter top tubes (35 μm), resuspended in PBS supplemented with 1% FBS, and analyzed using a LSRFortessa X-20 Flow cytometer (BD Bioscience). eCFP and eYFP were excited with a 405 nm and a 488 nm laser line, respectively. Emission filters were 525/50 and YFP-A. Quantification was carried out using FCS Express v.5 (De Novo Software). Mean intensity values were determined by gating 25.5% or more of the total cell population. Imaging flow cytometry (Amnis ImageStreamX) to measure colocalization of mGluR2 or 5-HT_{2A}R with the transferrin receptor at the single cell level was performed as previously reported, using an Amnis ImageStream flow cytometer[254]. Cells were considered to present a colocalized signal between the receptor constructs and transferrin receptor when their Bright Detail Similarity score was greater than 2. To detect cell surface receptors, cells were treated with DOI, LY379268 or vehicle

(60-min treatment), or with clozapine, M100907 or vehicle (overnight treatment). Cells were washed with ice-cold imaging buffer (PBS supplemented with 10% FBS) and incubated with human mGluR2 Alexa Fluor 647-conjugated antibody (R&D Systems, catalog no. IC4676R; 1:40) for 60 min on ice (~11-13°C). After two washes with ice-cold imaging buffer, cells were resuspended in ice-cold imaging buffer and loaded into the flow cytometer. 405 nm, 488 nm and 640 nm lasers were used to excite eCFP, eYFP and AF647, respectively. Data were subsequently gated and analyzed using the FCS Express 5 software. For the maturation pathway: IFC assays were performed on the Amnis ImageStreamX Mark II flow cytometer (IS). Prior to analysis, probe-free cells and single color channels controls were made in order to evaluate background autofluorescence and to set the compensation matrix parameters required to separate spectral overlap of fluorescent probes. For BiFC experiments, cells were transfected 24h before experiment on 10 cm plates using scaled up DNA/PEI concentrations. mCitrine and ER-Tr were illuminated with a 488 nm and a 561 nm lasers respectively. In-focused cells were acquired with a 60x objective and gated by gradients MAX and RMS controlling bright field focus quality, then proceeded to similarity analysis. The figure herein displays an example of negative control performed on the 5-$HT_{2A}R$ BiFC. Cells populations were gated by calculating the maximal threshold rendered from irrelevant colocalization of each channel with the bright field (>1.5) in ImageStream Data Exploration and Analysis Software (IDEAS). The BDS score is then determined and set to gate and identify highly colocalized populations[254]. BDS is a log-transformed Pearson Correlation Coefficient.

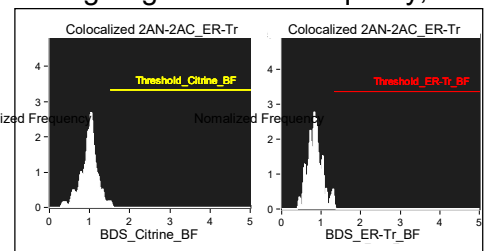

Figure A: Representative IS histograms displaying negative controls to set the BDS score. BDS is gated by the max point defined by cells population, colocalizing each probes with the bright field.

SensorFRET

SensorFRET assays were performed as previously reported[339]. Briefly, the fluorophores associated with uneven expression levels between the donor and acceptor. The fluorophores used as the FRET pair were eCFP (donor) and eYFP (acceptor) with quantum yields assumed to be

0.40 and 0.61, respectively[340]. This approach also requires knowledge of the fluorophore emission shapes (for linear unmixing of the spectra) as well as the relative molar extinction coefficients for the fluorophores at each excitation frequency (characterized by the γ parameter). The normalized emission shapes of both fluorophores as well as the autofluorescence at each excitation frequency were determined experimentally. The γ calibration term was also determined experimentally (γ = 0.114), following a previously described procedure[339]. Imaging was carried out using a Zeiss 710 confocal LSM at 405nm and 458 nm excitation frequencies and a 32-channel spectral detector spanning an emission range of 416nm to 718nm. In unfixed cells, short acquisition times (~ 600 ms) were necessary to minimize the shift due to vesicle movement during the time needed to acquire images at both excitation wavelengths. For assays involving TAT-tagged peptides, cells were briefly fixed with PFA (1%) for 5 min to avoid background caused by PFA fixation. A minimum of 30 cells were imaged for each experimental group. For the statistical analysis, the measured FRET efficiency of each vesicle was considered a single observation. Strict masking was carried out to include vesicles that met three criteria. First, only vesicles which remained stationary between the 405 and 458 nm images were included because even at short acquisition times, some population of vesicles showed appreciable movement. Second, only vesicles with a donor to acceptor stoichiometry within the range of 1:10 to 1:1 were included because the sensorFRET approach is not applicable when there are excess donor fluorophores[339]. Thus, below a 1:10 ratio the donor signal is so small that it is difficult to reliably distinguish it from auto fluorescence and noise. The stoichiometry was estimated by comparing the ratio of the donor and acceptor direct excitation in experimental vesicles to a unimolecular construct (both CFP and YFP are encoded as part of the same protein) where the stoichiometry is known to be 1:1. Marks were drawn only over pixels that showed colocalized eCFP and eYFP signal from both 405 nm and 458 nm images. Finally, only vesicles consisting of greater than 5 pixels were included so that mis-localization of proteins to small non-vesicle features was excluded, allowing each vesicle observation to be the average of multiple spectra and improving the signal to noise ratio.

Electron Microscopy

Electron microscopy assays were carried out as previously reported with minor modifications[252]. Briefly, four male mice (8 – 12 weeks old) per genotype were deeply anesthetized and perfused transcardially with 2% dextran (MW 70,000) in 0.1 M phosphate buffer (PB, pH 7.4), and then with a mixture of 4% paraformaldehyde and 0.125% glutaraldehyde in phosphate buffered saline (PBS). Brains were removed and post-fixed in the same perfusate overnight at 4°C. Approximately 0.5-mm-thick coronal slices were dissected from the regions of interest. Tissue blocks through superficial layers of prefrontal cortex were embedded in Lowicryl HM20 resin (Electron Microscopy Sciences, Fort Washington, PA) by freeze substitution and low-temperature embedding of the specimens using methods previously described[341–343]. Briefly, slices were cryoprotected by immersion in 4% D-glucose, followed with increasing concentrations of glycerol (from 10% to 30% PB). Sections were plunged rapidly into liquid propane cooled by liquid nitrogen (−190°C) in a Universal Cryofixation System KF80 (Reichert-Jung, Vienna, Austria). The samples were immersed in 0.5% uranyl acetate dissolved in anhydrous methanol (−90°C, 24 h) in a cryosubstitution AFS unit (Leica, Vienna, Austria). The temperature was raised from −90°C to −45°C in steps of 4°C/h. After washing with anhydrous methanol, the samples were infiltrated with Lowicryl HM20 resin at −45°C. Polymerization with ultraviolet light (360 nm) was performed for 48 h at −45°C, followed by 24 h at 0°C. Ultrathin sections (80 nm) were cut using a diamond knife on a Leica UC7 ultramicrotome, and mounted on 300 mesh nickel grids (EMS) coated using a Coat-Quick adhesive pen (EMS). Grids with sections were incubated in 0.1% sodium borohydride and 50 mM glycine for 6 minutes at room temperature, washed and incubated for 10 min in Tris-buffered saline with 0.1% Triton X-100 (TBST) containing 2% albumin. For immunolabeling, sections were incubated overnight in primary anti-mGluR2 antibody (Abcam, mouse monoclonal antibody catalog no. 15672, 10 µg/ml) in the same diluent as above, washed with TBST, and incubated with secondary anti-goat 10 nm gold-tagged antibody (EMS; 1:20) in TBST (2% albumin and polyethyleneglycol 20,000; 5 mg/ml) for two hours, washed and counter-stained with 1%

uranyl acetate (aq.). The specificity of the primary antibody against mGluR2 was previously confirmed in experiments with knockout mice[252]. Grids were viewed on a Hitachi 7000 transmission electron microscope and imaged at a final captured image magnification of 130K. Imaging concentrated on deep layer 2-3 of the prefrontal cortex. Excitatory (asymmetric) glutamatergic synapses were identified by the presence of a thickened postsynaptic density, synaptic cleft, and clusters of round presynaptic vesicles[344]. A synapse was scored as immunolabel-positive if it contained at least 3 gold particles in the synaptic compartments described above, and 25-35 labeled synapses were imaged per animal/group. Overall, ~90% of labeled synapses showed gold particles associated within the postsynaptic element, though a small population of synapses contained gold particles limited to its presynaptic compartment. Gold particle distribution with respect to plasmalemma was scored for each postsynaptic site as membrane only, intracellular only, or both. Membrane labelling was defined by gold particles falling within 25 n of the plasmalemma (a distance defined by the approximate size of the primary and secondary antibodies).

Data acquisition and statistical analysis

Statistical analysis was performed with a GraphPad Prism software version 8. Immunocytochemical assays were acquired using confocal fluorescence microscopy at identical settings for each of the experimental conditions. For colocalization assays, raw 16-bit image files (.czi) were imported into the Carl Zeiss ZEN software (Black version) and/or Fiji version 2.0.0 with Coloc 2 plugin. To assess colocalization, Pearson's and/or Manders' coefficients were calculated because these colocalization coefficients are based on pixel-intensity-correlation measurement and do not include object-recognition approaches. Pearson's coefficient, which ranges from +1 (total positive linear correlation) to -1 (total negative correlation; 0 defines absence of linear correlation) is sensitive to both signal cooccurrence and the more rigorous condition of signal correlation (pixel-for-pixel proportionality in the signal levels of the two channels). However, unlike Pearson's correlation coefficient, Manders' fractional overlap coefficients (M1 and M2), which

measure the fraction of a probe in a probe-tagged compartment and range from 0 (no overlap) to 1 (perfect overlap), strictly measures co-occurrence independent of signal proportionality[345,346]. Colocalization of two fluorescently labelled 7TMR constructs (5-HT_{2A}R-eCFP and mGluR2-eYFP) was assessed both by Manders' and Pearson's coefficients, whereas colocalization of a fluorescently labelled 7TMR construct with a marker of endosomal vesicles (Rab5) was assessed by Manders' coefficient. Both Manders' and Pearson's coefficients within the region of interest were calculated after setting single color thresholds by either colocalizing single probe channels or manually defining a threshold mask upon background subtraction in all channels using Rolling Ball Radius of the largest object in the image (~ 20 – 30 µm). Colocalization was scored in at least 25 cells per experimental condition in three independent assays where the experimenter was blinded to the experimental conditions. For Manders' and Pearson's coefficients, cell regions of interest were demarcated according to the eYFP signal located at the plasma membrane as a potential cell surface marker. For FRET signal, pixels of interest were demarcated based on their intracellular colocalization of eCFP and eYFP signal. For PLA signal, cell regions of interest were demarcated according to eYFP signal within previously defined eCFP-positive cells. For intracellular eYFP signal, cell regions of interest were randomly demarcated based on eCFP signal within intracellular vesicles. Signal intensity for intracellular eYFP was assessed with the Carl Zeiss ZEN software (Black version). The laser intensity was kept constant among all experimental conditions. Straight-line selections were drawn from the plasma membrane to the nucleus or across the cytoplasm, and pixel intensities across the line were measured using plot profile in Fiji. Pixels with maximum and minimum intensities were normalized to 100 and 0, respectively. The statistical significance of experiments involving three or more groups and two or more treatments was assessed by two-way ANOVA followed by Bonferroni's post hoc test. Statistical analysis of experiments involving three or more groups was assessed by one-way ANOVA followed by Bonferroni's post hoc test. Statistical analysis involving two groups was assessed by Student's *t*-test. For FRET analysis, statistical analysis was assessed by Mann-Whitney U test or one-way

non-parametric ANOVA (Kruskal-Wallis) with Dunn's post hoc test because FRET datasets show a Cauchy distribution with heavier tails. Normality and homoscedasticity assumptions were checked prior to any calculation. Radioligand binding saturation curves were analyzed using a nonlinear curve fitting approach. An extra-sum-of-squares (*F* test) was used to determine statistical significance for simultaneous analysis of binding saturation curves and [^{35}S]GTPγS binding assays. The level of significance was set at $P = 0.05$. Values included in the figure legends represent mean ± SEM, except for FRET assays where figure legends represent median with 95% confidence interval.

Results

I. Cellular distribution of mGluR2 and 5-HT$_{2A}$R alone and together in HEK293 cells

1. 5-HT$_{2A}$R distribution pattern in HEK293 cells

To first determine and compare expression patterns of human mGlu2 and 5-HT$_{2A}$ receptors in a heterologous cellular system and to validate previous findings showing an elevated intracellular localization of the 5-HT$_{2A}$R, we introduced the mCitrine sequence at the C-terminus to generate 5-HT$_{2A}$R-mCitrine. As shown before[251,347], HEK293 cells transfected with the 5-HT$_{2A}$R-mCitrine exhibit a fluorescent signal mostly localized in intracellular vesicles (Fig. 1A). To rule out a direct effect of the C-terminally tagged mCitrine on receptor trafficking, we used a second method where the epitope c-Myc was tagged to the N-terminus of the 5-HT$_{2A}$R construct. Similar to the distribution pattern observed with 5-HT$_{2A}$R-mCitrine, the c-Myc-5-HT$_{2A}$R construct was primarily located intracellularly (Fig. 1B).

2. Cotransfection of 5-HT$_{2A}$R and mGluR2

mGlu2 receptor exhibits a standard surface receptor distribution where most of the expression is visible at the plasma membrane area (Fig. 1C). However, when 5-HT$_{2A}$R and mGluR2 constructs were co-transfected, mGluR2 pattern of expression was dramatically changed. In contrast to the subcellular localization observed in HEK293 cells transfected with the mGluR2-mCitrine construct alone, coexpression of 5-HT$_{2A}$R-mCherry led to the partial internalization of mGluR2-mCitrine (Figs. 1, D and E), which can also be demonstrated by a high level of colocalization of mGluR2-mCitrine and 5-HT$_{2A}$R-mCherry in intracellular vesicles (Fig. 1F). Additionally, not all the cotransfected cells exhibited the observed relocalization of mGluR2, not in the same proportion. This suggests that the stoichiometry can affect the change responsible for the mGluR2 subcellular distribution.

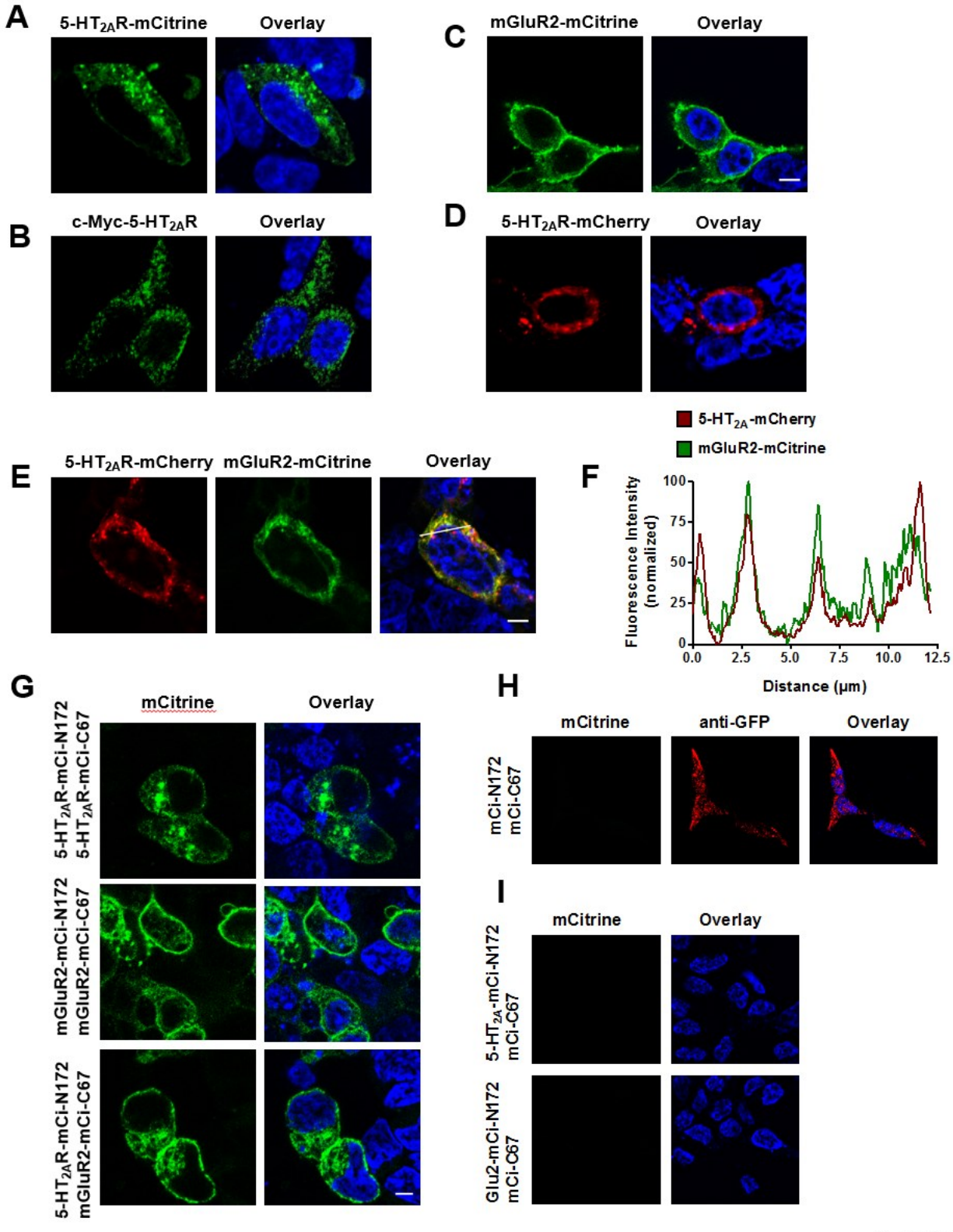
A
5-HT2AR-mCitrine
Overlay
B
c-Myc-5-HT2AR
Overlay
C
mGluR2-mCitrine
Overlay
D
5-HT2AR-mCherry
Overlay
E
5-HT2AR-mCherry
mGluR2-mCitrine
Overlay
F
5-HT2A-mCherry
mGluR2-mCitrine
Fluorescence Intensity (normalized)
100
75
50
25
0
0.0
2.5
5.0
7.5
10.0
12.5
Distance (µm)
G
mCitrine
Overlay
5-HT2AR-mCi-N172
5-HT2AR-mCi-C67
mGluR2-mCi-N172
mGluR2-mCi-C67
5-HT2AR-mCi-N172
mGluR2-mCi-C67
H
mCitrine
anti-GFP
Overlay
mCi-N172
mCi-C67
I
mCitrine
Overlay
5-HT2A-mCi-N172
mCi-C67
Glu2-mCi-N172
mCi-C67

(Fig 1)

Fig. 1. 5-HT_{2A}R affects localization of mGluR2. (**A** and **B**) Representative confocal micrographs of HEK293 cells transfected to express 5-HT_{2A}R-mCitrine (**A**) or c-Myc-5-HT_{2A}R (**B**). Nonpermeabilized cells were imaged to detect mCitrine (**A**), whereas permeabilized cells were stained with anti-c-Myc and secondary antibody, and imaged to detect anti-c-Myc (**B**). (**C** to **E**) HEK293 cells were transfected to express mGluR2-mCitrine alone (**C**), 5-HT_{2A}R-mCherry alone (**D**), or 5-HT_{2A}R-mCherry and mGluR2-mCitrine (**E**). (**F**) Representative line scan. (**G**) BiFC signal in HEK293 cells transfected to coexpress 5-HT_{2A}R-mCi-N172 and 5-HT_{2A}R-mCi-C67, mGluR2-mCi-N172 and mGluR2-mCi-C67, or 5-HT_{2A}R-mCi-N172 and mGluR2-mCi-C67. (**H** and **I**) Representative micrographs of BiFC controls. HEK293 cells co-transfected to express mCi-N172 and mCi-C67 (probes only) and submitted to immunofluorescence assay using antibody against GFP conjugated to a fluorescent secondary antibody (**H**). Absence of mCitrine signal when cells were cotransfected either with both 5-HT_{2A}R-mCi-N172 and mCi-C67 or with both mGluR2-mCi-N172 and mCi-C67 (**I**). Nuclei were stained in blue with Hoechst. Scale bars, 5 μm.

II. Intracellular localization of the 5-HT_{2A}R-mGluR2 heterocomplex

1. Intracellular complementation of 5-HT_{2A} and mGluR2

The 5-HT_{2A}-mGluR2 receptor heteromer study resembles a niche in the field of 7TMRs oligomers. Our laboratory has become an expert in the study of the structure and function of this heterocomplex. We thus expected to locate it at the cell boundaries, using several RRI assays.

To track the intracellular physical interaction between 5-HT_{2A}R and mGluR2 in HEK293 cells, we used bimolecular fluorescence complementation (BiFC) as a biophysical technique that allows visualization of protein complexes in transfected mammalian cells[348,349]. BiFC enables generation of a single fluorescent signal when each of the constructs fused to a fragment of the mCitrine fluorescent protein interact. The recovery of the protein quaternary structure attests the interaction between the two proteins. BiFC signal was detected in cells cotransfected with 5-HT_{2A}R fused to either the N-terminal 172 amino acid fragment or the C-terminal 67 amino acid fragment of mCitrine (mCi-N172 and mCi-C67, respectively) (Fig. 1G), which further corroborates the capability of 5-HT_{2A}R to form a family A GPCR homodimer[165]. Additionally, BiFC signal in cells coexpressing 5-HT_{2A}R-mCi-N172 and 5-HT_{2A}R-mCi-C67 was observed intracellularly (Fig. 1G), whereas BiFC signal in cells coexpressing mGluR2-mCi-N172 and mGluR2-mCi-C67 was mostly detected at the plasma membrane (Fig. 1G). Importantly, this pattern of BiFC signal was redistributed in cells coexpressing 5-HT_{2A}R-mCi-N172 and mGluR2-mCi-C67 (Fig. 1G), which suggests that physical interaction between 5-HT_{2A}R and mGluR2 can be detected both close to the cell surface as well as intracellularly. Internal controls to validate BiFC signal specificity included cotransfection of themCi-N172 and mCi-C67 constructs (Fig. 1H), as well as mCi-C67 and 5-HT_{2A}R-mCi-N172, or mCi-C67 and mGluR2-mCi-N172 (Fig. 1I).

III. GPCR heteromerization is necessary for the 5-HT_{2A}R-mediated mGluR2 internal relocalization

The use of stable cellular systems as a reductionist approach to observe trafficking events after receptor activation was chosen as a model for this study. This choice has several advantages, including overcoming expression variability and transfection efficiency issues – it is easy to routinely grow, treat and analyze, and to manage the expression levels. To that purpose, we devised an experimental Flp-In T-REx HEK293 cellular system that enables small molecule doxycycline (DOX)-inducible expression of the inserted human *HTR2A* gene construct along with the stable expression of mGlu2, mGlu3 or mGlu2ΔTM4 (see below) receptors. The Flp-In T-REx system allows expression of the inserted construct into the cell genome via Flp-In recombinase-mediated DNA recombination at the Flp recombination target (FRT) site, which can be controlled by the incorporation DOX to the cell culture medium. This model of stable cell lines has already been employed to great advantage in the study of receptor pharmacology, trafficking and oligomerization[45,335]. Here we used Flp-In T-REx HEK293 cells to further explore the effect of 5-HT_{2A}R on subcellular localization of mGluR2.

The c-Myc-5-HT_{2A}R-eCFP construct was inserted into the appropriate locus of the Flp-In expression system, and pools of positive Flp-In T-REx HEK293 cells were selected. No visible expression of the eCFP-tagged construct was observed in the absence of DOX (Fig. 2A). However, presence of DOX resulted in expression of the integrated construct as monitored by fluorescence corresponding to eCFP (Fig. 2B) and immunoblotting with anti-c-Myc antibody (Fig. 2C), which also serves as a concentration indicator of receptor expression. Induction of expression of c-Myc-5-HT_{2A}R-eCFP was concentration- and time-dependent, reaching maximal levels within 30 – 40 h upon 1 μg/mL [DOX] administration (Figs. 2, B and C), and lasted a couple of days, approximately. Additionally, as shown above in HEK293 cells transiently transfected with the 5-HT_{2A}R construct, visualization of living Flp-In T-REx HEK293 cells corroborated that the bulk of c-

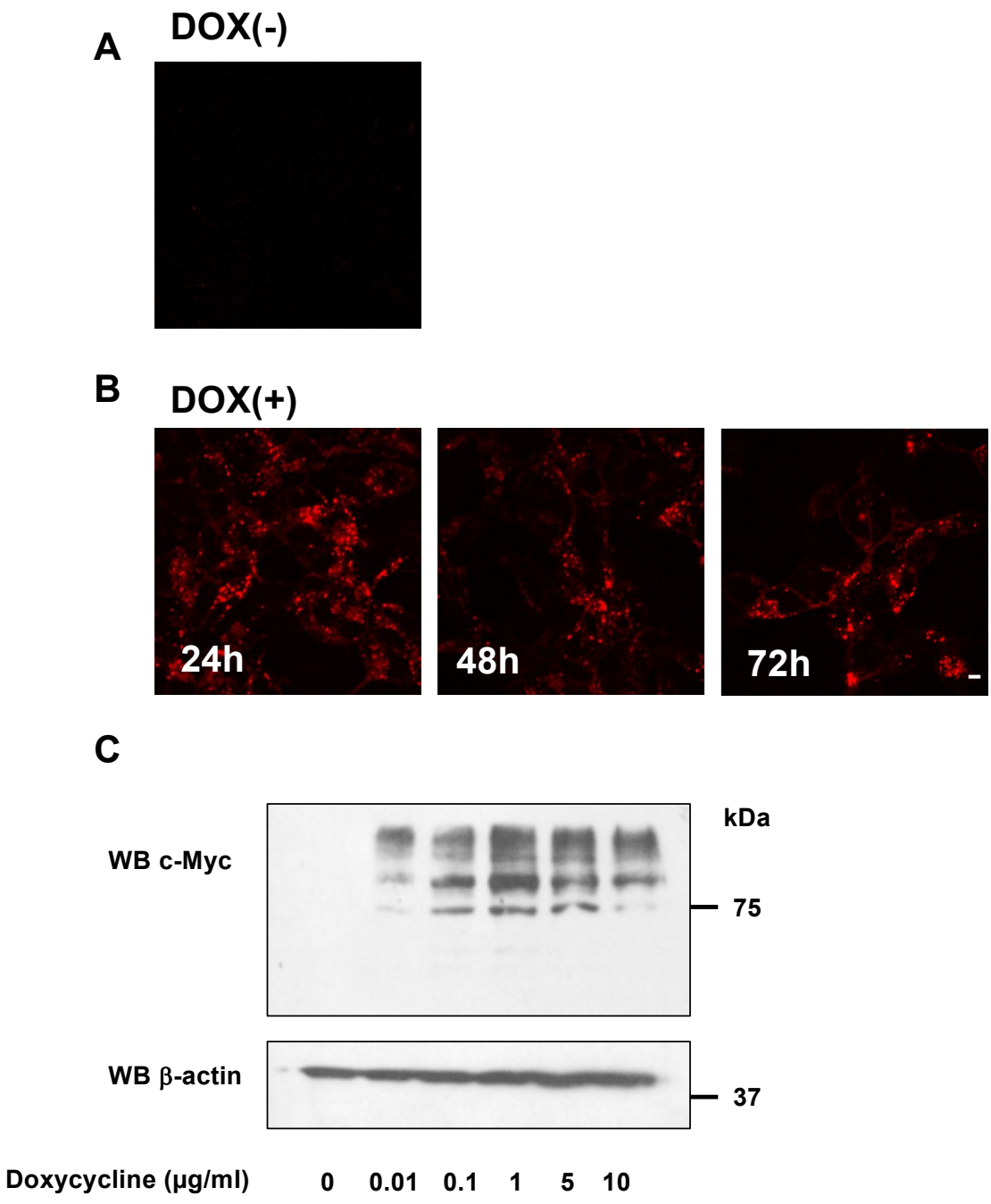
A
DOX(-)
B
DOX(+)
24h
48h
72h
C
WB c-Myc
kDa
75
WB β-actin
37
Doxycycline (μg/ml)
0
0.01
0.1
1
5
10

(Fig. 2)

Fig. 2. Confocal micrographs of Flp-In T-REx HEK293 cells expressing the 5-HT_{2A} receptor. (**A** and **B**) Representative live-cell confocal micrographs of Flp-In T-REx HEK293 cells harboring c-Myc-5-HT_{2A}R-eCFP at the inducible locus. Cells were left untreated [DOX(-)] (**A**) or treated for 24h, 48h, or 72 h with doxycycline [DOX(+)] (**B**). (**C**) Membranes from Flp-In T-REx HEK293 cells harboring c-Myc-5-HT_{2A}R-eCFP at the inducible locus left untreated or treated with doxycycline at the indicated concentration were immunoblotted with anti-c-Myc (upper panel) or anti-β-actin. Scale bar, 5 μm.

Myc-5-HT_{2A}R-eCFP was located intracellularly (Fig. 2B). Those experiments generated a series of parental clones expressing inducible 5-HT_{2A}R.

In order to demonstrate the involvement of 7TMR heteromerization in the relocalization of mGluR2 following its coexpression with 5-HT_{2A}R, we first based our negative controls with mGluR3 as well as with an mGluR2/mGluR3 chimeric construct that does not form a receptor heteromer with 5-HT_{2A}R. We selected the mGluR2/mGluR3 chimeric construct mGluR2ΔTM4 because, according to previous findings from substitution of residues Ala-677$^{4.40}$, Ala-681$^{4.44}$ and Ala-685$^{4.48}$ in mGluR2 for Ser-686$^{4.40}$, Phe-690$^{4.44}$ and Gly-694$^{4.48}$ in mGluR3 decreases signal that indicates heteromeric assembly. This was demonstrated based on the use of several independent experimental approaches, including flow cytometry-based fluorescence energy resonance transfer (FCM-based FRET), FRET microscopy, and coimmunoprecipitation in HEK293 cells[251,252].

The parental c-Myc-5-HT_{2A}R-eCFP expressing clones were then transfected with either mGluR2-eYFP, mGluR3-eYFP or mGluR2ΔTM4-eYFP, and individual clones constitutively eliciting eYFP signal were selected. Visual inspection of eYFP fluorescence confirmed that, in the absence of DOX, mGluR2-eYFP was localized at the cell boundaries (Fig. 3A). Remarkably, DOX-induced expression of 5-HT_{2A}R-eCFP dramatically affected the subcellular distribution of mGluR2-eYFP, now partially internalized in vesicles (Fig. 3A). This effect of 5-HT_{2A}R-eCFP expression was not observed in cells stably expressing either mGluR3-eYFP (Fig. 3B) or mGluR2ΔTM4-eYFP (Figs. 3C). Both mGluR3-eYFP and mGluR2ΔTM4-eYFP showed a higher degree of intracellular localization as compared to mGluR2-eYFP, yet both quantitative evaluation (Fig. 3D) and representative line scans (Figs. 3, E to G) demonstrated significantly less subcellular proximity between 5-HT_{2A}R-eCFP and mGluR3-eYFP or mGluR2ΔTM4-eYFP, as compared to the high degree of overlap between 5-HT_{2A}R-eCFP and mGluR2-eYFP. The subcellular distribution of the class A $G\alpha_{i/o}$ protein-coupled μ-opioid receptor, which is a prototypical plasma membrane-

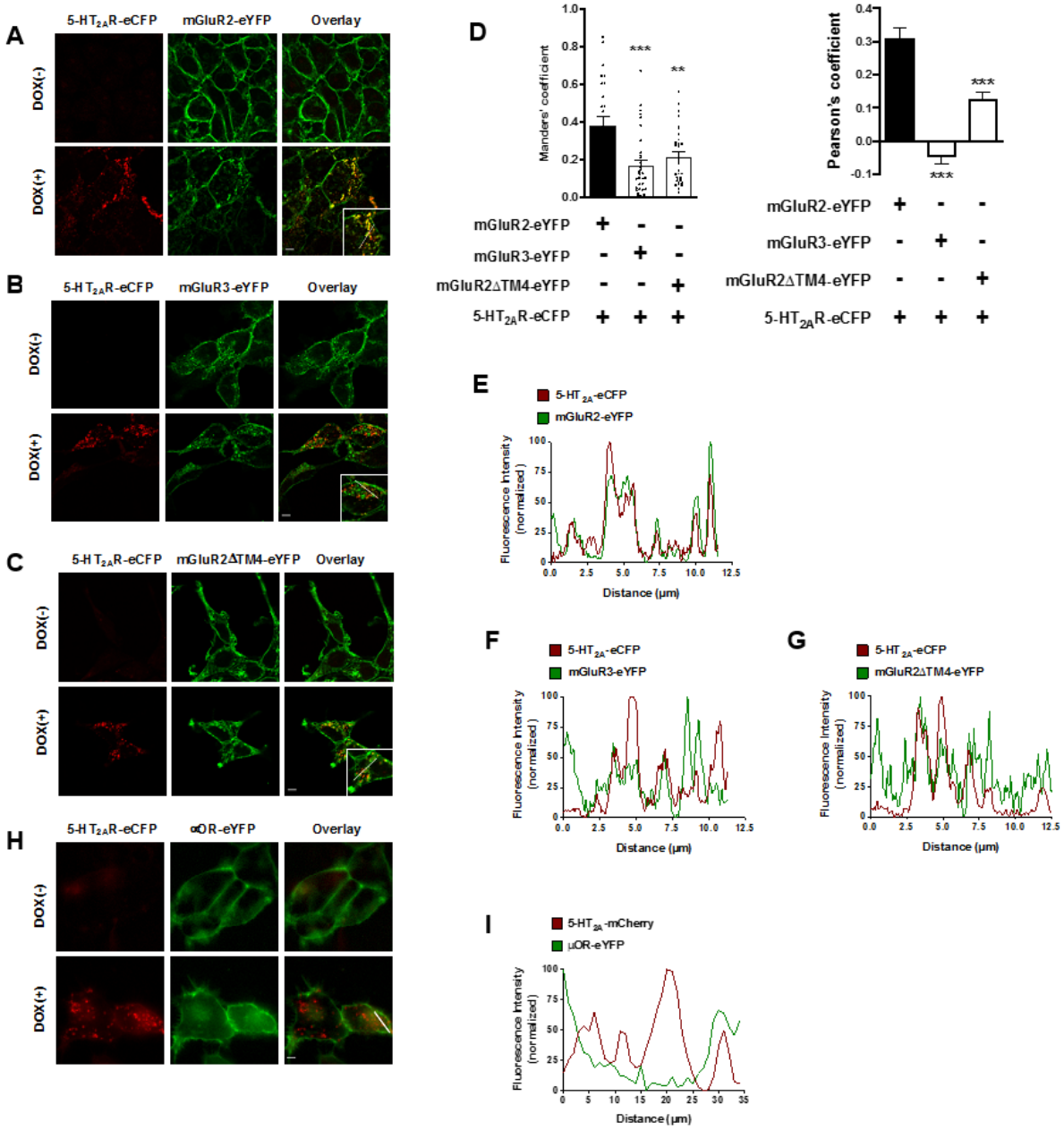
A
5-HT2AR-eCFP
mGluR2-eYFP
Overlay
DOX(-)
DOX(+)
B
5-HT2AR-eCFP
mGluR3-eYFP
Overlay
DOX(-)
DOX(+)
C
5-HT2AR-eCFP
mGluR2ΔTM4-eYFP
Overlay
DOX(-)
DOX(+)
H
5-HT2AR-eCFP
αOR-eYFP
Overlay
DOX(-)
DOX(+)
D
Manders' coefficient
1.0
0.8
0.6
0.4
0.2
0.0
***
**
mGluR2-eYFP + - -
mGluR3-eYFP - + -
mGluR2ΔTM4-eYFP - - +
5-HT2AR-eCFP + + +
Pearson's coefficient
0.4
0.3
0.2
0.1
0.0
-0.1
***
***
mGluR2-eYFP + - -
mGluR3-eYFP - + -
mGluR2ΔTM4-eYFP - - +
5-HT2AR-eCFP + + +
E
5-HT2A-eCFP
mGluR2-eYFP
Fluorescence Intensity (normalized)
100
75
50
25
0
0.0
2.5
5.0
7.5
10.0
12.5
Distance (μm)
F
5-HT2A-eCFP
mGluR3-eYFP
Fluorescence Intensity (normalized)
100
75
50
25
0
0.0
2.5
5.0
7.5
10.0
12.5
Distance (μm)
G
5-HT2A-eCFP
mGluR2ΔTM4-eYFP
Fluorescence Intensity (normalized)
100
75
50
25
0
0.0
2.5
5.0
7.5
10.0
12.5
Distance (μm)
I
5-HT2A-mCherry
μOR-eYFP
Fluorescence Intensity (normalized)
100
75
50
25
0
0
5
10
15
20
25
30
35
Distance (μm)

(Fig 3)

Fig. 3. Effect of 5-HT_{2A}R on localization of mGluR2 requires heteromerization. (**A** to **I**) Flp-In T-REx HEK293 cells stably expressing mGluR2-eYFP (**A**, **D** and **E**), mGluR3-eYFP (**B**, **D** and **F**), mGluR2ΔTM4-eYFP (**C**, **D** and **G**), or μOR-eYFP (**H** and **I**) and harboring 5-HT_{2A}R-eCFP at the inducible locus were untreated [DOX(-)] or treated with doxycycline [DOX(+)]. Representative confocal micrographs (**A** to **C** and **H**) and corresponding line scans (**E** to **G** and **I**). (**D**) Manders' and Pearson's colocalization coefficients analysis of eYFP- and eCFP-tagged constructs (n = 25 – 33 cell regions of interest in three independent experiments). Data are mean ± SEM (**D**). Statistical analysis was performed using the one-way ANOVA (**D**) with Bonferroni's *post hoc* test. ***P* < 0.01, ****P* < 0.001. Scale bars, 5 μm.

localized 7TMR, was not evidently affected by DOX-induced expression of 5-HT_{2A}R-eCFP (Figs. 3, H and I), further comforting the specificity of the relation between 5-HT_{2A}R and mGluR2.

IV. Characterization of the double stable cells lines

Radioligand binding assays with the 5-HT_{2A}R antagonist [^{3}H]ketanserin confirmed that addition of DOX resulted in 5-HT_{2A}R-eCFP expression in cells stably expressing mGluR2-eYFP, mGluR3-eYFP or mGluR2ΔTM4-eYFP (Figs. 4, A to C, and Table 1). Using the mGluR2/3 antagonist [^{3}H]LY341495, we also observed that DOX-induced expression of 5-HT_{2A}R-eCFP led to a statistically significant increase in the density of mGluR2-eYFP, an effect that was not observed in cells stably expressing mGluR3-eYFP or mGluR2ΔTM4-eYFP (Figs. 4, D to F, and Table 1). This effect of DOX-induced 5-HT_{2A}R-eCFP expression on augmentation of mGluR2-eYFP density was corroborated by fluorescence flow cytometry assays (Figs. 4, G and H).

We next assayed the effect of the mGluR2/3 agonist LY379268 on stimulation of [^{35}S]GTPγS binding as a functional readout of receptor-$G\alpha_{i/o}$ protein coupling. Interestingly, DOX-induced expression of 5-HT_{2A}R-eCFP reduced the functional properties of LY379268 augmenting [^{35}S]GTPγS binding in cells stably expressing mGluR2-eYFP (Fig. 4I), an allosteric event that was absent in cells stably expressing mGluR2ΔTM4-eYFP (Fig. 4J). Although activation of mGluR2 elicited a robust G protein signal after ligand binding, we were unable to test mGluR3 function with the [^{35}S]GTPγS assay on clones stably expressing mGluR3. In order to overcome this issue, $G\alpha_{i/o}$-coupled receptors mGluR (*i.e.*, mGluR2, mGluR3 and mGluR2ΔTM4) ability to trigger the phospholipase C pathway following activation of the G Protein, we transfect DOX(-) cells with the chimeric G protein $G\alpha_{qi9}$ and analyzed the fold increase in $[Ca^{2+}]_i$ (Fig. 4K) following application of 0.1 μM of the mGluR2/3 agonist LY379268. Together with the effects of 5-HT_{2A}R on mGluR2 subcellular redistribution (see above), these findings suggest that, although DOX-induced expression of 5-HT_{2A}R results in augmentation of total mGluR2 density, its functional properties for agonist-induced $G\alpha_{i/o}$ protein recruitment are diminished.

Activation of 5-HT_{2A}R stimulates the β-isoforms of phospholipase C (PLC-β) that catalyzes the hydrolysis of phosphatidylinositol bisphosphate (PIP_2), leading to the production of two second messengers, namely inositol triphospate (IP3) and diacylglycerol (DAG). The $G\alpha_q$-mediated signal is then transmitted through to those molecules: IP_3 binds to its ER localized receptor and open the channel allowing mobilization of the internal store and efflux of calcium in the cytosol. DAG binds to the plasma membrane to recruit the protein kinase C that is activated by Ca^{2+} and mediates several other pathways. Our previous results suggested that stimulation of cells coexpressing mGluR2 and 5-HT_{2A}R with the mGluR2/3 selective agonist LY379268 leads to a $G\alpha_{q/11}$ protein-dependent increase in the concentration of $[Ca^{2+}]_i$[251,253,254], a transactivation mechanism event that has been validated by some[170,350] but not all studies[351].

Besides physically interacting, 5-HT_{2A}R and mGluR2 have been shown to crosstalk by modulating their respective G proteins signaling. The endogenous ligands serotonin and glutamate tend to increase the $G\alpha_i$ signaling and reduce the $G\alpha_q$ signaling within the heterocomplex. Intracellular calcium mobilization mediated by inositol 1,4,5-triphosphate from endoplasmic reticulum compartments can be monitored by calcium-sensitive fluorescent dyes. The highly sensitive ratiometric calcium dye Fura-2 was used to assess calcium elevation in our clones expressing mGluR2 or mGluR2ΔTM4-eYFP along with the induction of 5-HT_{2A}R expression. Application of 10 μM of LY379268 was sufficient to increase the intracellular calcium concentration in cells expressing mGluR2, with a much lesser signal for the cells expressing the mutant receptor mGlu2ΔTM4-eYFP. This effect seemed dose-dependent as with 100 μM an even greater signal was observed (Figs. 4, L and M). As expected, neither serotonin (5-hydroxytryptamine, 5-HT) nor LY379268 had such an effect on Ca^{2+} release in DOX(-) Flp-In T-REx HEK293 cells, whereas 5-HT stimulated an increase in intracellular Ca^{2+} release in DOX(+) cells (Fig. 4N). An additional internal control included absence of effect of 5-HT on Ca^{2+} release in untransfected HEK293 cells (Fig. 4N). This findings indicate that we were able to reproduce the previous observed phenotype

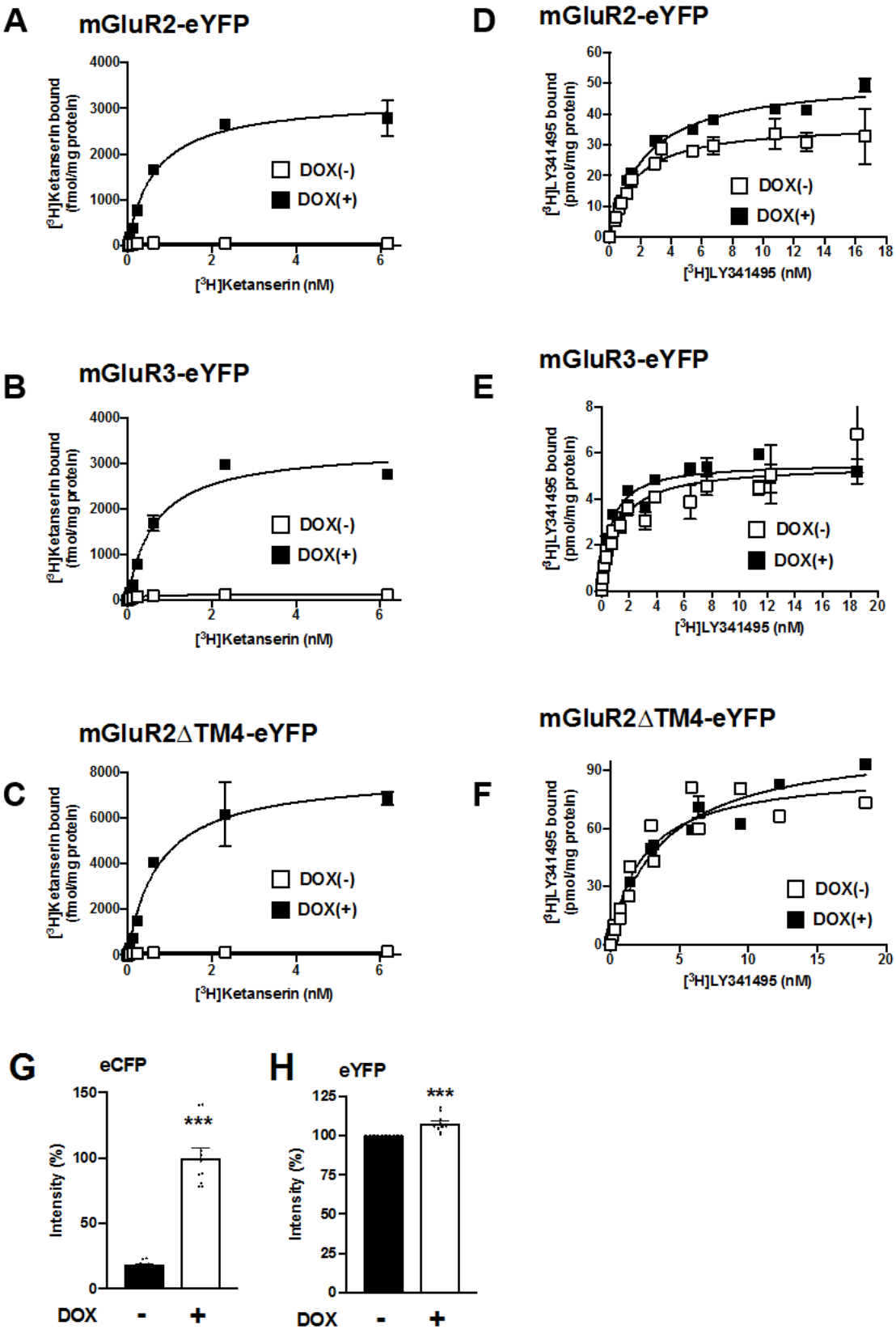
A
mGluR2-eYFP
[3H]Ketanserin bound (fmol/mg protein)
[3H]Ketanserin (nM)
DOX(-)
DOX(+)
B
mGluR3-eYFP
[3H]Ketanserin bound (fmol/mg protein)
[3H]Ketanserin (nM)
DOX(-)
DOX(+)
C
mGluR2ΔTM4-eYFP
[3H]Ketanserin bound (fmol/mg protein)
[3H]Ketanserin (nM)
DOX(-)
DOX(+)
D
mGluR2-eYFP
[3H]LY341495 bound (pmol/mg protein)
[3H]LY341495 (nM)
DOX(-)
DOX(+)
E
mGluR3-eYFP
[3H]LY341495 bound (pmol/mg protein)
[3H]LY341495 (nM)
DOX(-)
DOX(+)
F
mGluR2ΔTM4-eYFP
[3H]LY341495 bound (pmol/mg protein)
[3H]LY341495 (nM)
DOX(-)
DOX(+)
G
eCFP
Intensity (%)
***
DOX
-
+
H
eYFP
Intensity (%)
***
DOX
-
+

(Fig. 4)

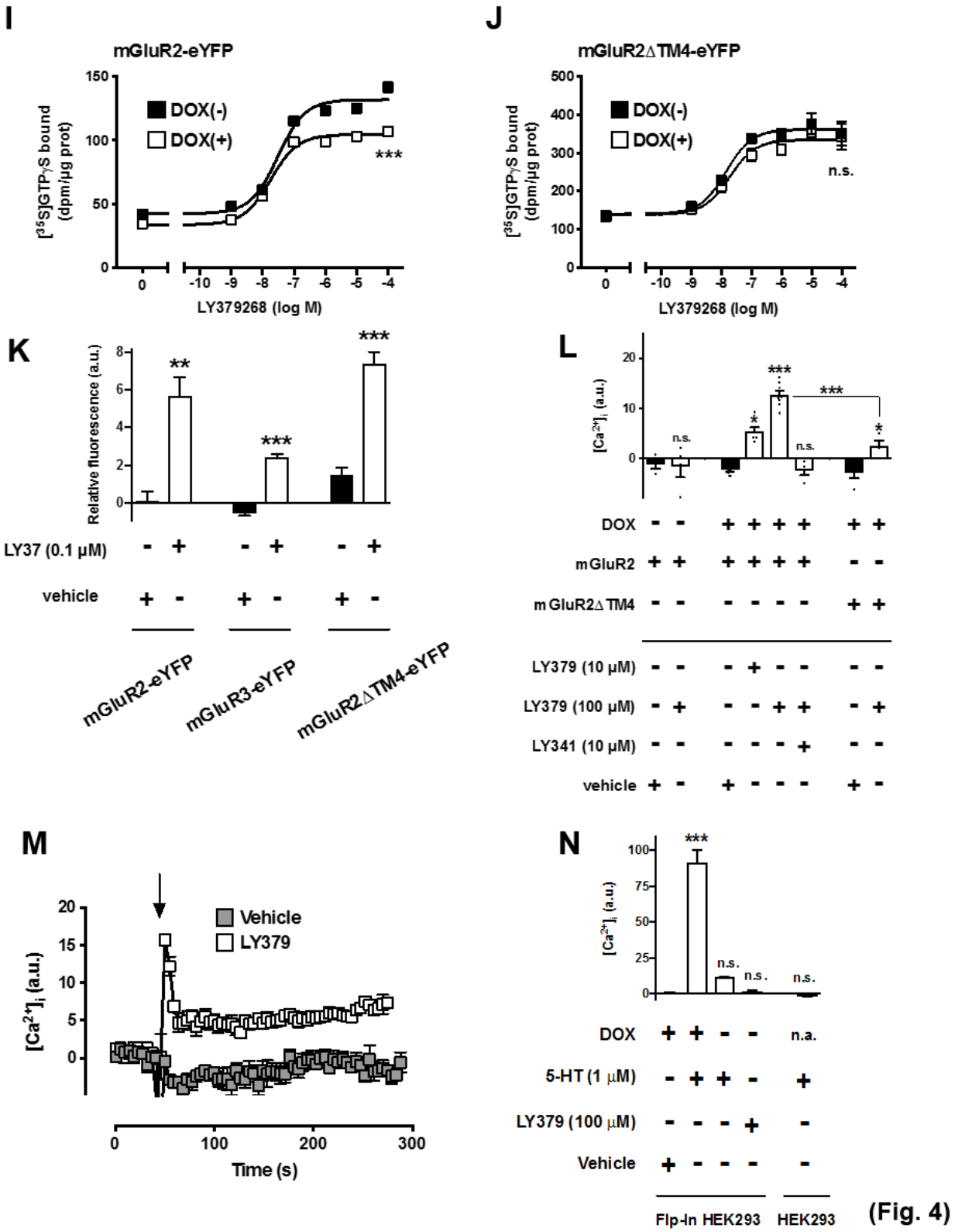
I
mGluR2-eYFP
DOX(-)
DOX(+)
[35S]GTPγS bound (dpm/μg prot)
LY379268 (log M)
***
J
mGluR2ΔTM4-eYFP
n.s.
K
Relative fluorescence (a.u.)
LY37 (0.1 μM)
vehicle
mGluR2-eYFP
mGluR3-eYFP
mGluR2ΔTM4-eYFP
L
[Ca2+]i (a.u.)
DOX
mGluR2
mGluR2ΔTM4
LY379 (10 μM)
LY379 (100 μM)
LY341 (10 μM)
vehicle
M
Vehicle
LY379
Time (s)
N
DOX
5-HT (1 μM)
LY379 (100 μM)
Vehicle
n.a.
Flp-In HEK293
HEK293

(Fig. 4)

Fig. 4. Characterization of the double stable cells lines. (**A** to **C**) Density of 5-HT_{2A}R as measured by [^{3}H]ketanserin binding in cell membrane preparations of Flp-In T-REx HEK293 cells stably expressing mGluR2-eYFP (**A**), mGluR3-eYFP (**B**), or mGluR2ΔTM4-eYFP (**C**) and harboring 5-HT_{2A}R-eCFP at the inducible locus. Cells were left untreated [DOX(-)] or treated with doxycycline [DOX(+)] (representative results of three independent experiments performed in duplicate; see also Table 1). (**D** to **F**) Density of mGluR2/3 shown as [^{3}H]LY341495 binding in cell membrane preparations of Flp-In T-REx HEK293 cells stably expressing mGluR2-eYFP (**D**), mGluR3-eYFP (**E**), or mGluR2ΔTM4-eYFP (**F**) and harboring 5-HT_{2A}R-eCFP at the inducible locus. Cells were untreated [DOX(-)] or treated with doxycycline [DOX(+)] (representative results of three independent experiments performed in duplicate; see also Table 1). (**G** and **H**) Cells were untreated [DOX(-)] or treated with doxycycline [DOX(+)], and densities of 5-HT_{2A}R-eCFP and mGluR2-eYFP with eCFP (**G**) and eYFP (**H**), respectively, were assessed by FACS assays (n = 10 independent experiments with 8459 – 9710 cells per experimental condition). (**I** and **J**) Effect of the mGluR2/3 agonist LY379268 on [^{35}S]GTPγS binding in membrane preparations of Flp-In T-REx HEK293 cells stably expressing mGluR2-eYFP (**I**) or mGluR2ΔTM4-eYFP (**J**) and harboring 5-HT_{2A}R-eCFP at the inducible locus. (**K**) $[Ca^{2+}]_i$ mobilization of mGluRs clones by activation of the chimeric Gα protein $Gα_{qi9}$. Flp-In T-REx HEK293 cells stably expressing mGluR2-eYFP, mGluR3-eYFP or mGluR2ΔTM4-eYFP and harboring 5-HT_{2A}R-eCFP at the inducible locus were untreated [DOX(-)], loaded with Fura-2 and monitored for intracellular calcium concentration after administration of LY379269 (0.1 μM), or vehicle. To allow efficient coupling of $Gα_{i/o}$-coupled receptors (mGluR2, mGluR3 and mGluR2ΔTM4) to the PLC pathway, cells were also transfected with the chimeric Gα protein $Gα_{qi9}$. Analysis of the fold increase in $[Ca^{2+}]_i$ (n = 4 independent experiments, representative results of three independent experiments performed in duplicate). (**L** and **M**) Flp-In T-REx HEK293 cells stably expressing mGluR2-eYFP or mGluR2ΔTM4-eYFP and harboring 5-HT_{2A}R-eCFP at the inducible locus were untreated [DOX(-)] or treated with doxycycline [DOX(+)], loaded with Fura-2 and monitored for intracellular calcium concentration after sequential administration of LY341495 and/or LY379268, or vehicle. Representative time course of Ca^{2+} release. The arrowhead indicates the time when drugs were added (**M**). Analysis of the fold increase in intracellular calcium concentration (**L**; n = 4 – 8 independent experiments). (**N**) $[Ca^{2+}]_i$ mobilization of mGluRs clones expressing 5-HT_{2A}R only, or untransfected HEK293 cells. Flp-In T-REx HEK293 cells stably expressing mGluR2-eYFP and harboring 5-HT_{2A}R-eCFP at the inducible locus or untransfected HEK293 cells were treated with doxycycline (or left untreated), loaded with Fura-2 and monitored for intracellular calcium concentration after administration of 5-HT (1 μM) or LY379268 (100 μM), or vehicle (n = 4 independent experiments). Data are mean ± SEM (**D, I, J, K, L** and **N**). Statistical analysis was performed using the *F* test (**A** to **F**), Student's *t*-test (**G** and **H**) one-way (**D, K** and **N**) or two-way (**M**) ANOVA with Bonferroni's *post hoc* test, or the *F* test (**A** to **F**). **P* < 0.05, ***P* < 0.01, ****P* < 0.001, n.s., not significant.

with our cell system and that the receptors stoichiometry allowing the crosstalk between 5-HT_{2A}R and mGluR2 is conserved[254].

V. mGluR2 and 5-HT_{2A}R interact intracellularly

Besides attesting of the coupling of mGluR2 and 5-HT2AR assessed by the above-mentioned BiFC assay, this experiment also showed that the distribution of the fluorescence produced by the complementation of the two mCitrine fluorescent protein moieties held by each receptor is at the cell borders but more importantly, intracellular (Fig. 1G). To further explore where the interaction between these two receptors is localized, we tested RRI using two different methods: sensorFRET, which enables quantitative measurement of FRET efficiency, and proximity ligation assay (PLA), which permits direct detection of molecular interactions between two proteins without the need of resonance energy transfer assays. Using the sensorFRET approach, we observed a significant decrease of FRET efficiency between eCFP and eYFP in DOX(+) cells stably expressing mGluR2ΔTM4-eYFP as compared to that observed in cells stably expressing mGluR2-eYFP (Figs. 5, A to C and Fig. A1). This confirms the impaired ability of the mGluR2/mGluR3 chimeric construct to physically interact with 5-HT_{2A}R. More importantly, the FRET signal between 5-HT_{2A}R-eCFP and mGluR2-eYFP was located intracellularly in vesicles positive for both eCFP and eYFP fluorescence signal (Fig. 5A). Following DOX-dependent induction of 5-HT_{2A}R-eCFP expression, PLA signal between 5-HT_{2A}R and mGluR2 was observed in the form of punctate staining (Fig. 5D). Quantification of PLA dots was significantly reduced in cells induced to express 5-HT_{2A}R-eCFP along with mGluR2ΔTM4-eYFP (Figs. 5, E and F). As anticipated, no PLA signal was observed in the absence of doxycycline in cells expressing mGluR2-eYFP only (Fig. 5F). Additional internal controls included omission of one of the primary antibodies in the PLA assays (Fig. 5F).

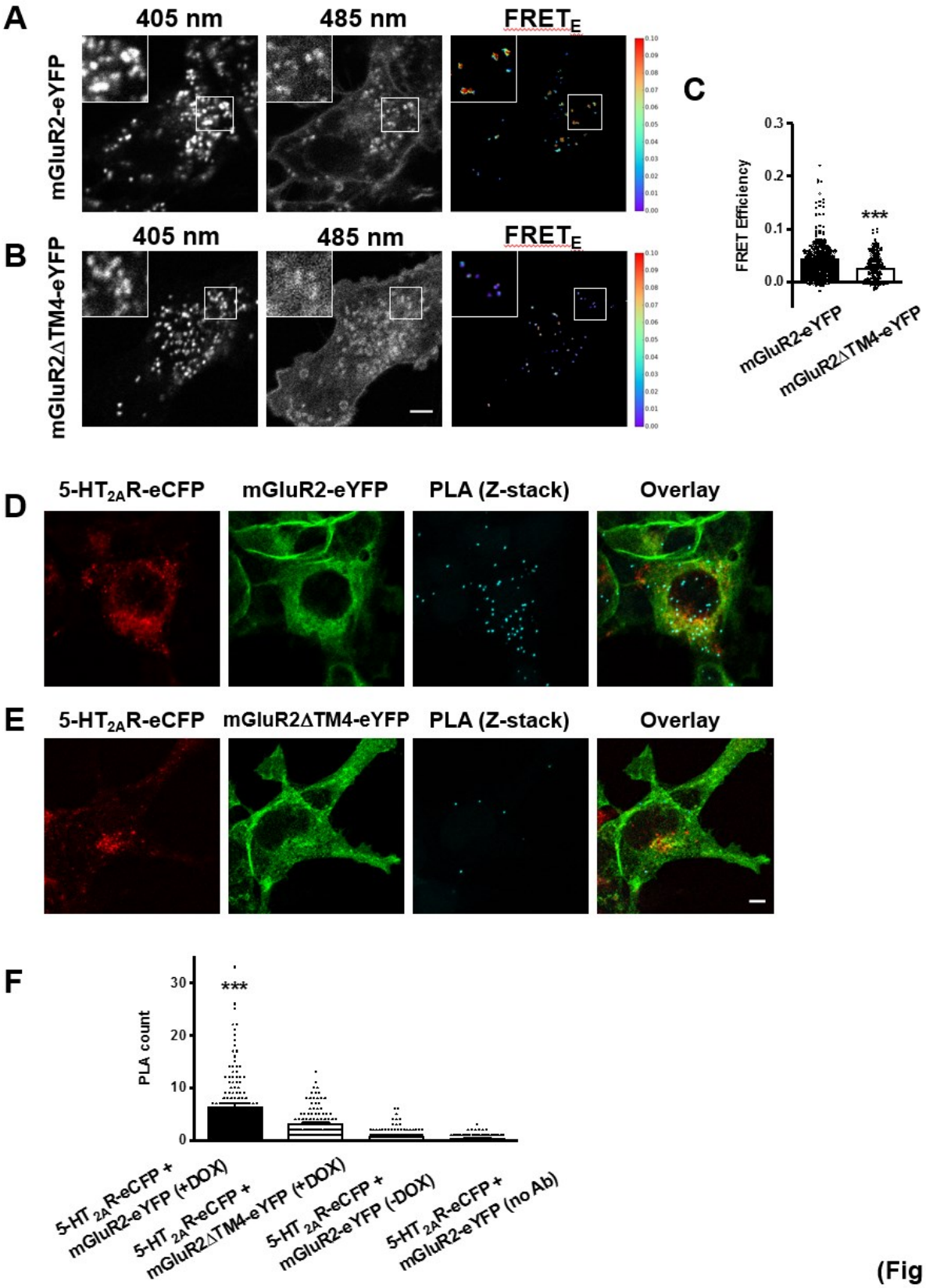
A
405 nm
485 nm
FRET$_E$
mGluR2-eYFP
B
405 nm
485 nm
FRET$_E$
mGluR2ΔTM4-eYFP
C
FRET Efficiency
0.3
0.2
0.1
0.0
***
mGluR2-eYFP
mGluR2ΔTM4-eYFP
D
5-HT$_{2A}$R-eCFP
mGluR2-eYFP
PLA (Z-stack)
Overlay
E
5-HT$_{2A}$R-eCFP
mGluR2ΔTM4-eYFP
PLA (Z-stack)
Overlay
F
PLA count
30
20
10
0
***
5-HT $_{2A}$R-eCFP + mGluR2-eYFP (+DOX)
5-HT $_{2A}$R-eCFP + mGluR2ΔTM4-eYFP (+DOX)
5-HT $_{2A}$R-eCFP + mGluR2-eYFP (-DOX)
5-HT $_{2A}$R-eCFP + mGluR2-eYFP (no Ab)

(Fig 5)

Fig. 5. Intracellular localization of the 5-HT_{2A}R-mGluR2 complex. (**A** to **C**) SensorFRET analysis of Flp-In T-REx HEK293 cells stably expressing mGluR2-eYFP (**A** and **C**) or mGluR2ΔTM4-eYFP (**B** and **C**), harboring 5-HT_{2A}R-eCFP at the inducible locus, and treated with doxycycline. Representative live-cell confocal images at 405 nm and 458 nm excitation frequencies (**A** and **B**), and (**C**) quantification of FRET efficiencies (n = 249 – 364 regions of interest in three independent experiments). (**D** to **F**) Flp-In T-REx HEK293 cells stably expressing mGluR2-eYFP (**D** and **F**) or mGluR2ΔTM4-eYFP (**E** and **F**) and harboring c-Myc-5-HT_{2A}R-eCFP at the inducible locus were treated with doxycycline, permeabilized and stained with anti-rabbit antibody selective for c-Myc and anti-mouse antibody selective for mGluR2, followed by incubation with species-specific PLA probes. Representative confocal micrographs of eCFP- or eYFP-tagged constructs and PLA signal (cyan dots, Z-stack projection) (**D** and **E**). Quantification of PLA dots (**F**). Note that PLA signal was decreased in DOX(-) cells, and when primary antibodies were not added (n = 57 – 94 cell regions of interest demarcated according to eYFP signal within previously defined eCFP-positive cells in three independent experiments). Data are median with 95% confidence interval (**C**) or mean ± SEM (**F**). Statistical analysis was performed using Mann-Whitney U test (**C**) or one-way ANOVA with Bonferroni's *post hoc* test (**F**). ***P < 0.001. Scale bars, 5 µm, inserts edge ~ 14.3 µm.

VI. Expression of 5-HT_{2A}R augments localization of mGluR2 in endosomal compartments

Our data thus far show that, under steady state conditions, colocalization of mGluR2 with markers of endocytic vesicles increased upon coexpression with 5-HT_{2A}R. However, the nature of these intracellular compartments remains unknown. It is classically established that agonist binding and activation of most 7TMRs usually results in the rapid removal of the receptor from the plasma membrane by two complementary mechanisms, desensitization and endocytosis. To evaluate the components of the intracellular trafficking pathway in which 5-HT_{2A}R affects subcellular distribution of mGluR2, we next tested the effect of DOX-induced expression of 5-HT_{2A}R on colocalization of mGluR2 with endosomal markers. Using fixed cell confocal immunofluorescence microscopy, we found that colocalization of mGluR2-eYFP with Rab5, which regulates clathrin-mediated endocytosis from the plasma membrane to early/sorting endosome pools, showed a modest, yet statistically significant, increase in DOX(+) cells as compared to DOX(-) cells (Figs. 6, A to D). Additionally, DOX-induced expression of 5-HT_{2A}R substantially augmented localization of mGluR2-eYFP with Rab7 as a late endosome maker (Figs. 6, E to H).

This localization of mGluR2 in Rab7 endosomes was surprising. Are those receptors directed to degradation, or Rab7 endosomes serve as storage compartments that are deeper or later used after endocytosis? To address that question, colocalization of mGluR2 in Rab7 endosomes was assessed following activation of the 5-HT_{2A} receptor. Application of DOI resulted in the reversal of the previous pattern; mGluR2 population was now greater in Rab5 than it was in Rab7 endosomes (Fig. 6I). This observation suggests that following activation of 5-HT_{2A}R, a Rab transition demobilized the Rab5 pool of mGluR2 to Rab7. It is possible that 5-HT_{2A}R activation leads to the migration of mGluR2 from Rab7 to Rab5 endosomes. This could explain why at basal state, *i.e.* in absence of 5-HT_{2A}R and mGluR2 ligand, the conservation of mGluR2 is maintained in late endosomes.

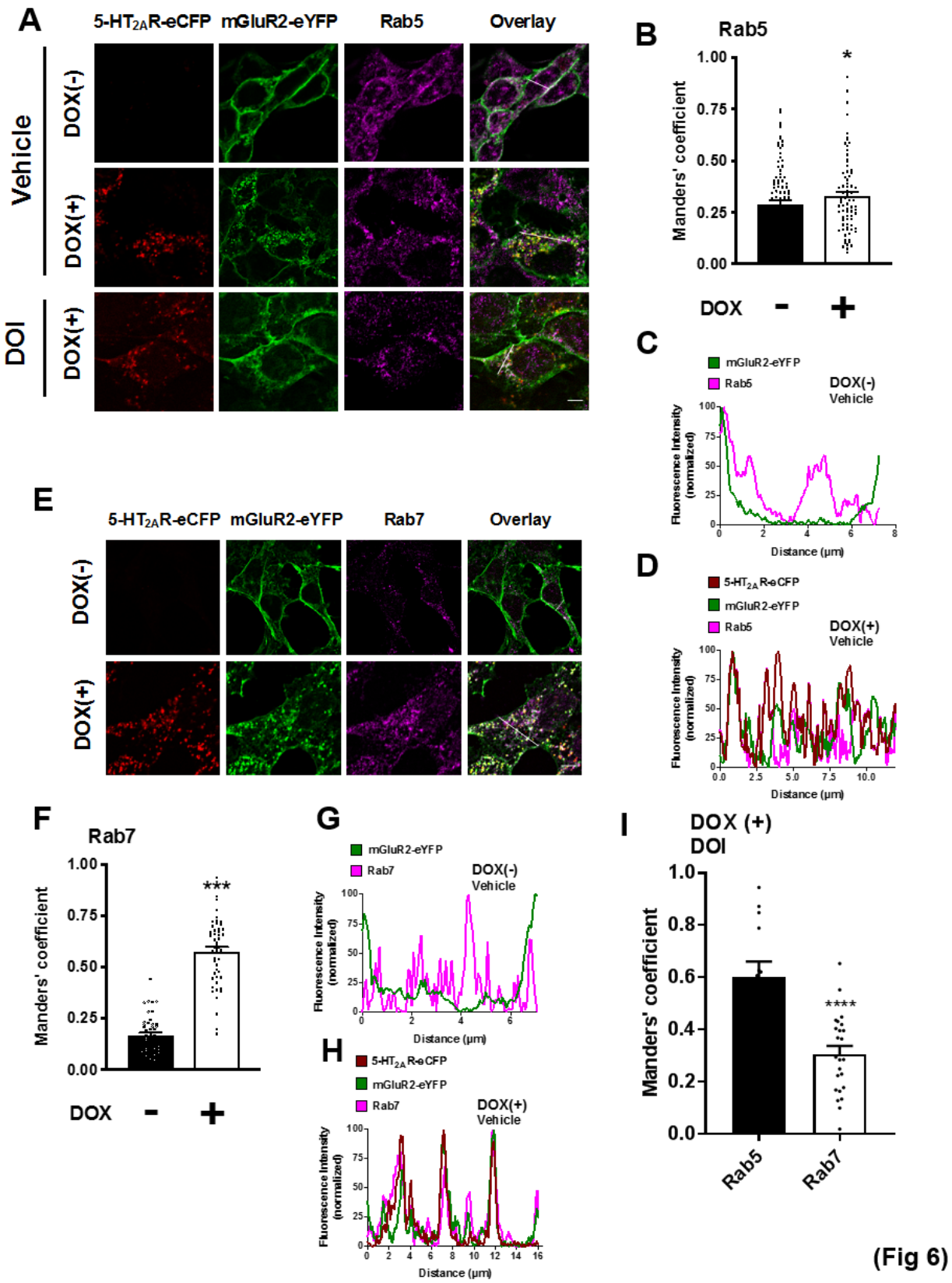
A
5-HT2AR-eCFP
mGluR2-eYFP
Rab5
Overlay
Vehicle
DOI
DOX(-)
DOX(+)
B
Rab5
Manders' coefficient
1.00
0.75
0.50
0.25
0.00
*
DOX
-
+
C
mGluR2-eYFP
Rab5
DOX(-)
Vehicle
Fluorescence Intensity (normalized)
Distance (μm)
D
5-HT2AR-eCFP
mGluR2-eYFP
Rab5
DOX(+)
Vehicle
Fluorescence Intensity (normalized)
Distance (μm)
E
5-HT2AR-eCFP
mGluR2-eYFP
Rab7
Overlay
DOX(-)
DOX(+)
F
Rab7
Manders' coefficient
***
DOX
-
+
G
mGluR2-eYFP
Rab7
DOX(-)
Vehicle
Fluorescence Intensity (normalized)
Distance (μm)
H
5-HT2AR-eCFP
mGluR2-eYFP
Rab7
DOX(+)
Vehicle
Fluorescence Intensity (normalized)
Distance (μm)
I
DOX (+)
DOI
Manders' coefficient
****
Rab5
Rab7

(Fig 6)

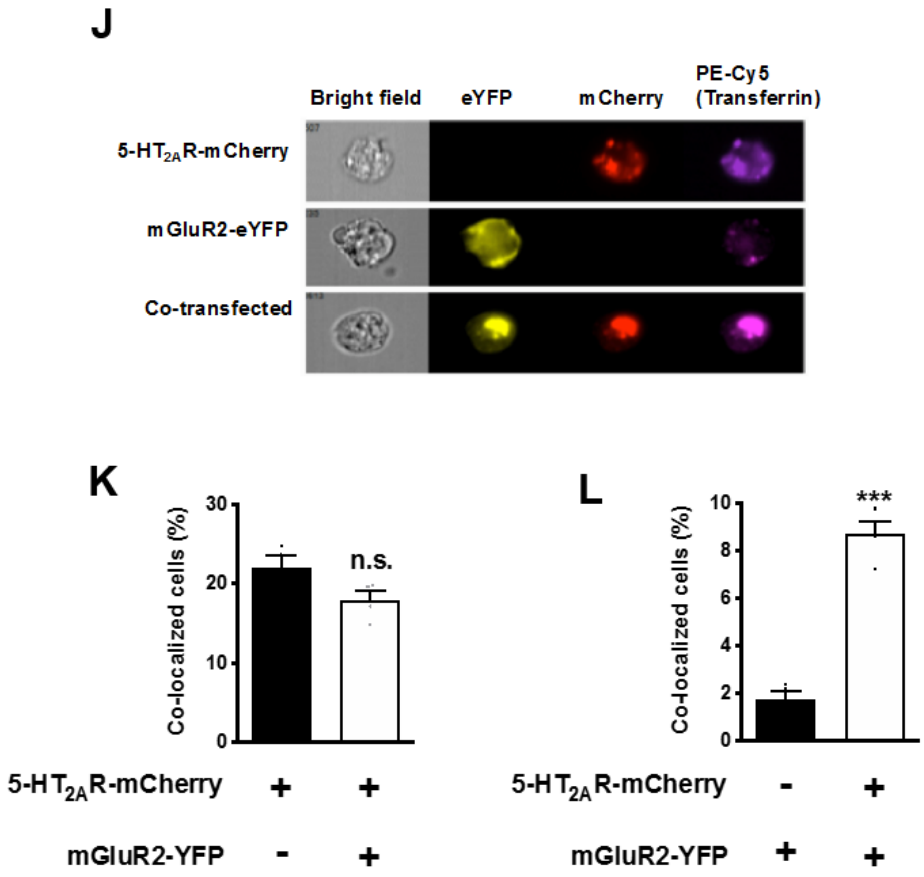
J
Bright field
eYFP
mCherry
PE-Cy5
(Transferrin)
5-HT2AR-mCherry
mGluR2-eYFP
Co-transfected
K
Co-localized cells (%)
30
20
10
0
n.s.
5-HT2AR-mCherry + +
mGluR2-YFP - +
L
Co-localized cells (%)
10
8
6
4
2
0
***
5-HT2AR-mCherry - +
mGluR2-YFP + +

(Fig 6)

Fig. 6. Agonist activation of either 5-HT_{2A}R or mGluR2 differentially affects mGluR2 trafficking and downregulation. (**A** to **L**) Flp-In T-REx HEK293 cells stably expressing mGluR2-eYFP and harboring c-Myc-5-HT_{2A}R-eCFP at the inducible locus were untreated [DOX(-)] or treated with doxycycline [DOX(+)], and exposed for 60 min to DOI (1 μM). Cells were then permeabilized and stained with anti-Rab5 or anti-Rab7 and secondary antibody, and imaged by confocal microscopy to detect eCFP, eYFP, anti-Rab5, or anti-Rab7. Representative confocal micrographs (**A** and **E)** and corresponding line scans (**C** and **D**, **G** and **H**), and Manders' colocalization coefficient analysis of anti-Rab5 (**A** and **B**; n = 33 – 134 cell regions of interest in three independent experiments) or anti-Rab7 (**E** and **F**; n = 48 – 49 cell regions of interest in three independent experiments) and eYFP-tagged construct. (**I**) Manders' colocalization coefficient analysis between Rab5 and Rab7 in [DOX(+)] cells and treated with DOI (1 μM) (36 cell regions of interest in two independent experiments). (**J** to **L**) FACS analysis of internalized mGlu2 receptors along with the transferrin marker. (**J** and **L**) HEK293 cells were transfected to express 5-HT_{2A}R-mCherry alone, mGluR2-eYFP alone, or 5-HT_{2A}R-mCherry and mGluR2-eYFP together, permeabilized, stained with PE-Cy5-tagged anti-transferrin receptor antibody, and imaged with an Amnis ImageStream flow cytometer. (**J**) Representative images. (**K**) Colocalization of 5-HT_{2A}R-mCherry and transferrin receptor with or without coexpression of mGluR2-eYFP (n = 4 independent experiments). (**L**) Colocalization of mGluR2-eYFP and transferrin receptor with or without coexpression of 5-HT_{2A}R-mCherry (n = 4 independent experiments). Data are mean ± SEM (**B**, **F**, **I**, **K** and **L**). Statistical analysis was performed using the Student's *t*-test (**B**, **F**, **I**, **K** and **L**). **P* < 0.05, ***P* < 0.01, ****P* < 0.001, *****P* < 0.0001, n.s., not significant. Scale bars, 5 μm.

To pursue quantitative comparison of variant receptor trafficking, and to validate our previous findings with an independent marker of clathrin-mediated endosomes, we assessed colocalization of 5-HT_{2A}R-mCherry or mGluR2-eYFP with the transferrin receptor, which transits through clathrin-coated pits and behaves as a marker of early endosomes, using imaging flow cytometry. As above with Rab5 and Rab7, our data show that localization between 5-HT_{2A}R-mCherry and the transferrin receptor was higher as compared to that observed between mGluR2-eYFP and transferrin receptor (Fig. 6J). Additionally, we show that whereas colocalization between 5-HT_{2A}R-mCherry and transferrin receptor was not affected upon cotransfection of the mGluR2-eYFP construct (Fig. 6K), transfection of the 5-HT_{2A}R-mCherry construct led to a significant increase in colocalization between mGluR2-eYFP and the transferrin receptor (Fig. 6L).

VII. DOI and LY379268 differentially affect localization of mGluR2 in Rab5-positive endosomes

To gain further insight into how cells control the subcellular localization of a 7TMR complexes, we next investigated the effects of different serotonergic and glutamatergic agonists on trafficking processes in cells coexpressing 5-HT_{2A}R and mGluR2.

We first explored the effect of the endogenous neurotransmitter serotonin (5-HT) or the 5-HT_{2A}R agonist DOI on localization of mGluR2 within Rab5-positive endosomes. Our data showed that colocalization of mGluR2-eYFP and Rab5 was significantly increased after either 5-HT or DOI treatment in cells stably expressing mGluR2-eYFP and induced to express 5-HT_{2A}R-eCFP (Figs. 6A, and 7A, and B). To rule out any effect of DOI on mGluR2 trafficking, we confirmed that treatment with DOI does not affect localization of mGluR2-eYFP and Rab5 in cells stably expressing mGluR2-eYFP and uninduced (DOX[-]) to express 5-HT_{2A}R-eCFP (Fig. 7C).

To test whether 5-HT_{2A}R and mGluR2 receptor heteromer is required for this trafficking event, we used synthetic peptides with the amino acid sequence of TM4 of mGluR2 fused to the HIV

transactivator of transcription (TAT) peptide, which determines the orientation of the peptide when inserted in the plasma membrane. To begin with, we wanted to test whether the interfering peptide can reduce or even prevent the interaction between 5-HT_{2A} and mGluR2. As expected and based on our above findings, incubation with TAT-TM4, but not with TAT-TM1 or TAT-tagged scrambled peptide (TAT-SCR), significantly decreased FRET signal in cells coexpressing 5-HT_{2A}R-eCFP and mGluR2-eYFP (Fig. 7D). Notably, incubation with TAT-TM4 reduced the effect of DOI on colocalization of mGluR2-eYFP and Rab5 (Fig. 7E). Exposure to TAT-TM4, however, did not affect colocalization between mGluR2-eYFP and Rab5 in vehicle-treated cells (Fig. 7E). To gain further insight into the endocytic process at work, endocytosis was pharmacologically blocked by an inhibitor. Dynamin is a GTPase protein that is essential for membrane fission during clathrin-mediated endocytosis. Dynasore acts as a potent inhibitor of endocytic pathways known to depend on dynamin by rapidly blocking coated vesicle formation within seconds of its application. Cells coexpressing 5-HT_{2A}R and mGluR2 was submit to dynasore mediated endocytosis inhibition and treated with DOI. As a result, a diminution of the effect of DOI on augmentation of colocalization between mGluR2-eYFP and Rab5 was observed (Fig. 7F).

To validate some of above findings with a different approach, and to track mGluR2 internalization upon different treatments, we processed the cells to flow cytometry, where cell surface localization of mGluR2-eYFP is detected thanks to an Alexa Fluor 647 (AF647)-tagged antibody targeting an epitope of the N-terminal of mGluR2. Surprisingly, mGluR2 surface distribution was unaffected by DOI in DOX(+) cells (Fig. 7G). As expected, however, cell surface AF647 signal was augmented upon dynasore treatment (Fig. 7G). This lack of effect of DOI exposure on cell surface mGluR2-eYFP was further supported by radioligand binding assays. [^{3}H]LY341495 binding was comparable in DOX(+) cells treated with DOI and vehicle (Fig. 7H). Together with the absence of effect of DOI treatment on FRET (Fig. 7I) and PLA (Fig. 7J) signal between 5-HT_{2A}R-eCFP and mGluR2-eYFP, these data suggest that whereas exposure to DOI augments subcellular

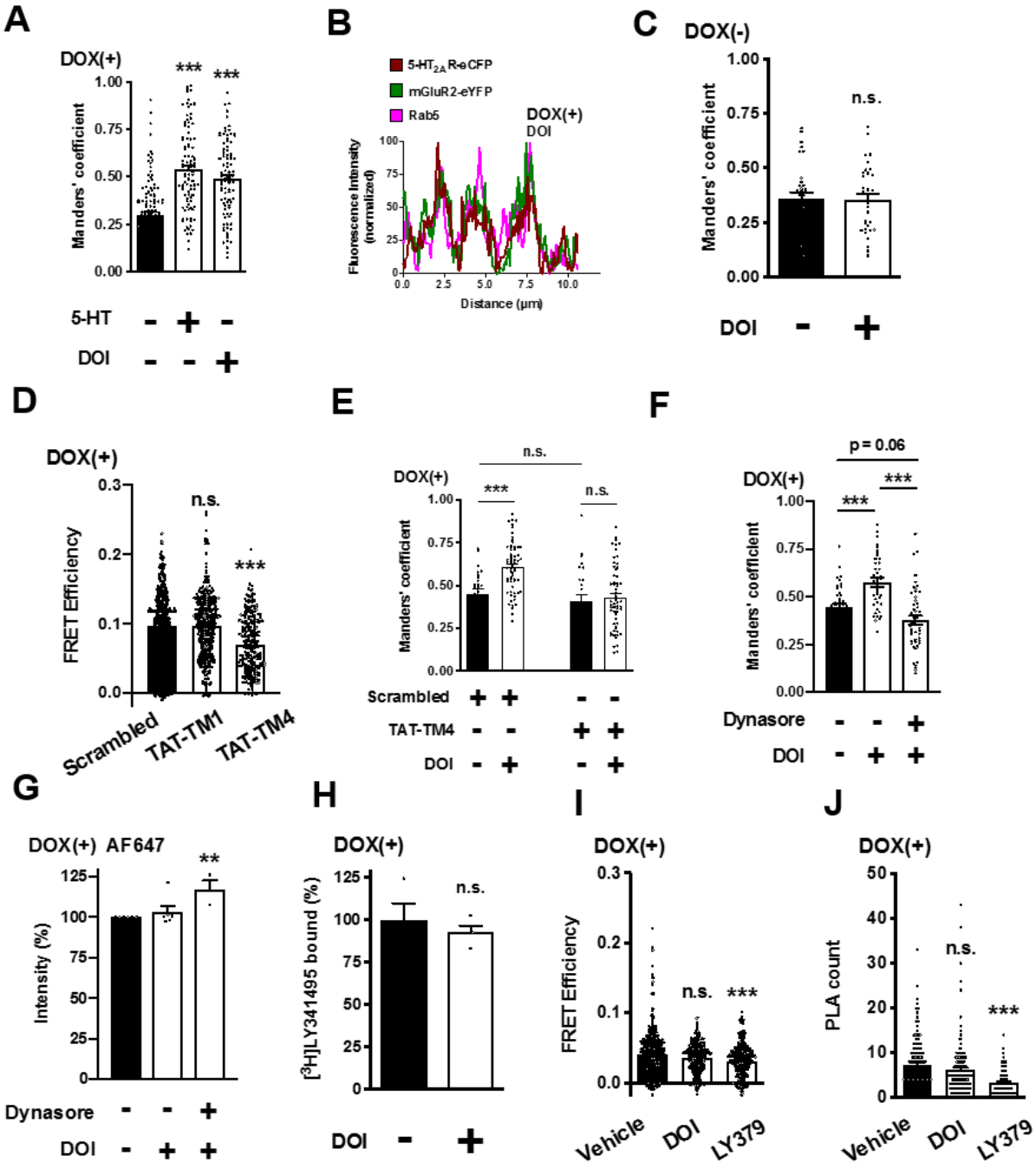
A
DOX(+)
Manders' coefficient
1.00
0.75
0.50
0.25
0.00
***
***
5-HT - + -
DOI - - +
B
5-HT2AR-eCFP
mGluR2-eYFP
Rab5
DOX(+)
DOI
Fluorescence Intensity (normalized)
100
75
50
25
0
0.0
2.5
5.0
7.5
10.0
Distance (μm)
C
DOX(-)
Manders' coefficient
1.00
0.75
0.50
0.25
0.00
n.s.
DOI - +
D
DOX(+)
FRET Efficiency
0.3
0.2
0.1
0.0
n.s.
***
Scrambled
TAT-TM1
TAT-TM4
E
n.s.
DOX(+)
Manders' coefficient
1.00
0.75
0.50
0.25
0.00
***
n.s.
Scrambled + + - -
TAT-TM4 - - + +
DOI - + - +
F
p = 0.06
DOX(+)
Manders' coefficient
1.00
0.75
0.50
0.25
0.00
***
***
Dynasore - - +
DOI - + +
G
DOX(+) AF647
Intensity (%)
125
100
75
50
25
0
**
Dynasore - - +
DOI - + +
H
DOX(+)
[3H]LY341495 bound (%)
125
100
75
50
25
0
n.s.
DOI - +
I
DOX(+)
FRET Efficiency
0.3
0.2
0.1
0.0
n.s.
***
Vehicle
DOI
LY379
J
DOX(+)
PLA count
50
40
30
20
10
0
n.s.
***
Vehicle
DOI
LY379

(Fig 7)

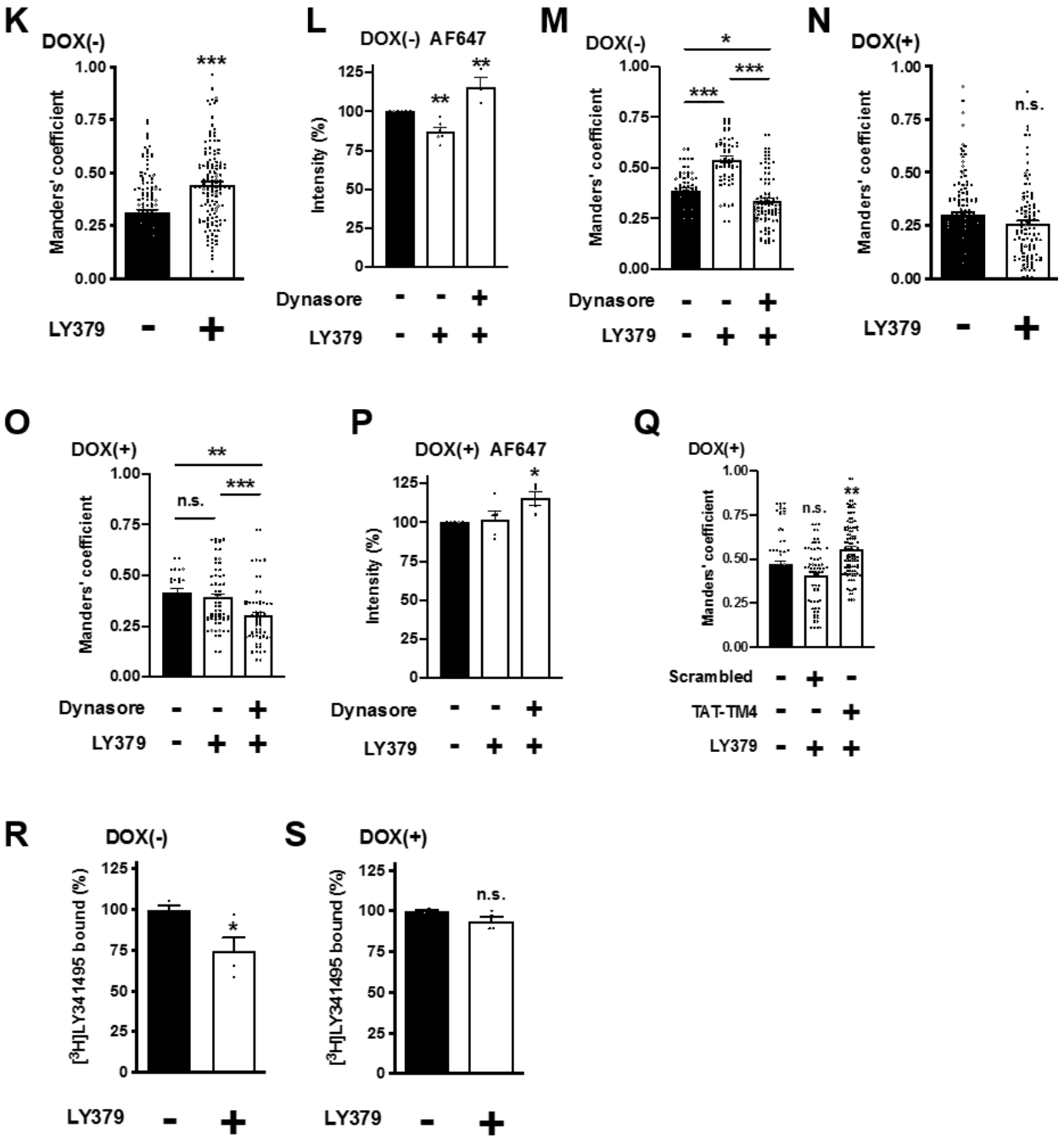
K
DOX(-)
Manders' coefficient
1.00
0.75
0.50
0.25
0.00
***
LY379 - +
L
DOX(-) AF647
Intensity (%)
125
100
75
50
25
0
**
**
Dynasore - - +
LY379 - + +
M
DOX(-)
Manders' coefficient
*
***
***
Dynasore - - +
LY379 - + +
N
DOX(+)
Manders' coefficient
n.s.
LY379 - +
O
DOX(+)
Manders' coefficient
**
n.s.
***
Dynasore - - +
LY379 - + +
P
DOX(+) AF647
Intensity (%)
*
Dynasore - - +
LY379 - + +
Q
DOX(+)
Manders' coefficient
n.s.
**
Scrambled - + -
TAT-TM4 - - +
LY379 - + +
R
DOX(-)
[3H]LY341495 bound (%)
*
LY379 - +
S
DOX(+)
[3H]LY341495 bound (%)
n.s.
LY379 - +

(Fig 7)

Fig. 7. DOI and LY379268 differentially affect localization of mGluR2 in Rab5-positive endosomes. (**A** to **C, K** and **N**) Flp-In T-REx HEK293 cells stably expressing mGluR2-eYFP and harboring c-Myc-5-HT_{2A}R-eCFP at the inducible locus were untreated [DOX(-)] or treated with doxycycline [DOX(+)], and exposed for 60 min to serotonin (5-HT, 1 μM), DOI (1 μM) or LY379268 (10 μM), or vehicle. Cells were then permeabilized and stained with anti-Rab5 and secondary antibody, and imaged by confocal microscopy to detect eCFP, eYFP, anti-Rab5 (**Fig. 6A 3rd line**). Representative line scan of DOI treated cells (**B**). Cells were incubated (60 min; 10 μM) with TAT-fused peptide corresponding to TM1 (TAT-TM1) or TM4 (TAT-TM4) of mGluR2, or scrambled control peptide and then processed for sensorFRET (n = 248 – 393 regions of interest in three independent experiments) (**D**). (**E** and **Q**) Manders' coefficient colocalization analysis of anti-Rab5 and eYFP-tagged construct. Cells were exposed for 60 min to DOI (1 μM, **E**), LY379268 (10 μM, **Q**), or vehicle. TAT-tagged peptides (10 μM) were added 5 min before drug or vehicle administration (n = 27 – 103 cell regions of interest in three independent experiments). (**F**, **M** and **O**) Manders' coefficient colocalization analysis of anti-Rab5 and eYFP-tagged construct. Cells were exposed for 60 min to DOI (1 μM, **F**), LY379268 (10 μM, **M** and **O**), or vehicle. Dynasore (80 μM) was added 5 min before drug or vehicle administration (n = 28 – 88 cell regions of interest in three independent experiments). (**G**, **L** and **P**) Cell surface localization of mGluR2-eYFP assessed by flow cytometry assays with an Alexa Fluor 647 (AF647)-tagged antibody. Cells were exposed for 60 min to DOI (1 μM, **G**), LY379268 (10 μM, **L** and **P**), or vehicle. Dynasore (80 μM) was added 5 min before drug or vehicle administration (n = 3 – 6 independent experiments with 8508 – 10048 cells per experimental condition). (**H**, **R** and **S**) Density of mGluR2 shown as [^{3}H]LY341495 binding in membrane preparations of DOX(+) (**H** and **S**) or DOX(-) (**R**) cells exposed for 60 min to DOI (1 μM, **H**), LY379268 (10 μM, **R** and **S**), or vehicle. Data are shown as percentage of specific binding in DOI- or LY379268-treated cells as compared to vehicle (n = 4 independent groups of membrane preparations). (**I** and **J**) Cells were exposed for 60 min to DOI (1 μM), LY379268 (10 μM), or vehicle. Quantification of FRET efficiencies (**I**, n = 281 – 536 regions of interest in three independent experiments). Quantification of PLA dots (**J**, n = 82 – 148 cell regions of interest demarcated according to eYFP signal within previously defined eCFP-positive cells in three independent experiments). Data are mean ± SEM (**A**, **C, E** to **H**, **K** to **S**) or median with 95% confidence interval (**D**, **I** and **J**). Statistical analysis was performed using Student's *t*-test (**C**, **H**, **K**, **N**, **R**, **S**), one-way ANOVA with Bonferroni's *post hoc* test (**A**, **F**, **G**, **L**, **M**, **O**, and **P** and **Q**), two-way ANOVA with Bonferroni's *post hoc* test (**E**), or one-way non-parametric ANOVA (Kruskal-Wallis) with Dunn's *post hoc* test (**D**, **I** and **J**). **P* < 0.05, ***P* < 0.01, ****P* < 0.001, n.s., not significant.

localization of mGluR2 within Rab5-positive endosomes through a mechanism that requires heteromerization between 5-HT_{2A}R and mGluR2, activation of the 5-HT_{2A}R receptor does not affect mGluR2 cell surface density, total density or heteromerization with 5-HT_{2A}R.

We next tested whether DOX-induced expression of 5-HT_{2A}R-eCFP modulates the effect of the mGluR2/3 agonist LY379268 on mGluR2's subcellular localization and trafficking. Consistent with the paradigmatic description of 7TMR endocytosis after ligand binding, in DOX(-) cells, incubation with LY379268 led to both an increase of colocalization between mGluR2-eYFP and Rab5 (Fig. 7K), and reduced cell surface AF647 signal (Fig. 7L), phenotypes that were prevented by dynasore (Figs. 7, L and M). Importantly, this effect of LY379268 on subcellular localization of mGluR2 was not observed in DOX(+) cells (Figs. 7, N, O and P), although dynasore augmented the surface location of mGluR2. This effect was rescued in DOX(+) cells treated with TAT-TM4 (Fig. 7Q). Additionally, our radioligand bindings assays with the mGluR2/3 antagonist [^{3}H]LY341495 showed that mGluR2 density was reduced in DOX(-) cells treated with LY379268 (Fig. 7R), whereas LY379268 treatment did not affect [^{3}H]LY341495 binding in cells stably expressing mGluR2-eYFP and induced to express 5-HT_{2A}R-eCFP (Fig. 7S). By contrast, we observed that, in DOX-treated cells, molecular proximity between 5-HT_{2A}R-eCFP and mGluR2-eYFP, as assessed by sensorFRET (Fig. 7I) and PLA (Fig. 7J), was reduced upon previous exposure to LY379268. Together, these data indicate that the 5-HT_{2A}R agonist DOI and the mGluR2/3 agonist LY379268 differentially affect mGluR2 density as well as localization of mGluR2 with markers of endocytic compartments in cells expressing mGluR2 alone, or together with 5-HT_{2A}R.

VIII. Psychedelic and non-psychedelic compounds have different effects on the 5-HT_{2A}R-mediated endocytosis of mGluR2

Our system thus far showed that 5-HT_{2A}R agonists such as DOI and 5-HT displaced mGluR2 to different marked compartment of the endocytic system, and that is dependent on the 5-HT_{2A}-

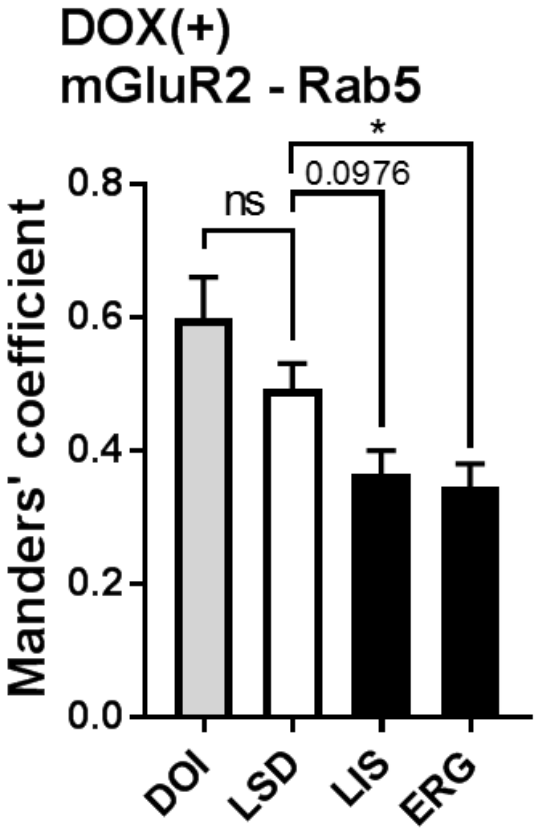
DOX(+)
mGluR2 - Rab5
Manders' coefficient
0.0
0.2
0.4
0.6
0.8
ns
0.0976
*
DOI
LSD
LIS
ERG

(Fig 8)

Fig. 8. Activation of 5-HT_{2A}R by hallucinogenic or nonhallucinogenic agonists differently mediate Rab5-dependent trafficking of mGluR2. Flp-In T-REx HEK293 cells stably expressing mGluR2-eYFP and harboring c-Myc-5-HT_{2A}R-eCFP at the inducible locus were treated with doxycycline [DOX(+)], and exposed for 60 min to DOI (1 μM), LSD (1μM), lisuride (1μM) or ergotamine (1μM). Cells were then permeabilized and stained with anti-Rab5 and secondary antibody, and imaged by confocal microscopy to detect eCFP, eYFP, anti-Rab5. Manders' coefficient colocalization analysis of anti-Rab5 (n = 33 cell regions of interest in one experiment) and eYFP-tagged construct. Data are mean ± SEM. Statistical analysis was performed using one-way ANOVA with Bonferroni's post hoc test. *P < 0.05, n.s., not significant.

mGluR2 receptor heterocomplex. Although serotonin is not hallucinogenic at physiological concentration, unlike DOI, we wanted to gain more insights into how propsychotic molecules such as 5-HT_{2A}R hallucinogens (HAL) can affect mGluR2 trafficking as compared to non-hallucinogenic agents (NHAL). Hallucinogenic 5-HT_{2A}R agonists such as LSD and psilocybin have been categorized as propsychotic compounds because of their ability to mimic some of the schizophrenia positive symptoms. Conversely, molecules that are very close in structure but not hallucinogenic, such as lisuride and ergotamine, seem to evoke different internalization and signaling mechanism, such as bias agonism[114,352] and transphosphorylation[350.] Given that HAL and NHAL have different effects on the internalization of 5-HT_{2A}R and that it can phosphorylate mGluR2 to affect its Gαi/o signaling and probably its internalization following exposure to the drugs, we hypothesized that similar to those findings, HAL and NHAL would have different effects on the internalization of mGluR2 in Rab5 endosomes in cells coexpressing both receptors. Consistently with previous findings[163,350], and similar to the findings with 5-HT and DOI, cells treated with LSD and psilocybin tended to have a greater colocalization index between mGluR2 and Rab5 (Fig. 8) (Fig. 8). Conversely, no increase was observed with NHAL treatments such as lisuride and ergotamine, indicating that only 5-HT_{2A}R hallucinogenic agonists have the potency to affect mGluR2 trafficking (Fig. 8).

IX. Exposure to clozapine down-regulates mGluR2 via GPCR heteromerization with 5-HT_{2A}R

1. Effect of 5-HT_{2A}R antagonists on receptor's subcellular distribution

Recent reports suggest that presence of 5-HT_{2A}R antagonists/inverse agonists affects intracellular localization of 5-HT_{2A}R constructs in living mammalian cell cultures. As an example, upon addition of ligands such as mianserin, cells show 5-HT_{2A}Rs predominantly at the plasma membrane[335]. To corroborate these findings, we used our Flp-In T-REx system expressing 5-HT_{2A}R-eCFP only (*i.e.*, without stable expression of mGluR2-eYFP, mGluR3-eYFP or mGluR2ΔTM4) in an inducible

manner. Following addition of DOX, cells were treated overnight with the 5-HT_{2A}R antagonist/inverse agonist M100907 (also known as volinanserin or MDL 100,907), or vehicle. Our data indicated that, opposite to that observed in vehicle-treated cells, 5-HT_{2A}R-eCFPs were essentially localized at the plasma membrane of cells treated with M100907 (Fig. 9A to C). Similar results were obtained with the 5-HT_{2A}R antagonist/inverse agonist altanserin (Fig. 9A and D). Surprisingly, the clozapine's analog olanzapine had the same effect on the localization of 5-HT_{2A}R (Fig. 9A). Together, these data suggest that, at steady state, the bulk of 5-HT_{2A}R-eCFP is present in punctate intracellular vesicles, and that treatment with the 5-HT_{2A}R antagonists/inverse agonists enhances the otherwise restricted cell surface localization of the 5-HT_{2A}R.

2. Effect of clozapine on 5-HT_{2A}R's subcellular distribution

Clozapine, however, is an antipsychotic medication that presents peculiar properties as it normally behaves as a 5-HT_{2A}R antagonist/inverse agonist, thus blocking or inhibiting 5-HT_{2A}R-dependent principal signaling pathways such as activation of $G\alpha_{q/11}$ proteins, yet is also able to activate certain pathways such as Akt. Additionally, and opposite to what is usually observed with most antagonists and inverse agonists (see above), our data showed that following DOX-induced expression of 5-HT_{2A}R-eCFP, clozapine exposure did not discernibly affect the subcellular distribution of the 5-HT_{2A}R construct (Fig. 9A and E). Nevertheless, our previous findings in whole animal models showed that long-lasting exposure to clozapine induces mGluR2 down-regulation in brain regions such as the frontal cortex. Consequently, we tested whether clozapine affectsmGluR2 localization and density in cells coexpressing 5-HT_{2A}R and mGluR2, as well as the extent to which 5-HT_{2A}R-mGluR2 heteromerization is necessary for this trafficking event.

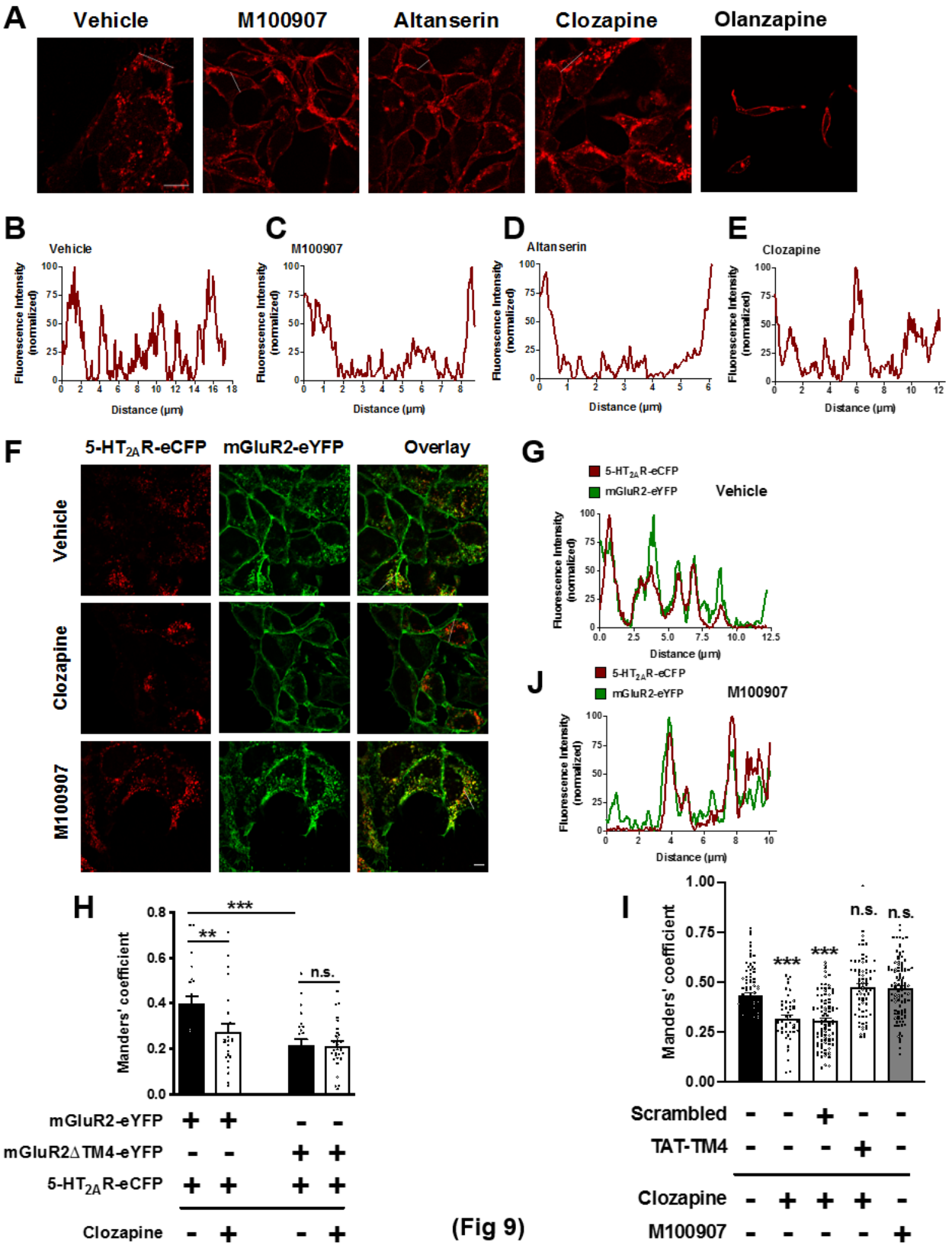
A
Vehicle
M100907
Altanserin
Clozapine
Olanzapine
B
Vehicle
C
M100907
D
Altanserin
E
Clozapine
Fluorescence Intensity (normalized)
Distance (µm)
F
5-HT2AR-eCFP
mGluR2-eYFP
Overlay
Vehicle
Clozapine
M100907
G
5-HT2AR-eCFP
mGluR2-eYFP
Vehicle
J
M100907
H
Manders' coefficient
***
**
n.s.
mGluR2-eYFP
mGluR2ΔTM4-eYFP
5-HT2AR-eCFP
Clozapine
I
Manders' coefficient
***
***
n.s.
n.s.
Scrambled
TAT-TM4
Clozapine
M100907

(Fig 9)

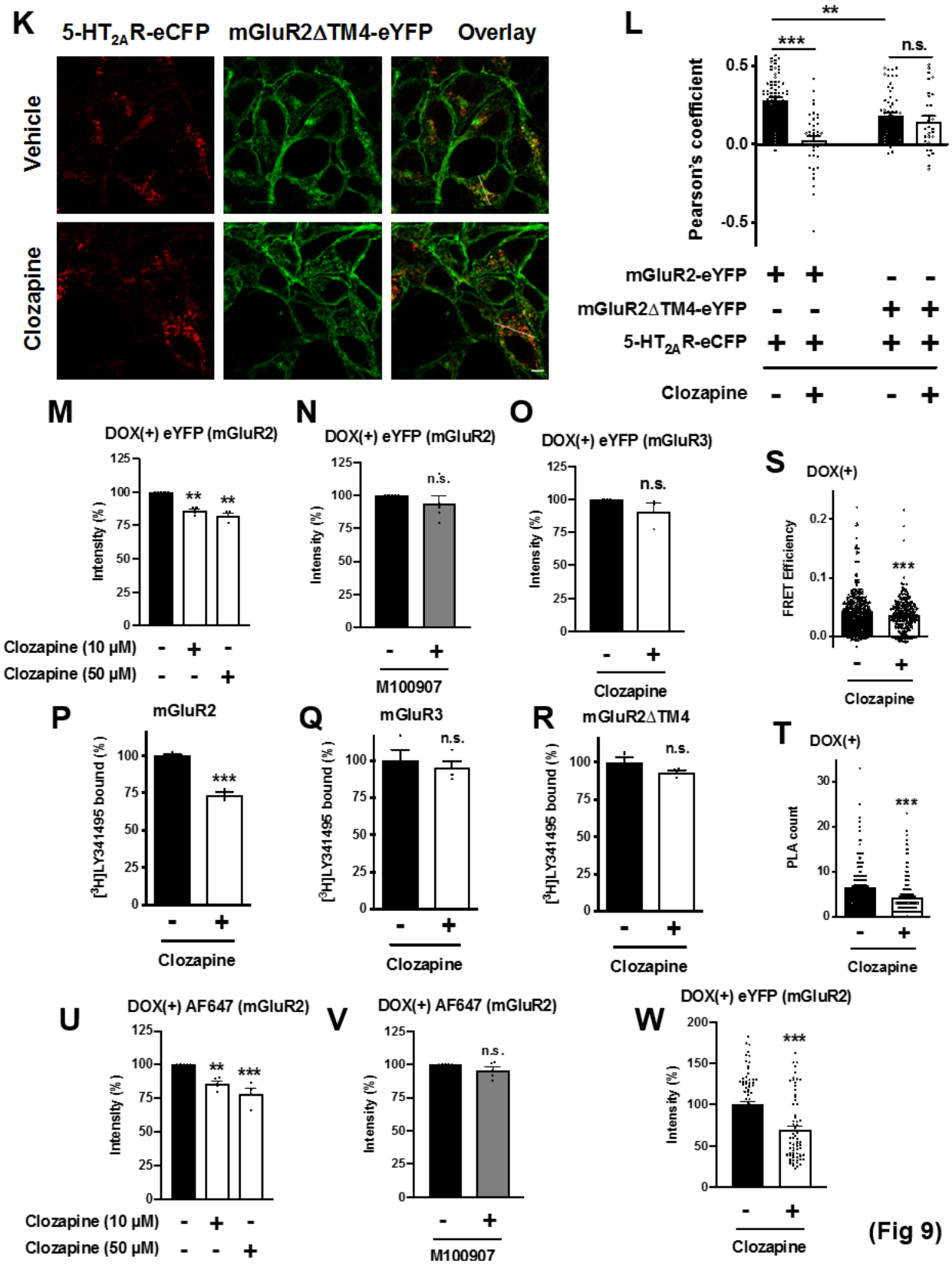
K
5-HT2AR-eCFP
mGluR2ΔTM4-eYFP
Overlay
Vehicle
Clozapine
L
Pearson's coefficient
0.5
0.0
-0.5
**
***
n.s.
mGluR2-eYFP + + - -
mGluR2ΔTM4-eYFP - - + +
5-HT2AR-eCFP + + + +
Clozapine - + - +
M
DOX(+) eYFP (mGluR2)
Intensity (%)
125
100
75
50
25
0
**
**
Clozapine (10 μM) - + -
Clozapine (50 μM) - - +
N
DOX(+) eYFP (mGluR2)
n.s.
- +
M100907
O
DOX(+) eYFP (mGluR3)
n.s.
- +
Clozapine
S
DOX(+)
FRET Efficiency
0.2
0.1
0.0
***
- +
Clozapine
P
mGluR2
[3H]LY341495 bound (%)
100
75
50
25
0
***
- +
Clozapine
Q
mGluR3
n.s.
- +
Clozapine
R
mGluR2ΔTM4
n.s.
- +
Clozapine
T
DOX(+)
PLA count
30
20
10
0
***
- +
Clozapine
U
DOX(+) AF647 (mGluR2)
Intensity (%)
125
100
75
50
25
0
**
***
Clozapine (10 μM) - + -
Clozapine (50 μM) - - +
V
DOX(+) AF647 (mGluR2)
n.s.
- +
M100907
W
DOX(+) eYFP (mGluR2)
Intensity (%)
200
150
100
50
0
***
- +
Clozapine

(Fig 9)

Fig. 9. Clozapine treatment affects mGluR2 trafficking and downregulation via 5-HT$_{2A}$R-mGluR2. (**A**) Representative confocal micrographs and representative line scans of Flp-In T-REx HEK293 cells harboring 5-HT$_{2A}$R-eCFP at the inducible locus were treated with doxycycline, and then exposed overnight to M100907 (**C**) (10 μM), altanserin (**D**) (10 μM) or clozapine (**E**) (10 μM), olanzapine (10 μM) or vehicle (**B**). (**F** to **H** and **K, J**) Flp-In T-REx HEK293 cells stably expressing mGluR2-eYFP (**F**, **G** to **L**, **N**, **P**, and **U, V, W**), mGluR2ΔTM4-eYFP (**H, L, R**), or mGluR3-eYFP (**O**, **Q**) and harboring 5-HT$_{2A}$R-eCFP at the inducible locus were treated with doxycycline and then exposed overnight to clozapine (10 μM or 50 μM) or M100907 (10 μM), or vehicle. Representative confocal micrographs and line scans (**F, G, J, K**). (**H**) Manders' coefficient colocalization analysis of eYFP- and eCFP-tagged constructs (n = 30 – 74 cell regions of interest in three independent experiments). (**I**) Manders' coefficient colocalization analysis of eYFP- and eCFP-tagged constructs in cells stably expressing mGluR2-eYFP and harboring 5-HT$_{2A}$R-eCFP at the inducible locus. Cells were treated with doxycycline, and then exposed overnight to clozapine (10 μM) or M100907 (10 μM), or vehicle. TAT-tagged peptides were added both 5 minutes before clozapine or vehicle administration and 65 minutes before cell fixation (n = 44 – 98 cell regions of interest in three independent experiments). (**M** to **O**, **U, V, W**) Cell surface localization of mGluR2-eYFP with an Alexa Fluor 647 (AF647)-tagged antibody (**U**, **V**, **W**) and mGluR2-eYFP (**M, N**) or mGluR3-eYFP (**O**) density with eYFP were assessed by flow cytometry assays (n = 3 – 5 independent experiments with 8148 – 10418 cells per experimental condition). (**P** to **R**) Density of mGluR2 (**P**), mGluR3 (**Q**) or mGluR2ΔTM4 (**R**) shown as [^{3}H]LY341495 binding in membrane preparations of cells exposed overnight to clozapine (10 μM), or vehicle (n = 4 independent groups of membrane preparations). (**S**) Quantification of FRET efficiencies (n = 315 – 364 regions of interest in three independent experiments). (**T**) Quantification of PLA dots (n = 160 – 253 cell regions of interest demarcated according to eYFP signal within previously defined eCFP-positive cells in three independent experiments). (**W**) Intracellular eYFP signal in cells stably expressing mGluR2-eYFP and harboring 5-HT$_{2A}$R-eCFP at the inducible locus. Cells were treated with doxycycline, and then exposed overnight to clozapine (10 μM), or vehicle (n = 73 – 68 cell regions of interest demarcated based on eCFP signal within intracellular vesicles in three independent experiments). Data are mean ± SEM (**H,** and **I, L** to **R**, and **T** to **W**) or median with 95% confidence interval (**S**). Statistical analysis was performed using Student's *t*-test (**N** to **R**, **S, T**, and **W**), one-way ANOVA with Bonferroni's *post hoc* test (**M** and **U**), two-way ANOVA with Bonferroni's *post hoc* test (**H, I, L**), or Mann-Whitney U test (**S**). $^{**}P < 0.01$, $^{***}P < 0.001$, n.s., not significant. Scale bars, 5 μm.

3. Effect of clozapine on mGluR2's subcellular distribution

Cells induced to express 5-HT_{2A}R-eCFP and stably expressing mGluR2-eYFP were incubated with clozapine or vehicle. As before (see Fig. 3A, above), induction of 5-HT_{2A}R-eCFP corroborated a high level of colocalization between 5-HT_{2A}R-eCFP and mGluR2-eYFP in intracellular vesicles of vehicle-treated cells (Fig. 9F, G and L). Importantly, addition of clozapine resulted in an observable reduction of colocalization between mGluR2-eYFP and 5-HT_{2A}R-eCFP (Figs. 9, F and Hand L). This effect was not observed after addition of M100907 (Figs. 9, F and I), and was prevented by TAT-TM4 (Fig. 9I). Interestingly, and opposite to the effect observed in cells expressing 5-HT_{2A}R-eCFP alone (see Fig. 9A, above), both 5-HT_{2A}R-eCFP and mGluR2-eYFP remained intracellularly colocalized upon exposure to M100907 (Fig. 9F and J). As expected (see Fig. 3C, above), colocalization was less observable in cells coexpressing 5-HT_{2A}R-eCFP and mGluR2ΔTM4-eYFP (Figs. 9H, K, L), yet this low degree of colocalization was unaffected upon clozapine exposure (Figs. 9F, H and L)). Together, these data suggest that clozapine, and not M100907, reduces subcellular colocalization of 5-HT_{2A}R-eCFP and mGluR2-eYFP through a mechanism that requires their molecular proximity.

4. Effect of clozapine on mGluR2 density and expression and its heteromeric association with 5-HT_{2A}R

We next tested whether clozapine treatment affects mGluR2's density via the 5-HT_{2A}R-mGluR2 heteromer. Our flow cytometry analysis shows that, in DOX(+) cells stably expressing mGluR2-eYFP, clozapine treatment reduced intensity of eYFP (Fig. 9F), an effect that was not observed upon M100907 treatment (Fig. 9N) or in cells stably expressing mGluR3-eYFP (Fig. 9O). Similarly, density of mGluR2-eYFP, as determined by binding saturation curves with [^{3}H]LY341495, was reduced upon clozapine treatment in cells induced to express 5-HT_{2A}R-eCFP and stably expressing mGluR2-eYFP (Fig. 9P and Fig. A2 A). This clozapine-dependent effect, however, was not observed in cells induced to express 5-HT_{2A}R-eCFP and stably expressing either mGluR3-

eYFP (Fig. 9Q and Fig. A2 B) or mGluR2ΔTM4-eYFP (Fig. 9R and Fig. A2 C). Treatment with clozapine also diminished both FRET efficiency (Fig. 9S) and PLA signal (Fig. 9T) between 5-HT_{2A}R-eCFP and mGluR2-eYFP. Most importantly, although clozapine (Fig. 9U), but not M100907 (Fig. 9V), decreased cell surface immunoreactivity of mGluR2-eYFP, this effect was more evident on the subpopulation of mGluR2 located intracellularly (Fig. 9W). Additional controls included absence of effect of clozapine on cell surface mGluR2-eYFP immunoreactivity (Fig. A2 D5Q) and eYFP signal (Fig. A2 E) in DOX(-) cells.

X. Absence of 5-HT_{2A}R expression affects mGluR2 localization in cortical pyramidal neurons

1. Colocalization of mGluR2 and Rab5 in mouse cortical primary neurons

Previous neuroanatomical studies showed that 5-HT_{2A}R and mGluR2 colocalize in frontal cortex pyramidal neurons. Our current data so far suggest that expression of 5-HT_{2A}R modulates mGluR2 trafficking and localization in a mammalian tissue culture model. To ensure that this phenomenon occurs in a primary cell culture system, we examined whether localization of mGluR2 in Rab5-positive endosomes is affected in cortical neuron cultures of 5-HT_{2A}R knockout (*5-$HT_{2A}R^{-/-}$*) mice and wild-type (*5-$HT_{2A}R^{+/+}$*) littermates. Notably, colocalization of anti-mGluR2 immunoreactivity and Rab5 was significantly reduced in cortical primary neuron cultures of *5-$HT_{2A}R^{-/-}$* mice, as compared to *5-$HT_{2A}R^{+/+}$* animals (Figs. 10, A and B).

2. Effect of 5-HT_{2A}R expression on mGluR2 subcellular localization in mouse frontal cortex synapses

To assess whether the subcellular localization of mGluR2 is regulated by its interactions with 5-HT_{2A}R in native tissue, we examined the distribution of anti-mGluR2 immunoreactivity relative to the plasmalemma in the frontal cortex of *5-$HT_{2A}R^{+/+}$* and *5-$HT_{2A}R^{-/-}$* mice using immunogold

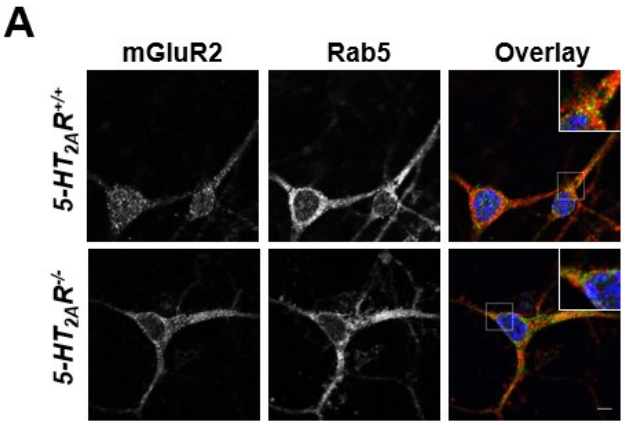
A
mGluR2
Rab5
Overlay
5-HT2AR+/+
5-HT2AR-/-

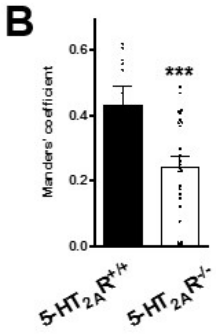
B
Manders' coefficient
0.6
0.4
0.2
0.0
***
5-HT2AR+/+
5-HT2AR-/-

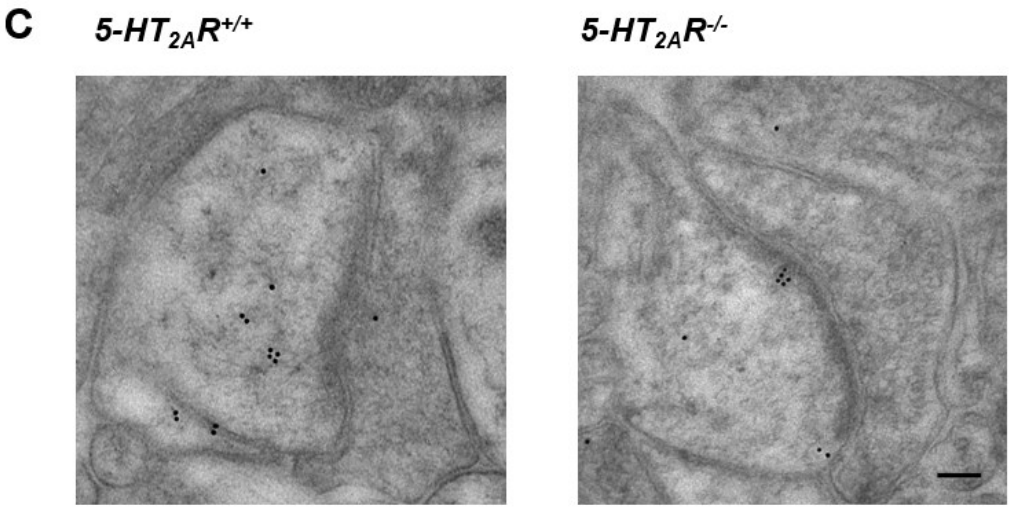
C
5-HT2AR+/+
5-HT2AR-/-

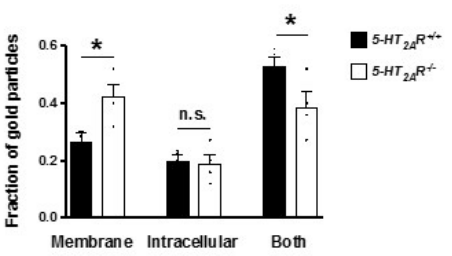
D
Fraction of gold particles
0.6
0.4
0.2
0.0
*
n.s.
*
Membrane
Intracellular
Both
5-HT2AR+/+
5-HT2AR-/-

(Fig 10)

Fig. 10. Localization of mGluR2 is dysregulated in the frontal cortex of *5-HT$_{2A}$R$^{-/-}$* mice. (**A** and **B**) Colocalization analysis of anti-mGluR2 and anti-Rab5 immunoreactivity in cortical primary cultures of *5-HT$_{2A}$R$^{+/+}$* and *5-HT$_{2A}$R$^{-/-}$* mice. Representative confocal micrographs (**A**). Manders' coefficient colocalization analysis (B) (n = 30 to 74 cell regions of interest in two independent experiments). Nuclei were stained in blue with Hoechst 33342. (**C** and **D**) Immunogold labeling for anti-mGluR2 immunoreactivity in the frontal cortex of *5-HT$_{2A}$R$^{+/+}$* and *5-HT$_{2A}$R$^{-/-}$* mice (n = 4 mice per genotype and 25 to 35 synapses per mouse). Representative photomicrographs showing excitatory synapses in mouse frontal cortex (**C**). Quantification of relative distribution of gold particles within postsynaptic spines (**D**). Data are means ± SEM (**B** and **D**). Statistical analysis was performed using Student's t test (B) or two-way ANOVA with Bonferroni's post hoc test (**D**). *P < 0.05 and ***P < 0.001. Scale bars, 5 μm (**A**) and 100 nm (**C**). n.s., not significant.

labeling. We focused our analysis solely on excitatory postsynaptic dendritic spines which in the frontal cortex region are the principal sites of glutamatergic input onto pyramidal neurons, and our previous data showed that 5-HT_{2A}R and mGluR2 crosstalk in this population of cortical cells. Within postsynaptic dendritic spines, particle clusters were observed at plasma membrane, inside the cytoplasm, or distributed on both plasmalemma and intracellularly (Fig. A3). For each synapse, distribution was scored based on these three categories. In neurons from *5-$HT_{2A}R^{+/+}$* mice, the largest proportion of synapses showed both plasma membrane and intracellular labeling (Figs. 10, C and D). Additionally, there was a significantly greater proportion of gold particle clusters at the plasma membrane alone in neurons from *5-$HT_{2A}R^{-/-}$* mice relative to *5-$HT_{2A}R^{+/+}$* littermates (Figs. 10, C and D). Together, these findings indicate that subcellular localization of mGluR2 is affected by expression of 5-HT_{2A}R in mouse cortical pyramidal neurons.

XI. 5-HT_{2A}R-mGluR2 fluorescence complementation in the HEK293 maturation pathway

1. In the endoplasmic reticulum

To address whether homo or heterodimeric receptor's complexes can be matured in the ER, we assessed by confocal microscopy the colocalization and the codistribution of the BiFC signal with the ER dye ER-Tracker, using the same quantitative colocalization analyses. 5-HT_{2A}, mGlu2 and mGlu3 homodimers complementation signals overlapped with the red dye, suggesting post-translational assembling in this organelle (Fig.11A, B, C, E and F). More importantly, 5-HT_{2A}-mGlu2 BiFC signal colocalized with the reticulum (Fig. 11D). 5-HT_{2A}R homodimer exhibited a significantly higher index of colocalization index (Manders $p<0.001$), accounting for ±80% of probes co-occurrence (Fig. 11E). No significant variation of mCitrine amount was measured (±0.6) between the mGlu2 mGlu3 and 5-HT_{2A}-mGlu2 receptor formations (Fig. 11E). The 5-HT_{2A}R

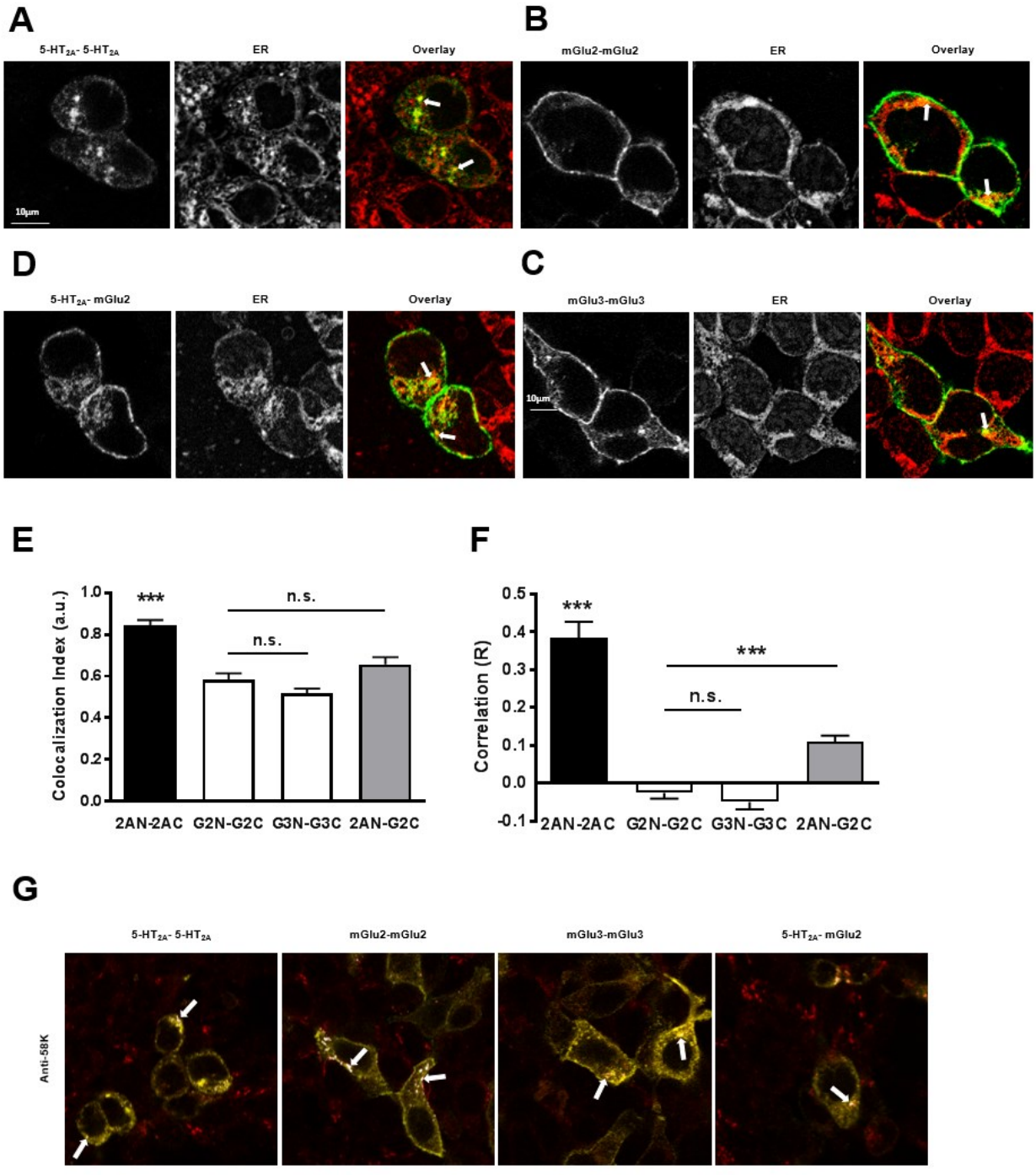
A
5-HT2A- 5-HT2A
ER
Overlay
10µm
B
mGlu2-mGlu2
ER
Overlay
D
5-HT2A- mGlu2
ER
Overlay
C
mGlu3-mGlu3
ER
Overlay
10µm
E
Colocalization Index (a.u.)
1.0
0.8
0.6
0.4
0.2
0.0
***
n.s.
n.s.
2AN-2AC
G2N-G2C
G3N-G3C
2AN-G2C
F
Correlation (R)
0.5
0.4
0.3
0.2
0.1
0.0
-0.1
***
***
n.s.
2AN-2AC
G2N-G2C
G3N-G3C
2AN-G2C
G
5-HT2A- 5-HT2A
mGlu2-mGlu2
mGlu3-mGlu3
5-HT2A- mGlu2
Anti-58K

(Fig 11)

H

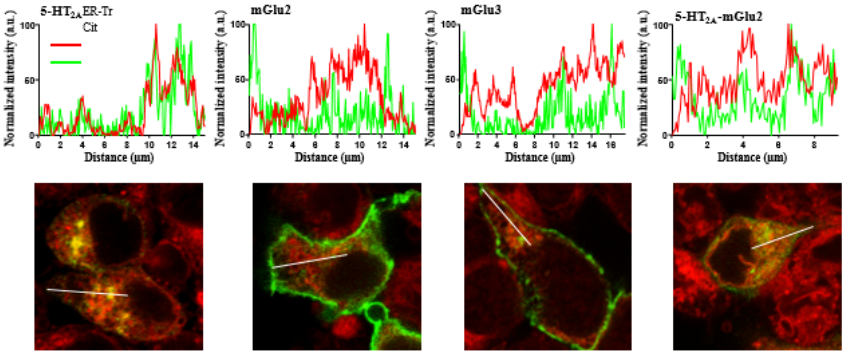
5-HT2AER-Tr
Cit
mGlu2
mGlu3
5-HT2A-mGlu2
Normalized intensity (a.u.)
Distance (µm)

I

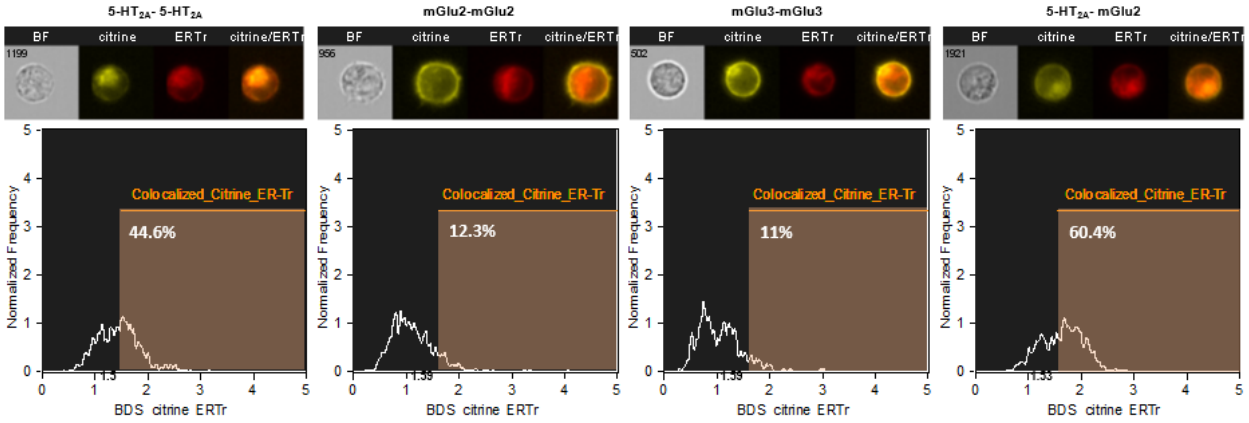
5-HT2A- 5-HT2A
mGlu2-mGlu2
mGlu3-mGlu3
5-HT2A- mGlu2
BF
citrine
ERTr
citrine/ERTr
Colocalized_Citrine_ER-Tr
44.6%
12.3%
11%
60.4%
Normalized Frequency
BDS citrine ERTr

(Fig 11)

Fig. 11. 5-HT_{2A}R-mGluR2 fluorescence complementation in the maturation pathway of HEK293. (**A**) Quantitative colocalization analysis of BiFC signals and the endoplasmic reticulum. (**A** to **D**) Single channel confocal micrographs of BiFC signal in HEK293 cells transfected to coexpress 5-HT_{2A}R-mCi-N172 and 5-HT_{2A}R-mCi-C67 (2AN-2AC), mGluR2-mCi-N172 and mGluR2-mCi-C67 (G2N-G2C), mGluR3-mCi-N172 and mGluR3-mCi-C67 (G3N-G3C), or 5-HT_{2A}R-mCi-N172 and mGluR2-mCi-C67 (2AN-G2C)and treated with the ER dye ER-Tracker. (**E** and **F**) Manders' and Pearson's coefficient colocalization analysis of BiFC mCitrine (yellow) and ER-Tracker (red) signal. (**G**) Colocalization between BiFC of 5-HT_{2A}R-mCi-N172 and 5-HT_{2A}R-mCi-C67, mGluR2-mCi-N172 and mGluR2-mCi-C67, mGluR3-mCi-N172 and mGluR3-mCi-C67, or 5-HT_{2A}R-mCi-N172 and mGluR2-mCi-C67 and the Golgi apparatus 58K. Immnunofluorescence using a primary antibody against 58K protein and secondary AF568. Arrows point white pixels indicating positive signals for both probes. (**H**) Intensities distributions line scans from the membrane to the nucleus areas. Fluorescence intensity profiles illustrate the spatial codistribution of the two probes, BiFC and ER-Tracker. The relative similarity probes profiles in the case of 5-HT2AR are consistent with relatively high and concentrated yellow pixels, as depicted by the image. mGluRs absence of paired profiles was reflected by absence of correlation. (**I**) ImageStream IFC-based BiFC of dual positive cell populations gated according to their Bright Details Similarity scores (BDS)**.** Orange areas represent gated colocalized cell populations after indicated BDS calculation. Percentages of colocalized cells are shown. Images represent flowed cells and fluorescence profiles in each population acquired with a 60x objective. n=: 5-HT_{2A}: 579; mGlu2: 811; mGlu3: 281; 5-HT_{2A}-mGlu2: 974. Data are means ± SEM for 2 experiments (**A** to **D**, and **I**), one experiment (**G**). Statistical analysis was performed using one-way ANOVA with Bonferroni's *post hoc* test (**E** and **F**) and a Pearson logarithm transformation for the BDS score calculation (**I**). ***p<0.001, n.s. not significant. Scale bar is 10 µm.

homodimer elicited a high fractional overlap with the ER dye (Fig. 11E). Probes intensity codistribution analysis by Pearson correlation index (PCC) confirmed a relatively high index of codistribution between the signals, suggesting a linear correlation of their intensity in the organelle (Fig. 11F). This was supported by the intensity profiles plotted by line scans crossing the intracellular cell's area from the membrane to the nucleus (Fig. 11G). There was no such correlation in the case of the mGluRs (Fig. 11F). The PCC value of the 5-HT_{2A}-mGlu2 receptor heteromer with the ER dye was significantly higher than the mGluR homodimers but lower than the 5-HT_{2A}R homodimer, suggesting a partial overlap with the ER (Fig. 11F). Noticeably, the expression pattern of the heterocomplex was both plasma membranous and intracellular (Fig. 11D). Together, these colocalization analyses suggest that 5-HT_{2A} and mGluR2, come in close proximity within the ER.

2. In the Golgi apparatus

We used an immunofluorescence approach to detect the presence of the 5-HT_{2A}-mGlu2 receptor heteromer in the Golgi apparatus (GA) with an anti-58k antibodies targeting the resident protein 58K, conjugated to AlexaFluor568 secondary antibody. Due to the reduced area covered by the Golgi apparatus within cells compared to that of the ER, we qualitatively assessed the presence of the BiFC signal attesting the formation of the 5-HT_{2A}R-mGlu2 heterocomplex (Fig. 11H). Homomeric 5-HT_{2A} mGluR2 and mGlu3 receptors were found is small proportion in the Golgi apparatus, consistent with the upward flow of the protein biosynthesis (Fig. 11H). 5-HT_{2A}-mGlu2 heterocomplex colocalized with the GA. This suggests that the heterodimer may also be matured in the GA in relatively same proportion as the homomeric structures.

3. Image Flow Cytometry-based BiFC colocalization of 5-HT_{2A}-mGlu2 heterocomplex with the ER

In order to confirm previous findings in a larger cell populations, we combined IFC with BiFC in cells transfected with paired constructs. Double fluorescent populations were analyzed by the

Bright Details Similarity score (BDS). Negative gates were set for each complementation experiment by colocalizing each probe with the bright field. As previously described, a BDS score of >1.5 indicates highly colocalized cell populations[254]. All calculated control gates provided BDS scores ≥ 1.5 (Fig. 11G). This score delineate the gate over which cell population can be interpreted as highly colocalized. BDS score of 1.5 showed that 44,6% of 5-HT_{2A} BIFC-positive population were highly colocalizing with the ER. Scores of 1.593 and 1.594 gated mGluR2 and mGluR3 populations accounting for 12.3% and 11%, respectively. The heterodimer scored 1.532 with 60.4% of colocalized cells. Thus, this experiment distinguished consistent amount of highly colocalized cells populations and provided a similar trend between the BiFC constructs, although the analysis technique was different.

Discussion

It has long been known that coexpression of multiple 7TMRs by individual cells can affect processes related to agonist-promoted receptor signaling, endocytosis and down-regulation[58,64,353–357]. The taste receptors provide a typical example. The finding that the class C heterodimer formed by T1R1 and T1R3 are sensors for the glutamate and aspartate amino-acid, commonly termed umami taste, while T1R2 and T1R3 associate to sense the sweet molecules, indicates that heteromerization is required for the perception of different taste stimuli. A change in the ligand binding domain (LBD) conformation relays an immediate restructuration of the dimeric interface, allowing to switch on downstream signals, which finally results in cell responses as diverse as taste perception can be[358–360]. Previous studies also suggested that for many documented 7TMRs heterocomplexes, such as δ-opioid-β_2-adrenergic[361], α_{2A} adrenergic-β_1-adrenergic[57], and adenosine A_{2A}-dopamine D_2 receptor[362], stimulation of only one of the components was sufficient to promote co-trafficking of the complex. Thus, the concept of 7TMRs co-trafficking in heterologous systems is not new. Pioneer observations suspected the co-internalization of two opioid receptors as a 7TMRs heterodimer, which were intensively studied for their pharmacology and their signaling as oligomers. The authors suggested that, etorphine treatment leads to internalization of δ-opioid receptor (δOR) when expressed alone, but not when it is coexpressed with κ-opioid receptor (κOR). However, they demonstrated that 30% of the surface fluorescence diminished indicating that δOR homodimer can be internalized in cells expressing both δOR and κOR. It was then proposed that heterodimerization may participate in mGluR2 co-internalization[64].

In the present study, our data suggest that expression of 5-HT_{2A}R affects the subcellular distribution of mGluR2 through a molecular mechanism that involves a physical interaction of the two protomers. We further show that in the same cells, mGluR2 responds differently to processes related to agonist-induced trafficking through endosomal compartments when expressed with 5-

$HT_{2A}R$. In addition, in glutamatergic excitatory postsynaptic elements of *HTR2A*$^{-/-}$ mouse frontal cortex, mGluR2 subcellular distribution is maintained close to the plasmalemma, similar to the prototypical localization observed in Flp-In T-REx stable HEK293 cells not induced to express 5-$HT_{2A}R$. Moreover, in cortical primary culture of 5-$HT_{2A}R$-deficient mice, the colocalization of mGluR2 and Rab5 is diminished, supporting the finding that 5-$HT_{2A}R$ expression favors Rab5-mediated internalization mGluR2.

Under basal state experimental conditions (*i.e.*, the dialyzed FBS used in the culture media is free of the endogenous neurotransmitter 5-HT) our data validate the intriguing observation that 5-$HT_{2A}R$ shows an elevated level of localization in intracellular vesicles, which could appear as an anomalous localization compared to most 7TMRs that are primarily addressed to the surface. This singular phenotype had previously been observed in several experimental systems, including HEK293 and CHO-K1 cells[40,88,363]. By assessing, in intact COS-7 cells, the interaction between 5-$HT_{2A}R$ and 5-$HT_{2C}R$'s PSD-95/Disc-large/Zonula occludens-1 (PDZ) domains and co-transfected pre or postsynaptic PDZ resident proteins, it was reported a prominent intracellular presence of 5-$HT_{2A}R$ when transfected alone, as a consequence of its interaction with specific sets of intracellular PDZ proteins[364]. Additionally, those protein sites together with PSD-95, being resident of the postsynaptic element, are in accordance with the main localization of 5-$HT_{2A}R$ in this compartment (see below). Although not mutually exclusive, the physical interaction of 5-$HT_{2A}R$ and PSD-95, besides providing structural localization, has also a functional role: PSD-95 enhances 5-$HT_{2A}R$-mediated activation of $G\alpha_q$ signaling as measured by IP accumulation in HEK 293 cells[365]. However, the direct interaction of 5-$HT_{2A}R$ and PSD-95 accounting for this phenotype was interpreted in two ways: PSD-95 would anchor 5-$HT_{2A}R$ in clusters to the cell surface, suggesting that its constitutive activity can be modulated by this postsynapytic proteins; and second, that this localization would favor interactions between 5-$HT_{2A}R$ and other downstream effectors to elicit agonist-induced signaling yet restricting agonist-dependent internalization of 5-$HT_{2A}R$[365]; here,

PSD-95 inhibits agonist-induced internalization of 5-HT_{2A}R in order to maintain the receptor near cell surface pools. This process is also thought to participate, through the recognition by PSD-95 of specific PDZ motifs borne by 5-HT_{2A}R, in its proper targeting to dendrites of pyramidal neurons[366]. In support of such cellular organization, it was also proposed that, similar to the agonist-independent G protein activation of 5-HT_{2C}R, 5-HT_{2A}R may also have constitutive activity in heterologous systems, although to a much lesser extent than the former receptor, hence its intracellular localization[367]. Later, the constitutive activity of the 5-HT_{2A}R has been reevaluated: using a cell-based functional assay, a stronger turnover was measured, that could be modulated by mutating residues in the helices 6 and 3 (interaction model) of the WT receptor[18,368]. Together, these reports in heterologous cellular systems addressed the nonstandard localization of 5-HT_{2A}R by providing functional and structural plausible explanations. Nonetheless, the 5-HT_{2A}R intracellular distribution is not restricted to such systems. Some of these regions contain neurons that express both 5-HT_{2A}R and mGluR2. While testing the subcellular distribution following the dendritic targeting mediated by the PDZ-binding domain of 5-HT_{2A}R, SFV-induced exogenous expression of 5-HT_{2A}R was found intracellularly, within dendrites of cortical primary neurons, in accordance with its endogenous distribution in culture[366].

Immunocytochemistry studies on rat cerebellar cortex and olfactory bulb demonstrated both intracellular and membranous expression of the 5-HT_{2A}R protein using two different antibodies, targeting either the receptor N-terminus or the C-terminus (both tested and exhibiting an intracellular presence in form of puncta in S2 cells)[369]. In the rat spinal cord and ganglia, the immuno-targeted 5-HT_{2A}R was observed in small and large neurons and also interpreted as intracellular, *i.e*. in “dot-like” cytoplasmic distribution[370]. The receptor was also immuno-reactive in the somata and dendrites of Purkinje cells and in neural bodies of deep cellular nuclei, where again, we could observed dot-like cytosolic patterns[133].

In the rat VTA, another study showed the prominent cytoplasmic localization of 5-HT_{2A}R-like immunoreactivity colocalizing with the enzyme tyrosine hydroxylase, marker of dopaminergic neurons in this region, where 92% of the immunogold particles was detected. Neurons where TH was not detected also displayed this intracellular pattern, and was interpreted as membrane recycling of surface receptors, with all the caution attributed to immunogold assays[127]. Given the highly probable constitutive activity of 5-HT_{2A}R (see above), it is possible to interpret this presence as agonist-independent activated receptor trafficking. Additionally, 5-HT_{2A}R immunoperoxidase stained other organelles such as the endoplasmic reticulum, Golgi apparatus, mitochondria and microtubules. This has also been observed in a study providing similar results in the rat cerebral cortex, using immunogold counterstaining and colocalization with the Microtubule Associated Protein 1A (MAP-1A)[371]. The authors validated previous findings addressing the large intracellular presence of 5-HT_{2A}R in the rat CNS[123], and specified the possible link between the intracellular enrichment of 5-HT_{2A}R in small dendrites of pyramidal neurons and the microtubule network, as a likely interaction with MAP-1A. This interaction could potentially generate more interactions with intracellular signaling molecules, and could also suggest an intracellular signaling role or a dynamic association between surface and cytosolic 5-HT_{2A}R[371]. A study focused on the caudate-putamen nucleus and the nucleus accumbens shell, attested that 5-HT_{2A}R and NMDAR colocalized in neuron's somata and dendrites. Interestingly, the intracellular presence of 5-HT_{2A}R was associated with cytoplasmic organelles rather than synaptic or extra-synaptic plasma membranes. Those neurons, assumed to be spiny striatal in the CPN and the NAc, were localized in dendrites and immuno-reacted with the endoplasmic reticulum and mitochondria. In the dorsolateral part of the CPN, labeling was more sharply localized in restricted areas between the plasma membrane and along mitochondria membranes, as well as in axon terminal endosomes, MVB, and small synaptic vesilcles[372]. In nociceptive neurons of rat lumbar dorsal root ganglia, 5-HT_{2A}R appeared in the cytoplasm, and at the junction of sensory and satellite cells, though also found at the plasma membrane of larger cell bodies[373]. While demonstrating the putative

interaction of 5-HT_{2C}R with 5-HT_{2A}R in the mPFC of rats, confocal images showed that in this critical region, 5-HT_{2A}R immunoreactivity was mostly intracellular[374]. In a study aiming to differentiate the anti-aversive action of serotonin inputs through activation of the 5-HT_{2A}R in the aversive system held within the midbrain periaqueductal grey matter, immunoreactivity was observed in both soma and dendrites of GABAergic interneurons[375]. The cytoplasmic localization of the 5-HT_{2A}R can also be found in unexpected cell types. Besides being observed in cell bodies and dendrites of pyramidal neurons in the cortex, the receptor was detected in Schwann cells using a newly developed monoclonal antibody targeting an epitope on the receptor N-terminal[376]. In rat hippocampus, 5-HT_{2A}R was detected in mossy fibers, indicating a presynaptic function of serotonin on glutamate axons. Additionally, the staining suggested that the receptor could be found on both excitatory and inhibitory neurons. Similar to the above findings, its intracellular presence was also recognized[377]. The approaches using immunoreactivity depends on the antibodies used, especially their reliability in terms of specificity[378]. It is possible, and often considered as a limitation, that several antibodies raised against different epitopes of the 5-HT_{2A}R receptor could lead to variable labelings of different cell types and subcellular localizations. However, the use of several antibodies at the same time followed by analysis of the matching profiles, allowed to validate and comfort the intracellular presence of the 5-HT_{2A}R[379]. The discrepancies could be attributed to the different conformations adopted by the receptor, *i.e.* different activation states that could reflect different levels of subcellular distribution: an antibody raised against the N-terminal end of the receptor would be likely inefficient to localized internalized vesicular receptors, because the N-terminal is in its lumen[126,380].

Conversely, the 5-HT_{2A}R was reported to be mostly located at the plasma membrane, in heterologous cell systems[261,381], or both intracellularly and at the cell surface[137]. In mouse cortical neurons, both the dendritic plasma membrane and the axon cytoplasm were positive for the serotonin receptor[252]. It is possible that the antibodies, used or the system itself, may contribute

to such variations in the distribution pattern of 5-HT_{2A}R. Another possibility is that, when the rat 5-HT_{2A}R is transfected in human cells, the trafficking proteins could not recognize its PDZ motif, which is different among species[382]. *In vivo*, ultrastructural studies of the rat spinal cord demonstrated a major localization of the 5-HT_{2A}R at the plasma membrane in many subregions[383]. However, the same study found substantial staining in intracellular organelles, such as endosomes and MVB. Moreover, 5-HT_{2A}R may take distinct functions whether localize in the spinal cord, as opposed to the cerebral cortex or the midbrain. This could explain such differences in its expression. In a more recent review, it was proposed and admitted that the 5-HT_{2A}R can actually function and traffic differently, in pre or post synaptic terminals, as well as in different cell types[384]. The mixed plasma membrane/cytoplasm distribution pattern of 5-HT_{2A}R was also observed in the intestine[385]. In non-human primates, similar findings have been reported[124].

Together, this collection of studies indicates that the 5-HT_{2A}R may be found in multiple brain regions where it adopts mixed distribution patterns, and more importantly, corroborates the intracellular distribution of the receptor. In heterologous cell systems, either the plasma membranous or the cytoplasmic pattern can be due to the absence of specific trafficking and signaling interacting partners that are present endogenously *in vivo*[386]. The presence or absence of ligand could also cause discrepancies. Moreover, the specific localization of a brain region and/or or cell type, determines the receptor's function; this is another point that could explain its mixed distribution pattern. Lastly, the technique in use and how it is carried out could also affect the results. Several hypotheses have been proposed to explain such atypical behavior for a class A 7TMR, such as constitutive activity, intracellular signaling and as a sensor for serotonin concentration. In accordance with our findings herein, another possibility may be explored in future work. The basal activity of the 5-HT_{2A}R was substancial in the stable cell line used, and this seemed to relocalize mGluR2, in absence of agonist. While the activation of 5-HT_{2A}R implicated Rab5-mediated internalization of mGluR2, it is possible that the serotonin receptor plays a role in

the internalization of unbound interacting receptors and promote their agonist-independent internalization. This is consistent with the observation that in presence of mGluR2 agonist LY379268, its colocalization with Rab5 is reversed. This mechanism is mediated by its heteromerization with 5-HT_{2A}R. Another possibility is that the heteromeric formation would signal from intracellular compartments, offering a novel functionally never observed previously.

Most 7TMRs are trafficked through the endocytic pathway after internalization[263,387]. We showed that, in the absence of 5-HT_{2A}R or mGluR2 agonists, the glutamate receptor colocalization indexes with endosome markers were higher when coexpressed with 5-HT_{2A}R, as compared to that obtained in HEK293 cells expressing mGluR2 alone. Our data also suggest that the presence of 5-HT_{2A}R in cells stably expressing mGluR2 increased mGluR2 colocalization with different markers of the endocytic pathway such as Rab5, Rab7, and the transferrin receptor. Considering that colocalization of mGluR2 and Rab5 was also reduced in *5-$HT_{2A}R^{-/-}$* mouse cortical primary cultures, these data provide evidence that 5-HT_{2A}R's constitutive activity affects the localization of mGluR2 within individual components of the endocytic pathway.

Although an important proportion of the 5-HT_{2A}R population is located intracellularly, we and others have validated the expected finding that addition of 5-HT_{2A}R agonists, including 5-HT or DOI, leads to activation of $G\alpha_{q/11}$ protein-dependent pathways, such as stimulation of phospholipase C (PLC) activity, which increases intracellular inositol triphosphate (IP3), diacylglycerol (DAG) and intracellular Ca^{2+} levels[251,254,388].

When HEK293 cells were transfected with both 5-HT_{2A}R-mCherry and mGluR2-mCitrine construct, we observed that mGluR2 is relocalized intracellularly like it is partially adopting the pattern of the serotonin receptor. However, this was not the case for all cells cotransfected with both constructs; while the 5-HT_{2A}R-mCherry was localized inside all the observed cells, mGluR2-eYFP was still maintained at the plasma membrane for some of them. It is likely that not all the cells express the same exact ratio of 5-HT_{2A}R/mGluR2 receptors. The relative stoichiometry, or

the amount of transfected DNA penetrating the cells in terms of copies, has been shown to affect the crosstalk between 5-HT_{2A}R and mGluR2, responsible for the mobilization of GIRK1/GIRK4 currents as a reporter of $G\alpha_i$ and $G\alpha_q$ activation. It has been already reported that in HEK 293 cells, the relative stoichiometry between the two cotransfected receptors is critical to elicit a robust crosstalk[251,254]. Because the functional crosstalk has been validated by several functional assays (GIRK current and Ca^{2+} mobilization), in this study we selected clones that elicited a robust cross-signaling in addition to their intracellular colocalization. In transfected cells that express 5-HT_{2A}R-mCherry and mGluR2-eYFP, the exact number of inserted genes was not assessed, and it is possible that the relative stoichiometry between the two receptors was not conserved. Together, these observations provide an interesting conclusion, suggesting that, in cells, a characteristic stoichiometry is necessary to elicit both the functional crosstalk and the co-trafficking of 5-HT_{2A}R and mGluR2. Further work would be required to determine what is the exact relative stoichiometry in neurons co-expressing the two receptors and likely prone to cross-signal, and compare the findings to the number of exogenous DNA copies inserted into the cell genome of crosstalk positive clones.

These above considerations incline to speculate that a critical stoichiometry between 5-HT_{2A}R and mGluR2 can either be beneficial (*i.e.* physiologic) or detrimental (over/under-expressed) for the neuron and its neurotransmission, and that the intracellular localization of 5-HT_{2A}R is an important factor of regulation. This is relevant to schizophrenia. Following the simplest hypothesis that trafficking controls proteins' subcellular spatial and temporal distribution, it is then possible that a defect in this synchronicity may lead to unbalanced ratio of receptors, which, if maintained for a substantial amount of time and because of the entanglement of receptor trafficking and signaling, increase the likelihood to generate a global failure, in a form of a neuropsychiatric disorder.

The implication of subcellular trafficking in schizophrenia was the topic of several symposia where, for the first time, to our knowledge, links were made between gene association and molecular

mechanisms[389]. In particular, several themes were related to endosomal trafficking and clathrin-coated dependent endocytosis, as well as the *DTBNP1* gene[390]. In post mortem tissues extracted from subjects with psychotic disorders, altered levels of several proteins interacting with clathrin, AP-2 and dynamin-1, among others, have been found[391]. These proteins regulate lysosome positioning and expression, endosomal trafficking and cell division (this review article lists several other proteins implicated in trafficking and detected in genetic or GWAS association studies). The *DTNBP1* gene is cited among several other primary candidates associated or altered in schizophrenia, such as *COMT*, *NRG1*, *RGS4*, *GRM3*, and *DISC1*[143,392,393].

Emerging hypotheses shedded light on a possible genetic dysregulation of the trafficking machinery and more specifically, the endosomal system, resulting in neurochemical and signaling abnormalities[390,391]. It is supported by genome wide analyses that detected several genes implicated in schizophrenia related to the endosomal trafficking, and in particular to the potential defects of the Biogenesis of Lysosome-related Organelles Complex-1 (BLOC-1). The dystrobrevin-binding protein 1 (*DTNBP1*) gene that encodes the dysbindin-1 protein, together with *MUTED*, are essential components of the BLOC-1 protein complex, and has become a highly scrutinized gene for its implication in schizophrenia[317,394], as well as in cognition in healthy subjects[395]. Dysbindin is widely expressed in neurons, in both presynaptic terminal and postsynaptic densities throughout the brain[395,396]. It is expressed in regions known to contain both 5-HT_{2A}R and mGluR2, such as the frontal and temporal cortexes, certain nuclei of the basal ganglia, the hippocampus, the thalamus, the amygdala, as well as the midbrain, which receives inputs from the claustrum that may control conditioning and sleep[397], a region that also receives main serotoninergic innervation from the DR[398]. Dysbindin mRNA is reduced in the dorsal prefrontal cortex and in the midbrain of patients with schizophrenia[399]. In the hippocampus of those patients, both mRNA and dysbindin protein are reduced. More importantly, this reduction in the contribution of dysbindin in the proper functioning of BLOC-1 has been shown to affect the surface

localization of D_2R, one of the main class A 7TMRs involved in both schizophrenia physiopathology and its treatment. The dopamine hypothesis indeed postulates that, within the PFC, the D_2R-D_1R ratio is imbalanced in favor of D_2R, resulting in a reduction of the cortical excitability concomitant with a reduction of the inhibitory strength of GABA interneurons[400]. In human SH-SY5Y neuroblastoma cells and in cultured cortical neurons, the reduction in dysbindin expression has been shown to augment the cell surface presence of D_2R, but not D_1R[401]. siRNA-induced downregulation of dysbindin decreased levels of SNAP25 and synapsin I, together with a reduction of glutamate release, suggesting that dysbindin plays a role in exocytosis of glutamate containing synaptic vesicles[402]. Similar findings have also been reported in the *sandy* mouse (a natural occurring null mutation of *DTNBP1*)[403]. Other components of the BLOC-1, such as snapin and pallidin, can respectively interact with SNAP25 and syntaxin 13[401], two members of the SNARE family, master regulators of membrane fusion[404,405]. It has also been proposed that, under elevated synaptic activity, pallidin interacts with Rab5 to recycle synaptic vesicles more efficiently in pools within early endosomes. Interestingly, in yeast, BLOC-1 may also regulate and participate to the early endosome maturation by interacting with Rab5 homolog[406]. These interactions, if altered, can also affect the dynamic and the spatial distribution of endosomes by disturbing the actin/microtubule cytoskeleton structure[407]. In the case of dysbindin, it has also been shown that the protein does not primarily regulate the endocytic trafficking, but rather influences later steps that lead to degradation. The overcharge of D_2R at the cell surface is a consequence of an inefficient degradation capacity. Additionally, the authors also suggest that this role of dysbindin is perhaps not strictly specific to D_2R but also to other 7TMRs, in various cell types[408]. The presynaptic reduction of dysbindin was also correlated with an augmentation of VGLUT-1 in the hippocampus of more than 75% of the studied schizophrenia population. It has thus been suspected that, because altered DTNBP1 in presynaptic glutamatergic terminals can cause BLOC-1 to dysfunction, the augmentation of VGLUT-1 can result from a lesser degradative

function of BLOC-1, thus providing a plausible cause of glutamate dysfunction in schizophrenia[399,409,410].

It is then tempting to speculate that a defect in receptor stoichiometry, for instance 5-HT_{2A}R and mGluR2, due to a defect in protein trafficking/signaling, and/or vice-versa, is a plausible explanation for the dysregulation observed in patients with schizophrenia syndrome[183]. What could be at the origin of such a breakdown of the trafficking system is beyond the scope of this study; it is possible that persistent epigenetic alterations can cause such deleterious effects in the core machinery of protein synthesis and recycling[411,412].

Many neuropsychiatric disorders, including schizophrenia, could be caused by alterations of the dopaminergic neurotransmission and related subcellular signaling[413]. Hyperdopaminergic activation in the prefrontal cortex (*i.e.*, increased D_2/D_1 ratio) associated with a lack of dopamine tone in the striatum, may account for both positive and negative symptoms of the schizophrenia syndrome[414–416]. The actual mechanism is complex but one model described that in dysbindin-deficient primary cortical neurons of *sandy* mice, BLOC-1-mediated trafficking of D_2R toward its degradation following ligand binding, corresponded to a reduction of dopamine-induced subcellular internalization of D_2R. As a result, abundant D_2R receptors at the cell surface seemed to traffic much faster than D_1R[400]. This excess of signaling has deleterious effects on the GABAergic neurons by reducing their excitability in the PFC and in the striatum, and more precisely, in the layer V of the PFC pyramidal neurons[400]. These defects could be the results of the dopamine neurotransmission imbalance observed in schizophrenia[400]. First generation antipsychotics have high affinity for the D_2R, although atypical antipsychotics target the receptor as well[309,314,415,417,418].

In the case of a defect in the 5-HT_{2A}R trafficking in the PFC, similar to the effects described above on D_2R, it is possible that a disruption of the constitutive activity of 5-HT_{2A}R, either by a defect of the endocytosis or the degradation processes, could lead to receptor overexpression and because

5-HT_{2A}R seemed to co-internalize mGluR2, the latter would also be downregulated, resulting in the loss of inhibition of glutamatergic transmission by the PFC neurons. This is consistent with the fact that agonists of mGluR2 have a potential antipsychotic activity. Thus, it would be interesting to search into the relationship between 5-HT_{2A}R mGluR2 and DTNBP1, although a study has implicated 5-HT_{2A}R and dysbindin in humans[419]. This is supported by the fact that the involvement of the *HTR2A* gene in the physiopathology of schizophrenia is not clear. Since neither apparent gene mutations, nor alteration of the receptor binding properties have been clearly demonstrated, it is possible to speculate that the regulation of the receptor is involved, rather than structural impairments of the peptide[420].

The potential role of heteromerization as the mechanism underlying the effect of 5-HT_{2A}R on subcellular localization of mGluR2 is supported by our findings demonstrating intracellular localization of the heterocomplex by BiFC, PLA and FRET. Surprisingly, we could not detect any FRET signal nor PLA association near the plasma membrane. As above-mentioned, most of the 5-HT_{2A}R seems located intracellularly, and despite being able to elicit a fast calcium mobilization, validating the fact that 5-HT_{2A}R can signal from the plasma membrane (as it is difficult to imagine that a monoamine like 5-HT crosses the plasma membrane and binds intracellular receptors), there was low to no interactions in this area. There was though a very faint eCFP fluorescence at the plasma membrane. This is puzzling and somewhat not consistent with the standard localization of most 7TMRs. If these findings are consistent, it will be necessary to further examine the role of receptor heteromers in the intracellular trafficking and signaling or 7TMRs.

Recent findings point towards instability of a family A 7TMR oligomeric interface[47,48,81]. Our current data demonstrating that the assembly of 5-HT_{2A}R and mGluR2 is able to modulate and affect dramatically the distribution of one of them can hardly be explained by a transient interaction lasting fractions of seconds as it has been demonstrated for other class A 7TMRs (kiss-and-fly model)[31,421–423]. Here, the interclass 7TMR heteromeric assembly supports the concept that 5-

$HT_{2A}R$ and mGluR2 are part of a stable receptor complex structure that is co-trafficked and can cross-signal consistently along different experiments[251,253,254,424]. Our findings in the maturation pathway, suggesting that 5-$HT_{2A}R$ and mGluR2 can come together in close enough proximity to be detected by BiFC confocal microcopy support that, at least in these compartments, the existence of a stable heteromer is conceivable. Further work, however, will be necessary to fully characterize the dynamics of this structural assembly. Given the active and structurally preferential TM domain involved in the homodimerization of mGluR2/3 and 5-$HT_{2A}R$, a recent photocrosslinking study addressed with high accuracy the potential TM domain at the interface of the heterocomplex formed by 5-$HT_{2A}R$ and mGluR2[89]. This indicates a potential site of stabilization that would explain herein results especially in the surprising case of DOI activating 5-$HT_{2A}R$-dependent trafficking of mGluR2 in Rab5 endosomes. Although previously thought as stable, the μ-opioid receptor dimer has recently been observed as a minor and negligible entity[51]. Whether 5-$HT_{2A}R$ association with mGluR2 it is stable or not, and whether this is a limitation, has to be addressed by additional experiments, such as single-molecule pull-down assay (SiMPull) assay[425–427].

An interesting observation was that whereas DOX-induced expression of 5-$HT_{2A}R$ augments the density of mGluR2, but not that of mGluR3 or mGluR2ΔTM4, $G\alpha_{i/o}$ protein coupling induced upon activation of mGluR2 was substantially reduced in DOX(+) cells as compared to DOX(−) cells. Although this finding further supports specificity of the cross-talk between 5-$HT_{2A}R$ and mGluR2, the exact mechanism remains to be investigated. Nevertheless, a potential explanation to reconcile these results is the existence of a compensatory pathway to rescue mGluR2-dependent function due to the higher degree of mGluR2 intracellular localization upon DOX-induced 5-$HT_{2A}R$ expression.

Acting through 5-$HT_{2A}R$, LY379268 and DOI differently affected the distribution of mGluR2 within Rab5-positive endocytic vesicles, as well as the physical interaction between 5-$HT_{2A}R$ and

mGluR2. Thus, we found that whereas coexpression of 5-HT_{2A}R prevented the effect of mGluR2 agonists on both mGluR2 endocytosis and down-regulation, agonist-induced activation of mGluR2 decreased its physical proximity with 5-HT_{2A}R. Our data also support the conclusion that agonist activation of 5-HT_{2A}R increased the colocalization between mGluR2 and Rab5. This effect required 5-HT_{2A}R–mGluR2 heteromeric assembly because it was reduced by the interfering peptide TAT-TM4. However, under the same experimental conditions, and opposite to the effects of LY379268, both mGluR2 density and 5-HT_{2A}R–mGluR2 heteromerization remained unchanged. These data suggest that whereas DOI augments intracellular distribution of mGluR2 within Rab5-positive and clathrin-dependent endosomes coexpressing 5-HT_{2A}R and mGluR2, internalized mGluR2 is not degraded after entering the late endosomal/lysosomal pathway. Sorting of mGluR2 into the recycling pathway could provide a potential explanation. Additional work will be necessary to determine the population of intracellular vesicles downstream of Rab5-positive endosomes responsible for increased endocytic uptake of mGluR2 without receptor down-regulation.

In the absence of DOI, colocalization of mGluR2 and Rab5 was comparable between cells exposed to either TAT-TM4 or the TAT-tagged scrambled peptide. This absence of effect of TAT-TM4 on colocalization of mGluR2 and Rab5 at steady-state conditions does not call into question the capability of the TAT-tagged peptide to reduce 5-HT_{2A}R–mGluR2 complex assembly. Instead, together with the effect of TAT-TM4 preventing DOI-induced augmentation of mGluR2 localization within Rab5-positive endosomes, these findings suggest that, in the absence of exogenous agonists such as DOI, disruption of 5-HT_{2A}R–mGluR2 heteromerization does not imply rapid mGluR2 trafficking from Rab5-positive endosomes to alternative endocytic compartments.

Although discovered in the late 1950's[428], clozapine still remains the gold standard for schizophrenia treatment[429]. It binds with relatively low affinity to dopamine D_2R and other monoaminergic neurotransmitter receptors, but similarly to other atypical antipsychotics, clozapine

shows a particularly high affinity for 5-HT_{2A}R[430,431]. Activation of mGluR2 by mGluR2/3 agonists, including pomaglumetad or LY2140023 (an oral prodrug of LY404039), has been proposed to treat tripartite symptoms in patients with schizophrenia[226], but pomaglumetad did not show enough clinical utility[432]. We previously proposed that chronic treatment with clozapine and other atypical antipsychotics induces a selective down-regulation of *mGluR2* expression through an epigenetic mechanism involving repressive histone modifications at the promoter region of the *mGluR2* (*GRM2*) gene in mouse and human frontal cortex[433,434]. These preclinical findings were validated by clinical work showing the absence of therapeutic effects of pomaglumetad in patients with schizophrenia previously treated with atypical antipsychotic medications[435]. Our current findings here propose an alternative, although not mutually exclusive, explanation by which long-lasting exposure to clozapine down-regulates mGluR2 density through a mechanism that requires its heteromerization with the 5-HT_{2A}R. We observed that subcellular colocalization between 5-HT_{2A}R and mGluR2 was reduced upon clozapine exposure. This effect was not induced by overnight exposure to M100907, was not observed in cells stably expressing mGluR2ΔTM4 and induced to express 5-HT_{2A}R, and was prevented by a TAT-tagged peptide that disrupts 5-HT_{2A}R–mGluR2 heteromerization. Similarly, clozapine, but not M100907, reduced total mGluR2 density and mGluR2 localization at both cell surface and in intracellular compartments. Thus, continued exposure to clozapine, but not M100907, affects mGluR2's subcellular distribution and density through a mechanism that requires 5-HT_{2A}R–mGluR2 complex formation. Further work will be necessary to better understand the trafficking pathway responsible for alterations in mGluR2 cellular distribution among 5-HT_{2A}R–positive intracellular vesicles and plasma membrane.

In the perspective of studying repressive epigenetic mechanisms at the *mGlu2* promoter, our lab showed that in mouse frontal cortex lacking the *HTR2A* gene, the mRNA level of *mGlu2* are also decreased, whereas *5-HT_{2C}* and *mGlu2* levels are not affected. Although these findings demonstrate in animal model an effect of 5-HT_{2A}R affecting mGlu2 at the transcription level, our

results in a cellular system showed that expression of 5-HT_{2A}R have a tendency to upregulate mGluR2 at the protein level. Although these two observations are distant to the mechanism of action, both seem to be consistent, although there is no evidence yet to prove it.

Exposure of GF-62 cells to 5-HT_{2A}R antagonists, including clozapine, has been shown to internalize the receptor which decreased its cell surface density. Similarly, an increase in the intracellular concentration of 5-HT_{2A}R in apical dendrites of rat pyramidal cells has been reported, following exposure to such drugs. An alternative mechanism to ligand-induced dynamin dependent endocytosis has been proposed, involving caveolae[436]. In the present study, we observed that in HEK293 cells induced to express 5-HT_{2A}R, several inverse agonists/antagonists relocated the receptor intracellular distribution to the plasma membrane area. Although it is not clear whether the receptor is actually spanning the membrane or stationing underneath in endosomes, only clozapine treatments seemingly failed to relocate the receptor. Even more surprising was that olanzapine, a clozapine analog, did affect 5-HT_{2A}R localization. Such puzzling finding would require fine investigations on how antagonists or inverse agonists affect the constitutive activity of 5-HT_{2A}R. The constitutive activity of 5-HT_{2A}R can affect ritanserin potency[18]. It is also a property of inverse agonists to affect the basal activity of 5-HT_{2A}R, while antagonist compounds should remain “inactive”[22]. A study *in vivo* provided more insights into this particular mode of action typical to 5-HT_{2A}R[437].

We were unable to characterize the function of our mGluR3 clones with the GTPγS assay. This is the reason why HEK293 were transfected with the chimeric G protein qi9, in order to test intracellular calcium release. The positive signal elicited by mGlu3 clones suggested that the cell line held a functional receptor. To note, we observed a large presence of intracellular eYFP-positive vesicles, attesting of a constitutive activity of the mGlu3 receptor. In the second step, we recently addressed the reason why mGluR3 was not able to efficiently mobilize $G\alpha_i$ protein signaling. In several brain tissues, GTPγS assays were performed in presence of the NAM

mGluR3. Robust signal was elicited accounting for the presence of mGluR2 and mGluR3 composite signals. Application of NAM reduced the signal elicited by LY379268 binding in the GTPγS readout (data not shown, in progress). Together, this indicates that mGluR3 can efficiently couple to G proteins, but for an unknown reason, this was not the case in our cell line. A consistent analogy is provided by a study that was able to distinguish mGluR2 signaling from mGluR3[230].

Considering our findings in this heterologous cellular system, the fact that over expression or overactivation of the 5-HT_{2A}R may as well induce over internalization of mGluR2 into more internalized compartment is consistent with a defect of activity. It would reduce the surface availability and the overall density of mGluR2, and likely damped the effect of antipsychotic glutamate agonists such as pomaglumetad. Our findings showed that coexpression of 5-HT_{2A}R and mGluR2 elicited some populations of more internal glutamate receptors, whereas as in average, unlike WT, 5-$HT_{2A}R^{-/-}$ mice postsynaptic area, mGluR2 tends to be nearby the plasmalemma.

Concluding remarks

Although some reported examples may reflect data overinterpretation or ambiguity due to the system in use, the concept that class A 7TMRs form receptor complexes is supported by numerous experimental approaches. As of yet, the functional importance of 7TMRs oligomerization remains controversial. Our data obtained with stable expression of mGluR2 or mGluR2/mGluR3 chimeric constructs and TAT-tagged peptides to disrupt 5-HT_{2A}R–mGluR2 complex formation support the conclusion that 5-HT_{2A}R affects the subcellular localization of mGluR2 through 7TMR heteromerization. The validity of this concept is further advanced by our findings showing alterations in mGluR2 cellular distribution in frontal cortex pyramidal neurons of *5-$HT_{2A}R^{-/-}$* mice as compared to control littermates. In short, these findings illuminate the importance of interclass heteromerization on 7TMRs localization and trafficking.

Limitations

The relatively low percentage of FRET efficiency is also consistent with the relative proportion but also the orientation of the fluorescent proteins. As we cannot establish a positive control to detect what is the maximum efficiency of this system, we could not compare our signal to a standard maximum FRETe. However, we showed that the mGluR2ΔTM4-eYFP chimera FRETe was reduced by 2 folds. This indicates that the interaction is less stable with the mutant or alternatively, we cannot rule out that the mutant's fluorescent protein is orientated differently. Orientation of the fluorescent protein is critical for the FRET to occur and its efficiency. Another possibility is that, as the KD of the mutant is higher than the WT (Table 1), the function of this receptor is affected and could not change its conformation as the WT does.

Another important question was the origin of mGluR2 trafficked by 5-HT_{2A}R. We showed that the application of the dynamin inhibitor dynasore prevented endocytosis of mGluR2 when 5-HT_{2A}R was coexpressed. Additionally, BiFC and FACS experiments suggested that the 5-HT_{2A}-mGlu2 receptor heteromer could be synthesized in the ER, and also detected in the Golgi apparatus. Several hypotheses can be provided: the heterocomplex is stable from it biosynthesis in the ER to the plasma membrane and it is trafficked as a stable entity; partially synthesized in the ER and partially assembled later at the cell surface or in endosomes; or mGlu2 provides an ER exit routes for 5-HT_{2A}R, similar to the $GABA_B$R or β_2AR, and the association is dynamic during the trafficking or upon ligand-induced G protein activation. An known limitation to those findings using the BiFC assay, is that complements of the fluorescent protein can be covalently fused and therefore, the heteromeric association is irreversible[438,439]. This has limited our studies to the maturation pathway, which suggested, even if the association is irreversible, that a close contact occurred. Additional work would be necessary to delineate and ascertain the directionality and the timeline of this association, for example by tracking 5-HT_{2A}R biosynthesis and trafficking in mGluR2$^{-/-}$ mice.

Although the HEK293 cells have been used extensively and reliably over the past decades as a neuronal model subrogate, they are not neurons. If they do not express mGluR2 and 5-HT_{2A}R, they still translate 7TMR interacting proteins, scaffolds and chaperones necessary for endogenous cellular operations and contain the basic machinery to robustly allow and maintain the structure and the function of overexpressed 7TMRs, or other transfected or stable receptors and transporters. It is interesting to have in mind the native receptor expressed by this cell line and control the expression of close and studied receptors to avoid any interference[440]. There is no serotonin in our DMEM, although serotonin is an important neurotransmitter and a hormone for the kidney function. *GRM2* and *GRM3* are also absent though it seems that *GRM2* has traces as assessed by a microarray study[440].

The question about the affinity of the mGlu2 chimera compared to the WT mGluR2 has not been addressed in this study. Whether the difference in affinity comes from the impaired association with 5-HT_{2A}R or the mutant by itself, constitutes a point to address.

Colocalization analyses sometime yielded high variances among and within experiments. This is perhaps due to the fact that not all cells elicit the same amount of 5-HT_{2A}R-eCFP after being induced, and because stoichiometry seems important, this can lead to a differential internalization of mGluR2 consistent with the level of 5-HT_{2A}R in Rab5 or Rab7.

The primary cortical cultured neurons were extracted from embryonic mice. Because we used the total cortical area, the exact nature of the neurons analyzed by immunofluorescence is not known, although we favored pyramidal shaped neurons in our collection.

The Pearson correlation coefficient is sensitive to the fluorescence intensity because the correlation is maximal when intensities are linearly associated. The use of Manders coefficient was more appropriate in those cases, and explains why the tandem was not systematically used in this study.

Table 1

[^{3}H]LY341495 binding saturation curves in Flp-In T-REx HEK293 cells

	DOX(-)		DOX(+)	
	K_D	**B_{max} (pmol/mg prot)**	**K_D**	**B_{max} (pmol/mg prot)**
mGluR2-eYFP	1.59 ± 0.21	36.94 ± 1.43	2.27 ± 0.15	51.81 ± 1.11
mGluR3-eYFP	1.16 ± 0.24	5.47 ± 0.30	0.68 ± 0.08	5.56 ± 0.16
mGluR2ΔTM4-eYFP	89.4 ± 4.84	2.33 ± 0.38	105.4 ± 4.03	3.77 ± 0.38

[^{3}H]LY341495 binding saturation curves in Flp-In T-REx HEK293 cells stably expressing mGluR2-eYFP, mGluR3-eYFP or mGluR2ΔTM40-eYFP and harboring 5-HT_{2A}R-eCFP at the inducible locus. Cells were untreated [DOX(-)] or treated with doxycycline [DOX(+)] (n = 2). The data are presented as the mean ± s.e.

[^{3}H]ketanserin binding saturation curves in Flp-In T-REx HEK293 cells

	DOX(-)		DOX(+)	
	K_D	**B_{max} (fmol/mg prot)**	**K_D**	**B_{max} (fmol/mg prot)**
mGluR2-eYFP	n/a	n/a	0.65 ± 0.07	3211 ± 115.9
mGluR3-eYFP	n/a	n/a	0.64 ± 0.09	3343 ± 153.7
mGluR2ΔTM4-eYFP	n/a	n/a	0.74 ± 0.12	7923 ± 416.0

[^{3}H]Ketanserin binding saturation curves in Flp-In T-REx HEK293 cells stably expressing mGluR2-eYFP, mGluR3-eYFP or mGluR2ΔTM40-eYFP and harboring 5-HT_{2A}R-eCFP at the inducible locus. Cells were untreated [DOX(-)] or treated with doxycycline [DOX(+)] (n = 2). The data are presented as the mean ± s.e. n/a, not applicable.

REFERENCE CITED

1. Cvicek, V., Goddard, W. A. & Abrol, R. Structure-Based Sequence Alignment of the Transmembrane Domains of All Human GPCRs: Phylogenetic, Structural and Functional Implications. *PLOS Comput. Biol.* **12**, e1004805 (2016).
2. JC Venter, M. A. E. M. P. L. R. M. G. S. *et al.* The sequence of the human genome. *Science (80-.).* **291**, 1304–1351 (2001).
3. Willyard, C. Expanded human gene tally reignites debate. *Nature* **558**, 334–335 (2018).
4. Gurevich, V. V. & Gurevich, E. V. GPCRs and Signal Transducers: Interaction Stoichiometry. *Trends Pharmacol. Sci.* **39**, 672–684 (2018).
5. Robinson, D. R., Wu, Y. M. & Lin, S. F. The protein tyrosine kinase family of the human genome. *Oncogene* **19**, 5548–5557 (2000).
6. Hauser, A. S., Attwood, M. M., Rask-andersen, M. & Schiöth, H. B. Trends in GPCR drug discovery: new agents, targets and indications Alexander. *Nat. Rev. Drug Discov.* **16**, 829–842 (2019).
7. Garland, S. L. Are GPCRs still a source of new targets? *Journal of Biomolecular Screening* **18**, 947–966 (2013).
8. Wei, H. *et al.* Independent β-arrestin 2 and G protein-mediated pathways for angiotensin II activation of extracellular signal-regulated kinases 1 and 2. *Proc. Natl. Acad. Sci. U. S. A.* **100**, 10782–10787 (2003).
9. Gesty-Palmer, D. *et al.* A β-arrestin-biased agonist of the parathyroid hormone receptor (PTH1R) promotes bone formation independent of G protein activation. *Sci. Transl. Med.* **1**, (2009).
10. Brzostowski, J. A. & Kimmel, A. R. Signaling at zero G: G-protein-independent functions for 7-TM receptors. *Trends Biochem. Sci.* **26**, 291–297 (2001).
11. Schöneberg, T., Hofreiter, M., Schulz, A. & Römpler, H. Learning from the past: evolution of GPCR functions. *Trends Pharmacol. Sci.* **28**, 117–121 (2007).
12. King, N., Hittinger, C. T. & Carroll, S. B. Evolution of key cell signaling and adhesion protein families predates animal origins. *Science (80-.).* **301**, 361–363 (2003).
13. Peroutka, S. J. & Howell, T. A. The molecular evolution of G protein-coupled receptors: Focus on 5-hydroxytryptamine receptors. *Neuropharmacology* **33**, 319–324 (1994).
14. Kolakowski, L. F. GCRDb: A G-protein-coupled receptor database. *Receptors and Channels* **2**, 1–7 (1994).
15. Pin, J. P., Bockaert, J. J. L. Molecular tinkering of G protein-coupled receptors : an evolutionary success. *EMBO J.* **18**, 1723–1729 (1999).
16. Fredriksson, R., Lagerström, M. C., Lundin, L.-G. G. & Schiöth, H. B. The G-protein-coupled receptors in the human genome form five main families. Phylogenetic analysis, paralogon groups, and fingerprints. *Mol. Pharmacol.* **63**, 1256–1272 (2003).
17. Massotte, D. & Kieffer, B. L. Structure—Function Relationships in G Protein-Coupled Receptors. in *The G Protein-Coupled Receptors Handbook* 3–31 (Humana Press, 2008). doi:10.1007/978-1-59259-919-6_1
18. Shapiro, D. A., Kristiansen, K., Weiner, D. M., Kroeze, W. K. & Roth, B. L. Evidence for a model of agonist-induced activation of 5-hydroxytryptamine 2A serotonin receptors that

involves the disruption of a strong ionic interaction between helices 3 and 6. *J. Biol. Chem.* **277**, 11441–11449 (2002).

19. Hu, G. M., Mai, T. L. & Chen, C. M. Visualizing the GPCR Network: Classification and Evolution. *Sci. Rep.* **7**, 1–15 (2017).

20. Mustafa, A. K., Gadalla, M. M. & Snyder, S. H. Signaling by Gasotransmitters. *Sci. Signal.* **2**, re2 (2009).

21. Hilger, D., Masureel, M. & Kobilka, B. K. Structure and dynamics of GPCR signaling complexes. *Nat. Struct. Mol. Biol.* **25**, 4–12 (2018).

22. Sullivan, L., Clarke, W. & Berg, K. Atypical antipsychotics and inverse agonism at 5-HT_2 receptors. *Curr. Pharm. Des.* **21**, 3732–3738 (2015).

23. Heuss, C., Scanziani, M., Gähwiler, B. H. & Gerber, U. G-protein-independent signaling mediated by metabotropic glutamate receptors. *Nat. Neurosci.* **2**, 1070–1077 (1999).

24. Heuss, C. & Gerber, U. G-protein-independent signaling by G-protein-coupled receptors. *Trends Neurosci.* **23**, 469–475 (2000).

25. Shenoy, S. K. *et al.* β-Arrestin-dependent, G Protein-independent ERK1/2 Activation by the β2 Adrenergic Receptor. *J. Biol. Chem.* **281**, 1261–1273 (2006).

26. Sun, Y. *et al.* Dosage-dependent switch from G protein-coupled to G protein-independent signaling by a GPCR. *EMBO J.* **26**, 53–64 (2007).

27. Cong, X., Topin, J. & Golebiowski, J. Class A GPCRs: Structure, Function, Modeling and Structure-based Ligand Design. *Curr. Pharm. Des.* **23**, 4390–4409 (2017).

28. Muto, T., Tsuchiya, D., Morikawa, K. & Jingami, H. Structures of the extracellular regions of the group II/III metabotropic glutamate receptors. *Proc. Natl. Acad. Sci. U. S. A.* **104**, 3759–3764 (2007).

29. Fonseca, J. M. & Lambert, N. A. Instability of a class A G protein-coupled receptor oligomer interface. *Mol. Pharmacol.* **75**, 1296–1299 (2009).

30. Kasai, R. S. *et al.* Full characterization of GPCR monomer-dimer dynamic equilibrium by single molecule imaging. *J. Cell Biol.* **192**, 463–480 (2011).

31. Kasai, R. S., Ito, S. V., Awane, R. M., Fujiwara, T. K. & Kusumi, A. The Class-A GPCR Dopamine D2 Receptor Forms Transient Dimers Stabilized by Agonists: Detection by Single-Molecule Tracking. *Cell Biochem. Biophys.* **76**, 29–37 (2018).

32. Hebert, T. E. *et al.* A peptide derived from a β 2-adrenergic receptor transmembrane domain inhibits both receptor dimerization and activation. *J. Biol. Chem.* **271**, 16384–16392 (1996).

33. González-Maeso, J. GPCR oligomers in pharmacology and signaling. *Mol. Brain* **4**, 20 (2011).

34. Gaitonde, S. A. & González-Maeso, J. Contribution of heteromerization to G protein-coupled receptor function. *Curr. Opin. Pharmacol.* **32**, 23–31 (2017).

35. Lan, T. H. *et al.* BRET evidence that β2 adrenergic receptors do not oligomerize in cells. *Sci. Rep.* **5**, 1–12 (2015).

36. Milligan, G. & Bouvier, M. *Methods to monitor the quaternary structure of G protein-coupled receptors. FEBS Journal* **272**, 2914–2925 (John Wiley & Sons, Ltd (10.1111), 2005).

37. Han, Y., Moreira, I. S., Urizar, E., Weinstein, H. & Javitch, J. A. Allosteric communication between protomers of dopamine class a GPCR dimers modulates activation. *Nat. Chem.*

Biol. **5**, 688–695 (2009).

38. Whorton, M. R. *et al.* Efficient coupling of transducin to monomeric rhodopsin in a phospholipid bilayer. *J. Biol. Chem.* **283**, 4387–4394 (2008).

39. Sartania, N., Appelbe, S., Pediani, J. D. & Milligan, G. Agonist occupancy of a single monomeric element is sufficient to cause internalization of the dimeric β2-adrenoceptor. *Cell. Signal.* **19**, 1928–1938 (2007).

40. Lopez-Gimenez, J. F., Canals, M., Pediani, J. D. & Milligan, G. The α1b-adrenoceptor exists as a higher-order oligomer: Effective oligomerization is required for receptor maturation, surface delivery, and function. *Mol. Pharmacol.* **71**, 1015–1029 (2007).

41. Ge, B. *et al.* Single-molecule imaging reveals dimerization/oligomerization of CXCR4 on plasma membrane closely related to its function. *Sci. Rep.* **7**, 1–9 (2017).

42. Smith, T. H., Li, J. G., Dores, M. R. & Trejo, J. A. Protease-activated receptor-4 and purinergic receptor P2Y12 dimerize, co-internalize, and activate Akt signaling via endosomal recruitment of -arrestin. *J. Biol. Chem.* **292**, 13867–13878 (2017).

43. Jin, J. *et al.* CCR5 adopts three homodimeric conformations that control cell surface delivery. *Sci. Signal.* **11**, 2869 (2018).

44. Dorsch, S., Klotz, K.-N., Engelhardt, S., Lohse, M. J. & Bünemann, M. Analysis of receptor oligomerization by FRAP microscopy. *Nat. Methods* **6**, 225–230 (2009).

45. Marsango, S. *et al.* A molecular basis for selective antagonist destabilization of dopamine D3 receptor quaternary organization. *Sci. Rep.* **7**, 1–17 (2017).

46. Dijkman, P. M. *et al.* Dynamic tuneable G protein-coupled receptor monomer-dimer populations. *Nat. Commun.* **9**, 1710 (2018).

47. Hern, J. A. *et al.* Formation and dissociation of M1 muscarinic receptor dimers seen by total internal reflection fluorescence imaging of single molecules. *Proc. Natl. Acad. Sci. U. S. A.* **107**, 2693–2698 (2010).

48. Pediani, J. D., Ward, R. J., Godin, A. G., Marsango, S. & Milligan, G. Dynamic regulation of quaternary organization of the m1 muscarinic receptor by subtype-selective antagonist drugs. *J. Biol. Chem.* **291**, 13132–13146 (2016).

49. Gavalas, A. *et al.* Segregation of family A G protein-coupled receptor protomers in the plasma membrane. *Mol. Pharmacol.* **84**, 346–352 (2013).

50. Felce, J. H. *et al.* Receptor Quaternary Organization Explains G Protein-Coupled Receptor Family Structure. *Cell Rep.* **20**, 2654–2665 (2017).

51. Meral, D. *et al.* Molecular details of dimerization kinetics reveal negligible populations of transient μ-opioid receptor homodimers at physiological concentrations. *Sci. Rep.* **8**, 7705 (2018).

52. Lavoie, C. *et al.* Beta 1/beta 2-adrenergic receptor heterodimerization regulates beta 2-adrenergic receptor internalization and ERK signaling efficacy. *J. Biol. Chem.* **277**, 35402–35410 (2002).

53. Lavoie, C. & Hébert, T. E. Pharmacological characterization of putative β 1 -β 2 -adrenergic receptor heterodimers. *Can. J. Physiol. Pharmacol.* **81**, 186–195 (2003).

54. Mercier, J.-F., Salahpour, A., Angers, S., Breit, A. & Bouvier, M. Quantitative assessment of beta 1- and beta 2-adrenergic receptor homo- and heterodimerization by bioluminescence resonance energy transfer. *J. Biol. Chem.* **277**, 44925–31 (2002).

55. Breit, A., Lagacé, M. & Bouvier, M. Hetero-oligomerization between beta2- and beta3-adrenergic receptors generates a beta-adrenergic signaling unit with distinct functional properties. *J. Biol. Chem.* **279**, 28756–65 (2004).

56. Stanasila, L., Perez, J.-B., Vogel, H. & Cotecchia, S. Oligomerization of the alpha 1a- and alpha 1b-adrenergic receptor subtypes. Potential implications in receptor internalization. *J. Biol. Chem.* **278**, 40239–51 (2003).

57. Xu, J. *et al.* Heterodimerization of alpha 2A- and beta 1-adrenergic receptors. *J. Biol. Chem.* **278**, 10770–10777 (2003).

58. Cvejic, S. & Devi, L. A. Dimerization of the δ opioid receptor: Implication for a role in receptor internalization. *J. Biol. Chem.* **272**, 26959–26964 (1997).

59. McVey, M. *et al.* Monitoring receptor oligomerization using time-resolved fluorescence resonance energy transfer and bioluminescence resonance energy transfer. The human delta -opioid receptor displays constitutive oligomerization at the cell surface, which is not regulate. *J. Biol. Chem.* **276**, 14092–9 (2001).

60. Perron, A. A. *et al.* Agonist-independent desensitization and internalization of the human platelet-activating factor receptor by coumermycin-gyrase B-induced dimerization. *J. Biol. Chem.* **278**, 27956–27965 (2003).

61. George, S. R. *et al.* Oligomerization of μ- and δ-opioid receptors: Generation of novel functional properties. *J. Biol. Chem.* **275**, 26128–26135 (2000).

62. Pfeiffer, M. *et al.* Heterodimerization of somatostatin and opioid receptors cross-modulates phosphorylation, internalization, and desensitization. *J. Biol. Chem.* **277**, 19762–19772 (2002).

63. Gomes, I. *et al.* Heterodimerization of mu and delta opioid receptors: A role in opiate synergy. *J. Neurosci.* **20**, RC110–RC110 (2000).

64. Jordan, B. A. & Devi, L. A. G-protein-coupled receptor heterodimerization modulates receptor function. *Nature* **399**, 697–700 (1999).

65. Jones, K. A. *et al.* GABA(B) receptors function as a heteromeric assembly of the subunits GABA(B)R1 and GABA(B)R2. *Nature* **396**, 674–679 (1998).

66. Margeta-Mitrovic, M., Jan, Y. N. & Jan, L. Y. A trafficking checkpoint controls GABA(B) receptor heterodimerization. *Neuron* **27**, 97–106 (2000).

67. Bouvier, M. Oligomerization of G-protein-coupled transmitter receptors. *Nat. Rev. Neurosci.* **2**, 274–286 (2001).

68. Doly, S. *et al.* GABA B receptor cell-surface export is controlled by an endoplasmic reticulum gatekeeper. *Mol. Psychiatry* **21**, 480–490 (2016).

69. Milligan, G. Oligomerisation of G-protein-coupled receptors. *J. Cell Sci.* **114**, 1265–1271 (2001).

70. Bulenger, S., Marullo, S. & Bouvier, M. Emerging role of homo- and heterodimerization in G-protein-coupled receptor biosynthesis and maturation. *Trends Pharmacol. Sci.* **26**, 131–137 (2005).

71. Doly, S. & Marullo, S. Gatekeepers Controlling GPCR Export and Function. *Trends Pharmacol. Sci.* **36**, 636–644 (2015).

72. El Moustaine, D. *et al.* Distinct roles of metabotropic glutamate receptor dimerization in agonist activation and G-protein coupling. *Proc. Natl. Acad. Sci. U. S. A.* **109**, 16342–16347

(2012).

73. Goudett, C. *et al.* Heptahelical domain of metabotropic glutamate receptor 5 behaves like rhodopsin-like receptors. *Proc. Natl. Acad. Sci. U. S. A.* **101**, 378–383 (2004).

74. Milligan, G., Ward, R. J. & Marsango, S. GPCR homo-oligomerization. *Curr. Opin. Cell Biol.* **57**, 40–47 (2019).

75. Romano, C., Yang, W. L. & O'Malley, K. L. Metabotropic glutamate receptor 5 is a disulfide-linked dimer. *J. Biol. Chem.* **271**, 28612–28616 (1996).

76. Lohse, M. J. Dimerization in GPCR mobility and signaling. *Curr. Opin. Pharmacol.* **10**, 53–58 (2010).

77. Gurevich, V. V. & Gurevich, E. V. How and why do GPCRs dimerize? *Trends Pharmacol. Sci.* **29**, 234–240 (2008).

78. Guidolin, D., Marcoli, M., Tortorella, C., Maura, G. & Agnati, L. F. *G protein-coupled receptor-receptor interactions give integrative dynamics to intercellular communication*. *Reviews in the Neurosciences* **29**, 703–726 (De Gruyter, 2018).

79. Rasmussen, S. G. F. *et al.* Crystal structure of the β 2 adrenergic receptor-Gs protein complex. *Nature* **477**, 549–557 (2011).

80. Seven, A. B. *et al.* G-protein activation by a metabotropic glutamate receptor. *Nature* (2021). doi:10.1038/s41586-021-03680-3

81. Calebiro, D. *et al.* Single-molecule analysis of fluorescently labeled G-protein-coupled receptors reveals complexes with distinct dynamics and organization. *Proc. Natl. Acad. Sci. U. S. A.* **110**, 743–748 (2013).

82. Fung, J. J. *et al.* Ligand-regulated oligomerization of B 2-adrenoceptors in a model lipid bilayer. *EMBO J.* **28**, 3315–3328 (2009).

83. Herrick-Davis, K., Grinde, E., Cowan, A. & Mazurkiewicz, J. E. Fluorescence correlation spectroscopy analysis of serotonin, adrenergic, muscarinic, and dopamine receptor dimerization: the oligomer number puzzle. *Mol. Pharmacol.* **84**, 630–42 (2013).

84. Milligan, G. The Prevalence, Maintenance, and Relevance of G Protein–Coupled Receptor Oligomerization. *Mol. Pharmacol.* **84**, 158–169 (2013).

85. Ferré, S. *et al.* Building a new conceptual framework for receptor heteromers. *Nat. Chem. Biol.* **5**, 131–134 (2009).

86. Gomes, I. *et al.* G Protein–Coupled Receptor Heteromers. *Annu. Rev. Pharmacol. Toxicol.* **56**, 403–425 (2016).

87. Porzionato, A. *et al.* Receptor–Receptor Interactions of G Protein-Coupled Receptors in the Carotid Body: A Working Hypothesis. *Front. Physiol.* **9**, 697 (2018).

88. Magalhaes, A. C. C. *et al.* CRF receptor 1 regulates anxiety behavior via sensitization of 5-HT2 receptor signaling. *Nat. Neurosci.* **13**, 622–629 (2010).

89. Shah, U. H. H., Toneatti, R., Gaitonde, S. A. A., Shin, J. M. M. & González-Maeso, J. Site-Specific Incorporation of Genetically Encoded Photo-Crosslinkers Locates the Heteromeric Interface of a GPCR Complex in Living Cells. *Cell Chem. Biol.* **27**, 1308-1317.e4 (2020).

90. Fotiadis, D. *et al.* Rhodopsin dimers in native disc membranes. *Nature* **421**, 127–128 (2003).

91. Fuxe, K. *et al.* Moonlighting proteins and protein-protein interactions as neurotherapeutic

targets in the G protein-coupled receptor field. *Neuropsychopharmacology* **39**, 131–155 (2014).

92. Jeffery, C. J. Protein moonlighting: what is it, and why is it important? *Philos. Trans. R. Soc. B Biol. Sci.* **373**, 20160523 (2018).

93. Jeffery, C. J. Moonlighting proteins: old proteins learning new tricks. *Trends Genet.* **19**, 415–417 (2003).

94. Turlejski, K. Evolutionary ancient roles of serotonin: Long-lasting regulation of activity and development. *Acta Neurobiol. Exp. (Wars).* **56**, 619–636 (1996).

95. Azmitia, E. C. Evolution of Serotonin: Sunlight to Suicide. in **21**, 3–22 (Elsevier, 2010).

96. Azmitia, E. C. & York, N. Serotonin. eLS. (2012).

97. Jayamohanan, H., Kumar, M. K. M. & Aneesh, T. P. 5-HIAA as a potential biological marker for neurological and psychiatric disorders. *Advanced Pharmaceutical Bulletin* **9**, 374–381 (2019).

98. Fairbanks, L. A., Melega, W. P., Jorgensen, M. J., Kaplan, J. R. & McGuire, M. T. Social impulsivity inversely associated with CSF 5-HIAA and fluoxetine exposure in vervet monkeys. *Neuropsychopharmacology* **24**, 370–378 (2001).

99. Bourgeois, M. Serotonin, impulsivity and suicide. *Hum. Psychopharmacol. Clin. Exp.* **6**, S31–S36 (1991).

100. Coccaro, E. F. Central serotonin and impulsive aggression. *Br. J. Psychiatry. Suppl.* 52–62 (1989).

101. Coccaro, E. F., Lee, R. & Kavoussi, R. J. Aggression, suicidality, and intermittent explosive disorder: serotonergic correlates in personality disorder and healthy control subjects. *Neuropsychopharmacology* **35**, 435–44 (2010).

102. Coccaro, E. F., Fanning, J. R., Phan, K. L. & Lee, R. Serotonin and impulsive aggression. *CNS Spectr.* **20**, 295–302 (2015).

103. Moberg, T. *et al.* CSF 5-HIAA and exposure to and expression of interpersonal violence in suicide attempters. *J. Affect. Disord.* **132**, 173–178 (2011).

104. Musshoff, F., Menting, T. & Madea, B. Postmortem serotonin (5-HT) concentrations in the cerebrospinal fluid of medicolegal cases. *Forensic Sci. Int.* **142**, 211–219 (2004).

105. Nordström, P. *et al.* CSF 5-HIAA Predicts Suicide Risk After Attempted Suicide. *Suicide Life-Threatening Behav.* **24**, 1–9 (1994).

106. Ninan, P. T. *et al.* CSF 5-hydroxyindoleacetic acid levels in suicidal schizophrenic patients. *Am. J. Psychiatry* **141**, 566–569 (1984).

107. Croonenberghs, J. *et al.* Peripheral markers of serotonergic and noradrenergic function in post- pubertal, caucasian males with autistic disorder. *Neuropsychopharmacology* **22**, 275–283 (2000).

108. Hérault, J. *et al.* Serotonin and autism: Biochemical and molecular biology features. *Psychiatry Res.* **65**, 33–43 (1996).

109. Launay, J. M. *et al.* Serotonin Metabolism and Other Biochemical Parameters in Infantile Autism. *Neuropsychobiology* **20**, 1–11 (1988).

110. Hoshino, Y. *et al.* Blood Serotonin and Free Tryptophan Concentration in Autistic Children. *Neuropsychobiology* **11**, 22–27 (1984).

111. Chakraborti, B. *et al.* Gender-Specific Effect of 5-HT and 5-HIAA on Threshold Level of Behavioral Symptoms and Sex-Bias in Prevalence of Autism Spectrum Disorder. *Front. Neurosci.* **13**, 1375 (2020).

112. Carlborg, A., Jokinen, J., Nordström, A. L., Jönsson, E. G. & Nordström, P. CSF 5-HIAA, attempted suicide and suicide risk in schizophrenia spectrum psychosis. *Schizophr. Res.* **112**, 80–85 (2009).

113. Berger, M., Gray, J. A. & Roth, B. L. The expanded biology of serotonin. *Annu. Rev. Med.* **60**, 355–366 (2009).

114. López-Giménez, J. F. & González-Maeso, J. Hallucinogens and Serotonin 5-HT2A Receptor-Mediated Signaling Pathways. in *Behavioral Neurobiology of Psychedelic Drugs* 45–73 (Springer Berlin Heidelberg, 2017).

115. Steinbusch, H. W. M., Dolatkhah, M. A. & Hopkins, D. A. Anatomical and neurochemical organization of the serotonergic system in the mammalian brain and in particular the involvement of the dorsal raphe nucleus in relation to neurological diseases. in *Progress in Brain Research* **261**, 41–81 (Elsevier B.V., 2021).

116. Römpler, H. *et al.* G protein-coupled time travel: Evolutionary aspects of GPCR research. *Molecular Interventions* **7**, 17–25 (2007).

117. A. J. Thompson and S.C.R.Lummis. 5-HT-3 Receptor. in *Curr Pharm Des* **12**, 1–7 (Elsevier, 2006).

118. Lummis, S. 5-HT 3 Receptors . *eLS* 1–7 (2018).

119. Hannon, J. & Hoyer, D. Molecular biology of 5-HT receptors. *Behav. Brain Res.* **195**, 198–213 (2008).

120. Garnovskaya, M. N., Nebigil, C. G., Arthur, J. M., Spurney, R. F. & Raymond, J. R. 5-Hydroxytryptamine(2A) receptors expressed in rat renal mesangial cells inhibit cyclic AMP accumulation. *Mol. Pharmacol.* **48**, 230–237 (1995).

121. McCorvy, J. D. & Roth, B. L. Structure and function of serotonin G protein-coupled receptors. *Pharmacol. Ther.* **150**, 129–142 (2015).

122. Johansen, A. *et al.* Human biodistribution and radiation dosimetry of the 5-HT2A receptor agonist Cimbi-36 labeled with carbon-11 in two positions. *EJNMMI Res.* **9**, 71 (2019).

123. Cornea-Hébert, V., Riad, M., Wu, C., Singh, S. K. & Descarries, L. Cellular and subcellular distribution of the serotonin 5-HT2A receptor in the central nervous system of adult rat. *J. Comp. Neurol.* **409**, 187–209 (1999).

124. Jakab, R. L. *et al.* 5-Hydroxytryptamine2A serotonin receptors in the primate cerebral cortex: Possible site of action of hallucinogenic and antipsychotic drugs in pyramidal cell apical dendrites. *Proc. Natl. Acad. Sci. U. S. A.* **95**, 735–740 (1998).

125. Marek, G. J., Wright, R. A., Schoepp, D. D., Monn, J. A. & Aghajanian, G. K. Physiological antagonism between 5-hydroxytryptamine(2A) and group II metabotropic glutamate receptors in prefrontal cortex. *J. Pharmacol. Exp. Ther.* **292**, 76–87 (2000).

126. Miner, L. A. H., Backstrom, J. R., Sanders-Bush, E. & Sesack, S. R. Ultrastructural localization of serotonin2A receptors in the middle layers of the rat prelimbic prefrontal cortex. *Neuroscience* **116**, 107–117 (2003).

127. Doherty, M. D. & Pickel, V. M. Ultrastructural localization of the serotonin 2A receptor in dopaminergic neurons in the ventral tegmental area. *Brain Res.* **864**, 176–185 (2000).

128. Barre, A. *et al.* Presynaptic serotonin 2A receptors modulate thalamocortical plasticity and associative learning. *Proc. Natl. Acad. Sci.* **113**, E1382–E1391 (2016).

129. Xu, T. & Pandey, S. C. Cellular localization of serotonin2A (5HT2A) receptors in the rat brain. *Brain Res. Bull.* **51**, 499–505 (2000).

130. López-Giménez, J. F., Mengod, G., Palacios, J. M. & Vilaró, M. T. Selective visualization of rat brain 5-HT(2A) receptors by autoradiography with [3H]MDL 100,907. *Naunyn. Schmiedebergs. Arch. Pharmacol.* **356**, 446–454 (1997).

131. Erritzoe, D. *et al.* Cortical and subcortical 5-HT2A receptor binding in neuroleptic-naive first-episode schizophrenic patients. *Neuropsychopharmacology* **33**, 2435–2441 (2008).

132. Burnet, P. W. J., Eastwood, S. L. & Harrison, P. J. 5-HT(1A) 5-HT(2A) receptor mRNAs and binding site densities are differentially altered in schizophrenia. *Neuropsychopharmacology* **15**, 442–455 (1996).

133. Geurts, F. J., De Schutter, E. & Timmermans, J. P. Localization of 5-HT2A, 5-HT3, 5-HT5A and 5-HT7 receptor-like immunoreactivity in the rat cerebellum. *J. Chem. Neuroanat.* **24**, 65–74 (2002).

134. Eastwood, S. L., Burnet, P. W. J., Gittins, R., Baker, K. & Harrison, P. J. Expression of serotonin 5-HT2A receptors in the human cerebellum and alterations in schizophrenia. *Synapse* **42**, 104–114 (2001).

135. Paterson, L. M., Kornum, B. R., Nutt, D. J., Pike, V. W. & Knudsen, G. M. 5-HT radioligands for human brain imaging with PET and SPECT. *Med. Res. Rev.* **33**, 54–111 (2013).

136. Ettrup, A. *et al.* Serotonin 2A receptor agonist binding in the human brain with [11 C]Cimbi-36. *J. Cereb. Blood Flow Metab.* **34**, 1188–1196 (2014).

137. Willins, D. L., Deutch, A. Y. & Roth, B. L. Serotonin 5-HT(2A) receptors are expressed on pyramidal cells and interneurons in the rat cortex. *Synapse* **27**, 79–82 (1997).

138. Vollenweider, F. X., Vollenweider-Scherpenhuyzen, M. F. I., Bäbler, A., Vogel, H. & Hell, D. Psilocybin induces schizophrenia-like psychosis in humans via a serotonin-2 agonist action. *Neuroreport* **9**, 3897–3902 (1998).

139. Nichols, D. E. Hallucinogens. *Pharmacol. Ther.* **101**, 131–181 (2004).

140. González-Maeso, J. *et al.* Hallucinogens Recruit Specific Cortical 5-HT2A Receptor-Mediated Signaling Pathways to Affect Behavior. *Neuron* **53**, 439–452 (2007).

141. Roth, B. L., Willins, D. L., Kristiansen, K. & Kroeze, W. K. Activation is hallucinogenic and antagonism is therapeutic: Role of 5- HT(2A) receptors in atypical antipsychotic drug actions. *Neuroscientist* **5**, 254–262 (1999).

142. Aghajanian, G. K. & Marek, G. J. Serotonin and hallucinogens. *Neuropsychopharmacology* **21**, 16S-23S (1999).

143. González-Maeso, J. & Sealfon, S. C. Psychedelics and schizophrenia. *Trends Neurosci.* **32**, 225–232 (2009).

144. Nichols, D. E. Psychedelics. 264–355 (2016).

145. Halberstadt, A. L. & Geyer, M. A. Serotonergic hallucinogens as translational models relevant to schizophrenia. *Int. J. Neuropsychopharmacol.* **16**, 2165–2180 (2013).

146. Leptourgos, P. *et al.* Hallucinations under Psychedelics and in the Schizophrenia Spectrum: An Interdisciplinary and Multiscale Comparison. *Schizophr. Bull.* **46**, 1396–1408 (2020).

147. Vollenweider, F. X. & Kometer, M. The neurobiology of psychedelic drugs: Implications for the treatment of mood disorders. *Nat. Rev. Neurosci.* **11**, 642–651 (2010).

148. Genís Ona, J. C. B. Can psychedelics be the treatment for the crisis in psychopharmacology. *Russ. Union Cat. Sci. Lit.* **6**, 1–6 (2013).

149. Gasser, P., Kirchner, K. & Passie, T. LSD-assisted psychotherapy for anxiety associated with a life-threatening disease: A qualitative study of acute and sustained subjective effects. *J. Psychopharmacol.* **29**, 57–68 (2015).

150. Szabo, A. Psychedelics and immunomodulation: Novel approaches and therapeutic opportunities. *Front. Immunol.* **6**, 1–11 (2015).

151. Palhano-Fontes, F. *et al.* Rapid antidepressant effects of the psychedelic ayahuasca in treatment-resistant depression: A randomized placebo-controlled trial. *Psychol. Med.* **49**, 655–663 (2019).

152. Kelly, J. R. *et al.* Psychedelic science in post-COVID-19 psychiatry. *Irish Journal of Psychological Medicine* **38**, 93–98 (2021).

153. Nutt, D., Erritzoe, D. & Carhart-Harris, R. Psychedelic Psychiatry's Brave New World. *Cell* **181**, 24–28 (2020).

154. Carhart-Harris, R. L. *et al.* Psilocybin with psychological support for treatment-resistant depression: an open-label feasibility study. *The Lancet Psychiatry* **3**, 619–627 (2016).

155. Rucker, J. J. H., Iliff, J. & Nutt, D. J. Psychiatry & the psychedelic drugs. Past, present & future. *Neuropharmacology* **142**, 200–218 (2018).

156. Young, J. W., Powell, S. B. & Geyer, M. A. Mouse pharmacological models of cognitive disruption relevant to schizophrenia. *Neuropharmacology* **62**, 1381–90 (2012).

157. Meyerhoefer, M. M. Serotonergic Hallucinogens. in *Addiction Medicine* 585–602 (Springer New York, 2010). doi:10.1007/978-1-4419-0338-9_27

158. Raote, I., Bhattacharya, A. & Panicker, M. M. *Serotonin 2A (5-HT2A) Receptor Function: Ligand-Dependent Mechanisms and Pathways*. *Serotonin Receptors in Neurobiology* (CRC Press/Taylor & Francis, 2007).

159. WILLINS, D. L. *et al.* Serotonergic Antagonist Effects on Trafficking of Serotonin 5-HT2A Receptors in Vitro and in Vivoa. *Ann. N. Y. Acad. Sci.* **861**, 121–127 (1998).

160. Gray, J. A. & Roth, B. L. Paradoxical trafficking and regulation of 5-HT2A receptors by agonists and antagonists. *Brain Res. Bull.* **56**, 441–451 (2001).

161. Berg, KA (Berg, KA); Maayani, S (Maayani, S); Goldfarb, J (Goldfarb, J); Clarke, WP (Clarke, W. Pleiotropic Behavior of 5-HT2A and 5-HT2C Receptor Agonists. *Ann. N. Y. Acad. Sci.* **861**, 104–110 (1998).

162. González-Maeso, J. *et al.* Transcriptome fingerprints distinguish hallucinogenic and nonhallucinogenic 5-hydroxytryptamine 2A receptor agonist effects in mouse somatosensory cortex. *J. Neurosci.* **23**, 8836–8843 (2003).

163. Karaki, S. *et al.* Quantitative phosphoproteomics unravels biased phosphorylation of serotonin 2A Receptor at Ser280 by hallucinogenic versus nonhallucinogenic agonists. *Mol. Cell. Proteomics* **13**, 1273–1285 (2014).

164. Canal, C. E. & Morgan, D. Head-twitch response in rodents induced by the hallucinogen 2,5-dimethoxy-4-iodoamphetamine: a comprehensive history, a re-evaluation of mechanisms, and its utility as a model. *Drug Test. Anal.* **4**, 556 (2012).

165. Brea, J. *et al.* Evidence for Distinct Antagonist-Revealed Functional States of 5HT2A Homodimers. *Mol. Pharmacol.* **75**, 1380–1391 (2009).

166. Bruno, A., Beato, C. & Costantino, G. Molecular dynamics simulations and docking studies on 3D models of the heterodimeric and homodimeric 5-HT(2A) receptor subtype. *Futur. Med Chem.* **3**, 665–81 (2011).

167. Shashack, M. J. *et al.* Synthesis and Evaluation of Dimeric Derivatives of 5-HT 2A Receptor (5-HT 2A R) Antagonist M-100907. *ACS Chem. Neurosci* **2**, 640–644 (2011).

168. Iglesias, A., Cimadevila, M., Cadavid, M. I., Loza, M. I. & Brea, J. Serotonin-2A homodimers are needed for signalling via both phospholipase A2 and phospholipase C in transfected CHO cells. *Eur. J. Pharmacol.* **800**, 63–69 (2017).

169. Moutkine, I., Quentin, E., Guiard, B. P., Maroteaux, L. & Doly, S. Heterodimers of serotonin receptor subtypes 2 are driven by 5-HT2C protomers. *J. Biol. Chem.* **292**, 6352–6368 (2017).

170. Poulie, C. B. M., Liu, N., Jensen, A. A. & Bunch, L. Design, Synthesis, and Pharmacological Characterization of Heterobivalent Ligands for the Putative 5-HT 2A /mGlu 2 Receptor Complex. *J. Med. Chem.* acs.jmedchem.0c01058 (2020).

171. Łukasiewicz, S. *et al.* Hetero-dimerization of serotonin 5-HT2A and dopamine D2 receptors. *Biochim. Biophys. Acta - Mol. Cell Res.* **1803**, 1347–1358 (2010).

172. Albizu, L., Holloway, T., González-Maeso, J. & Sealfon, S. C. Functional crosstalk and heteromerization of serotonin 5-HT2A and dopamine D2 receptors. *Neuropharmacology* **61**, 770–777 (2011).

173. Galindo, L. *et al.* Cannabis Users Show Enhanced Expression of CB1-5HT2A Receptor Heteromers in Olfactory Neuroepithelium Cells. *Mol. Neurobiol.* **55**, 6347–6361 (2018).

174. Maroteaux, L., Béchade, C. & Roumier, A. Dimers of serotonin receptors: Impact on ligand affinity and signaling. *Biochimie* **161**, 23–33 (2019).

175. Guinart, D. *et al.* Altered Signaling in CB1R-5-HT2AR Heteromers in Olfactory Neuroepithelium Cells of Schizophrenia Patients is Modulated by Cannabis Use. *Schizophr. Bull.* **46**, 1547–1557 (2020).

176. Borroto-Escuela, D. O. *et al. Dopamine D2 and 5-hydroxytryptamine 5-HT2A receptors assemble into functionally interacting heteromers*. *Biochemical and Biophysical Research Communications* **401**, (2010).

177. Van Heeringen, C. *et al.* Prefrontal 5-HT2a receptor binding index, hopelessness and personality characteristics in attempted suicide. *J. Affect. Disord.* **74**, 149–158 (2003).

178. Bryson, A., Carter, O., Norman, T. & Kanaan, R. 5-HT2A agonists: A novel therapy for functional neurological disorders? *International Journal of Neuropsychopharmacology* **20**, 422–427 (2017).

179. Camile, B. 5-HT2A mediated plasticity as a target in major depression : a narrative review connecting the dots from neurobiology to cognition and psychology. 1–35 (2020).

180. Akin, D., Manier, D. H., Sanders-Bush, E. & Shelton, R. C. Decreased serotonin 5-HT2A receptor-stimulated phosphoinositide signalling in fibroblasts from melancholic deppresed patients. *Neuropsychopharmacology* **29**, 2081–2087 (2004).

181. Benedetti, F. *et al.* Serotonin 5-HT2A receptor gene variants influence antidepressant response to repeated total sleep deprivation in bipolar depression. *Prog. Neuro-*

Psychopharmacology Biol. Psychiatry **32**, 1863–1866 (2008).

182. Yu, B. *et al.* Serotonin 5-hydroxytryptamine2A receptor activation suppresses tumor necrosis factor-α-induced inflammation with extraordinary potency. *J. Pharmacol. Exp. Ther.* **327**, 316–323 (2008).

183. González-Maeso, J. *et al.* Identification of a serotonin/glutamate receptor complex implicated in psychosis. *Nature* **452**, 93–97 (2008).

184. Huot, P. *et al.* Increased 5-HT2A receptors in the temporal cortex of Parkinsonian patients with visual hallucinations. *Mov. Disord.* **25**, 1399–1408 (2010).

185. Muguruza, C. *et al.* Dysregulated 5-HT2A receptor binding in postmortem frontal cortex of schizophrenic subjects. *Eur. Neuropsychopharmacol.* **23**, 852–864 (2013).

186. Guiard, B. P. & Giovanni, G. Di. Central serotonin-2A (5-HT2A) receptor dysfunction in depression and epilepsy: the missing link? *Front. Pharmacol.* **6**, 46 (2015).

187. Aznar, S. & Hervig, M. E. S. The 5-HT2A serotonin receptor in executive function: Implications for neuropsychiatric and neurodegenerative diseases. *Neuroscience and Biobehavioral Reviews* **64**, 63–82 (2016).

188. Vollenweiderl, F. X. *et al.* S54.04 A system model of altered consciousness: Integrating natural and drug-induced psychoses. *Eur. Psychiatry* **15**, 318s-318s (2000).

189. Muguruza, C. *et al.* Evaluation of 5-HT2A and mGlu2/3 receptors in postmortem prefrontal cortex of subjects with major depressive disorder: Effect of antidepressant treatment. *Neuropharmacology* **86**, 311–318 (2014).

190. Hayashi, T. Effects of sodium glutamate on the nervous system. *keio j. med.* **3**, 183–192 (1954).

191. Curtis, D. R. & Watkins, J. C. The excitation and depression of spinal neurones by structurally related amino acids. *j. neurochem.* **6**, 117–141 (1960).

192. Danbolt, N. C. Glutamate uptake. *Progress in Neurobiology* **65**, 1–105 (2001).

193. Greenamyre, J. T. The Role of Glutamate in Neurotransmission and in Neurologic Disease. *Arch. Neurol.* **43**, 1058–1063 (1986).

194. Schousboe, A., Bak, L. K. & Waagepetersen, H. S. Astrocytic control of biosynthesis and turnover of the neurotransmitters glutamate and GABA. *Frontiers in Endocrinology* **4**, 102 (2013).

195. Murphy-Royal, C., Dupuis, J., Groc, L. & Oliet, S. H. R. Astroglial glutamate transporters in the brain: Regulating neurotransmitter homeostasis and synaptic transmission. *J. Neurosci. Res.* **95**, 2140–2151 (2017).

196. Zhou, Y. & Danbolt, N. C. Glutamate as a neurotransmitter in the healthy brain. *Journal of Neural Transmission* **121**, 799–817 (2014).

197. Yao, H.-H. *et al.* Enhancement of glutamate uptake mediates the neuroprotection exerted by activating group II or III metabotropic glutamate receptors on astrocytes. *J. Neurochem.* **92**, 948–961 (2005).

198. Pinheiro, P. S. & Mulle, C. Presynaptic glutamate receptors: physiological functions and mechanisms of action. *Nature reviews. Neuroscience* **9**, 423–436 (2008).

199. Pin, J. P., De Colle, C., Bessis, A. S. & Acher, F. New perspectives for the development of selective metabotropic glutamate receptor ligands. *European Journal of Pharmacology* **375**,

277–294 (1999).

200. Pin, J. P. & Duvoisin, R. The metabotropic glutamate receptors: Structure and functions. *Neuropharmacology* **34**, 1–26 (1995).

201. Yasumatsu, K. *et al.* Multiple receptors underlie glutamate taste responses in mice. in *American Journal of Clinical Nutrition* **90**, (Am J Clin Nutr, 2009).

202. Tanabe, Y., Masu, M., Ishii, T., Shigemoto, R. & Nakanishi, S. A family of metabotropic glutamate receptors. *Neuron* **8**, 169–179 (1992).

203. Petralia, R. S., Wang, Y. X., Niedzielski, A. S. & Wenthold, R. J. The metabotropic glutamate receptors, MGLUR2 and MGLUR3, show unique postsynaptic, presynaptic and glial localizations. *Neuroscience* **71**, 949–976 (1996).

204. Wright, R. A. *et al.* CNS distribution of metabotropic glutamate 2 and 3 receptors: Transgenic mice and [3H]LY459477 autoradiography. *Neuropharmacology* **66**, 89–98 (2013).

205. Ohishi, H., Neki, A. & Mizuno, N. Distribution of a metabotropic glutamate receptor, mGluR2, in the central nervous system of the rat and mouse: an immunohistochemical study with a monoclonal antibody. *Neurosci. Res.* **30**, 65–82 (1998).

206. Tamaru, Y., Nomura, S., Mizuno, N. & Shigemoto, R. Distribution of metabotropic glutamate receptor mGluR3 in the mouse CNS: Differential location relative to pre- and postsynaptic sites. *Neuroscience* **106**, 481–503 (2001).

207. Jin, L. E. *et al.* mGluR2/3 mechanisms in primate dorsolateral prefrontal cortex: evidence for both presynaptic and postsynaptic actions LE. *Mol. Psychiatry* **22**, 1615–1625 (2017).

208. Scanziani, M., Salin, P. A., Vogt, K. E., Malenka, R. C. & Nicoll, R. A. Use-dependent increases in glutamate concentration activate presynaptic metabotropic glutamate receptors. *Nature* **385**, 630–634 (1997).

209. Forsythe, I. D. & Clements, J. D. Presynaptic glutamate receptors depress excitatory monosynaptic transmission between mouse hippocampal neurones. *J. Physiol.* **429**, 1–16 (1990).

210. Ozawa, S., Kamiya, H. & Tsuzuki, K. Glutamate receptors in the mammalian central nervous system. *Prog. Neurobiol.* **54**, 581–618 (1998).

211. Durand, D., Carniglia, L., Caruso, C. & Lasaga, M. mGlu3 receptor and astrocytes: Partners in neuroprotection. *Neuropharmacology* **66**, 1–11 (2013).

212. Jin, L. E. *et al.* mGluR2 versus mGluR3 Metabotropic Glutamate Receptors in Primate Dorsolateral Prefrontal Cortex: Postsynaptic mGluR3 Strengthen Working Memory Networks. *Cereb. Cortex* **28**, 974–987 (2017).

213. Cochilla, A. J. & Alford, S. Metabotropic glutamate receptor-mediated control of neurotransmitter release. *Neuron* **20**, 1007–1016 (1998).

214. Choi, S. & Lovinger, D. M. Metabotropic glutamate receptor modulation of voltage-gated Ca2+ channels involves multiple receptor subtypes in cortical neurons. *J. Neurosci.* **16**, 36–45 (1996).

215. Hanna, L. *et al.* Differentiating the roles of mGlu2 and mGlu3 receptors using LY541850, an mGlu2 agonist/mGlu3 antagonist. *Neuropharmacology* **66**, 114–121 (2013).

216. Wroblewska, B. *et al.* N-acetylaspartylglutamate selectively activates mGluR3 receptors in transfected cells. *J. Neurochem.* **69**, 174–181 (1997).

217. Neale, J. H., Bzdega, T. & Wroblewska, B. N-Acetylaspartylglutamate. *J. Neurochem.* **75**, 443–452 (2002).

218. Cid, J. M., Trabanco, A. A. & Lavreysen, H. Metabotropic glutamate receptor 2 activators. *Top. Med. Chem.* **13**, 101–142 (2015).

219. Muguruza, C., Meana, J. J. & Callado, L. F. Group II Metabotropic Glutamate Receptors as Targets for Novel Antipsychotic Drugs. *Front. Pharmacol.* **7**, 130 (2016).

220. González-Maeso, J. Metabotropic Glutamate 2 (mGlu2) Receptors and Schizophrenia Treatment. in 59–78 (Humana Press, Cham, 2017).

221. Sanger, H. *et al.* Pharmacological profiling of native group II metabotropic glutamate receptors in primary cortical neuronal cultures using a FLIPR. *Neuropharmacology* **66**, 264–273 (2013).

222. Kingston, A. E. *et al.* Neuroprotection by metabotropic glutamate receptor agonists: LY354740, LY379268 and LY389795. *Eur. J. Pharmacol.* **377**, 155–165 (1999).

223. Rorick-Kehn, L. M. *et al.* In vivo pharmacological characterization of the structurally novel, potent, selective mGlu2/3 receptor agonist LY404039 in animal models of psychiatric disorders. *Psychopharmacology (Berl).* **193**, 121–136 (2007).

224. Niswender, C. M. & Conn, P. J. Metabotropic glutamate receptors: Physiology, pharmacology, and disease. *Annu. Rev. Pharmacol. Toxicol.* **50**, 295–322 (2010).

225. Kinon, B. J. *et al.* A multicenter, inpatient, phase 2, double-blind, placebo-controlled dose-ranging study of LY2140023 monohydrate in patients with DSM-IV schizophrenia. *J. Clin. Psychopharmacol.* **31**, 349–355 (2011).

226. Patil S.T. *et al.* Activation of mGlu2/3 receptors as a new approach to treat schizophrenia: A randomized Phase 2 clinical trial. *Nat. Med.* **13**, 1102–1107 (2007).

227. Simmons, R. M. A., Webster, A. A., Kalra, A. B. & Iyengar, S. Group II mGluR receptor agonists are effective in persistent and neuropathic pain models in rats. *Pharmacol. Biochem. Behav.* **73**, 419–427 (2002).

228. Swanson C.J. *et al. Metabotropic glutamate receptors as novel targets for anxiety and stress disorders*. *Nature Reviews Drug Discovery* **4**, 131–144 (Nature Publishing Group, 2005).

229. Schiefer, J. *et al.* The metabotropic glutamate receptor 5 antagonist MPEP and the mGluR2 agonist LY379268 modify disease progression in a transgenic mouse model of Huntington's disease. *Brain Res.* **1019**, 246–254 (2004).

230. Woolley, M. L., Pemberton, D. J., Bate, S., Corti, C. & Jones, D. N. C. The mGlu2 but not the mGlu3 receptor mediates the actions of the mGluR2/3 agonist, LY379268, in mouse models predictive of antipsychotic activity. *Psychopharmacology (Berl).* **196**, 431–440 (2008).

231. Kufahl, P. R. *et al.* Attenuation of methamphetamine seeking by the mGluR2/3 agonist LY379268 in rats with histories of restricted and escalated self-Administration. *Neuropharmacology* **66**, 290–301 (2013).

232. Menezes, M. M. *et al.* The mGlu2/3 Receptor Agonists LY354740 and LY379268 Differentially Regulate Restraint-Stress-Induced Expression of c-Fos in Rat Cerebral Cortex. *Neurosci. J.* **2013**, 1–8 (2013).

233. Li, M. L., Hu, X. Q., Li, F. & Gao, W. J. Perspectives on the mGluR2/3 agonists as a

therapeutic target for schizophrenia: Still promising or a dead end? *Prog. Neuro-Psychopharmacology Biol. Psychiatry* **60**, 66–76 (2015).

234. Highland, J. N., Zanos, P., Georgiou, P. & Gould, T. D. Group II metabotropic glutamate receptor blockade promotes stress resilience in mice. *Neuropsychopharmacology* 1 (2019). doi:10.1038/s41386-019-0380-1

235. Fell, M. J., Svensson, K. A., Johnson, B. G. & Schoepp, D. D. Evidence for the role of metabotropic glutamate (mGlu)2 not mGlu3 receptors in the preclinical antipsychotic pharmacology of the mGlu2/3 receptor agonist (-)-(1R,4S,5S,6S)-4-amino-2-sulfonylbicyclo[3.1.0]hexane-4,6-dicarboxylic acid (LY404039). *J. Pharmacol. Exp. Ther.* **326**, 209–217 (2008).

236. Di Prisco, S. *et al.* Presynaptic, release-regulating mGlu 2 -preferring and mGlu 3 -preferring autoreceptors in CNS: pharmacological profiles and functional roles in demyelinating disease. *Br. J. Pharmacol.* **173**, 1465–1477 (2016).

237. Witkin, J., Marek, G., Johnson, B. & Schoepp, D. Metabotropic Glutamate Receptors in the Control of Mood Disorders. *CNS Neurol. Disord. - Drug Targets* **6**, 87–100 (2008).

238. Chaki, S. Group II metabotropic glutamate receptor agonists as a potential drug for schizophrenia. *European Journal of Pharmacology* **639**, 59–66 (2010).

239. De Filippis, B. *et al.* The role of group II metabotropic glutamate receptors in cognition and anxiety: Comparative studies in GRM2-/-, GRM3-/- and GRM2/3-/- knockout mice. *Neuropharmacology* **89**, 19–32 (2015).

240. Maksymetz, J., Moran, S. P. & Conn, P. J. Targeting metabotropic glutamate receptors for novel treatments of schizophrenia. *Mol. Brain* **10**, 15 (2017).

241. Ferraguti, F., Baldani-Guerra, B., Corsi, M., Nakanishi, S. & Corti, C. Activation of the extracellular signal-regulated kinase 2 by metabotropic glutamate receptors. *Eur. J. Neurosci.* **11**, 2073-2082X (1999).

242. Zammataro, M. *et al.* MGlu2 metabotropic glutamate receptors restrain inflammatory pain and mediate the analgesic activity of dual mGlu2/mGlu3 receptor agonists. *Mol. Pain* **7**, (2011).

243. Lyon, L. *et al.* Fractionation of Spatial Memory in GRM2/3 (mGlu2/mGlu3) Double Knockout Mice Reveals a Role for Group II Metabotropic Glutamate Receptors at the Interface Between Arousal and Cognition. **36**, (2011).

244. Pritchett, D. *et al.* Deletion of metabotropic glutamate receptors 2 and 3 (mGlu2 & mGlu3) in mice disrupts sleep and wheel-running activity, and increases the sensitivity of the circadian system to light. *PLoS One* **10**, e0125523 (2015).

245. Cohrs, S. Sleep disturbances in patients with schizophrenia: Impact and effect of antipsychotics. *CNS Drugs* **22**, 939–962 (2008).

246. Pritchett, D. *et al.* Evaluating the links between schizophrenia and sleep and circadian rhythm disruption. *Journal of Neural Transmission* **119**, 1061–1075 (2012).

247. Liu, J. J. *et al.* Allosteric control of an asymmetric transduction in a g protein-coupled receptor heterodimer. *Elife* **6**, (2017).

248. Moreno Delgado, D. *et al.* Pharmacological evidence for a metabotropic glutamate receptor heterodimer in neuronal cells. *Elife* **6**, (2017).

249. Lee, J. *et al.* Defining the Homo- and Heterodimerization Propensities of Metabotropic

Glutamate Receptors. *Cell Rep.* **31**, 107605 (2020).

250. Corti, C. *et al.* Altered Dimerization of Metabotropic Glutamate Receptor 3 in Schizophrenia. *Biol. Psychiatry* **62**, 747–755 (2007).

251. Moreno, J. L. *et al.* Allosteric signaling through an mGlu2 and 5-HT2A heteromeric receptor complex and its potential contribution to schizophrenia. *Sci. Signal.* **9**, 1–19 (2016).

252. Moreno, J. L. *et al.* Identification of three residues essential for 5-hydroxytryptamine 2A-metabotropic glutamate 2 (5-HT2A·mGlu2) receptor heteromerization and its psychoactive behavioral function. *J. Biol. Chem.* **287**, 44301–44319 (2012).

253. Fribourg, M. *et al.* Decoding the signaling of a GPCR heteromeric complex reveals a unifying mechanism of action of antipsychotic drugs. *Cell* **147**, 1011–1023 (2011).

254. Baki, L. *et al.* Cross-signaling in metabotropic glutamate 2 and serotonin 2A receptor heteromers in mammalian cells. *Pflugers Arch. Eur. J. Physiol.* **468**, 775–793 (2016).

255. Wischhof, L., Hollensteiner, K. J. & Koch, M. Impulsive behaviour in rats induced by intracortical DOI infusions is antagonized by co-administration of an mGlu2/3 receptor agonist. *Behav. Pharmacol.* **22**, 805–13 (2011).

256. Wischhof, L. & Koch, M. 5-HT2A and mGlu2/3 receptor interactions. *Behav. Pharmacol.* **27**, 1–11 (2016).

257. Kurita, M. *et al.* Repressive Epigenetic Changes at the mGlu2 Promoter in Frontal Cortex of 5-HT2A Knockout Mice. 1166–1175 (2013).

258. Scott, M. G. H. H. *et al.* An escort for GPCRs: implications for regulation of receptor density at the cell surface. *Trends Pharmacol. Sci.* **29**, 528–535 (2008).

259. Irannejad, R. & Von Zastrow, M. GPCR signaling along the endocytic pathway. *Curr. Opin. Cell Biol.* **27**, 109–116 (2014).

260. Irannejad, R. *et al.* Conformational biosensors reveal GPCR signalling from endosomes. *Nature* **495**, 534–538 (2013).

261. Bhatnagar, A. *et al.* The Dynamin-dependent, Arrestin-independent Internalization of 5-Hydroxytryptamine 2A (5-HT 2A) Serotonin Receptors Reveals Differential Sorting of Arrestins and 5-HT 2A Receptors during Endocytosis. *J. Biol. Chem.* **276**, 8269–8277 (2001).

262. Raote, I., Bhattacharyya, S. & Panicker, M. M. Functional selectivity in serotonin receptor 2A (5-HT2A) endocytosis, recycling, and phosphorylation. *Mol. Pharmacol.* **83**, 42–50 (2013).

263. Magalhaes, A. C., Dunn, H., Ferguson, S. S. G. S., Taylor, J. A. & Ferguson, S. S. G. S. Regulation of GPCR activity, trafficking and localization by GPCR-interacting proteins. *Br. J. Pharmacol.* **165**, 1717–1736 (2012).

264. Pfeffer, S. R. Rab GTPases: specifying and deciphering organelle identity and function. *Trends Cell Biol.* **11**, 487–491 (2001).

265. Kjos, I., Vestre, K., Guadagno, N. A., Borg Distefano, M. & Progida, C. Rab and Arf proteins at the crossroad between membrane transport and cytoskeleton dynamics. *Biochimica et Biophysica Acta - Molecular Cell Research* **1865**, 1397–1409 (2018).

266. Horgan, C. P. & McCaffrey, M. W. Rab GTPases and microtubule motors. *Biochem. Soc. Trans.* **39**, 1202–1206 (2011).

267. Jordens, I. *et al.* The Rab7 effector protein RILP controls lysosomal transport by inducing the recruitment of dynein-dynactin motors. *Curr. Biol.* **11**, 1680–1685 (2001).

268. Zerial, M. & McBride, H. Rab proteins as membrane organizers. *Nat. Rev. Mol. Cell Biol.* **2**, 107–117 (2001).

269. Bucci, C. *et al.* The small GTPase rab5 functions as a regulatory factor in the early endocytic pathway. *Cell* **70**, 715–728 (1992).

270. Poteryaev, D., Datta, S., Ackema, K., Zerial, M. & Spang, A. Identification of the switch in early-to-late endosome transition. *Cell* **141**, 497–508 (2010).

271. Pfeffer, S. R. Rab GTPase regulation of membrane identity. *Curr. Opin. Cell Biol.* **25**, 414–419 (2013).

272. Pfeffer, S. R. Rab GTPases: master regulators that establish the secretory and endocytic pathways. (2017). doi:10.1091/mbc.E16-10-0737

273. Seachrist, J. L. & Ferguson, S. S. G. Regulation of G protein-coupled receptor endocytosis and trafficking by Rab GTPases. *Life Sci.* **74**, 225–235 (2003).

274. Oakley, R. H., Laporte, S. A., Holt, J. A., Caron, M. G. & Barak, L. S. Differential affinities of visual arrestin, βarrestin1, and βarrestin2 for G protein-coupled receptors delineate two major classes of receptors. *J. Biol. Chem.* **275**, 17201–17210 (2000).

275. Seachrist, J. L., Anborgh, P. H. & Ferguson, S. S. G. β2-Adrenergic Receptor Internalization, Endosomal Sorting, and Plasma Membrane Recycling Are Regulated by Rab GTPases. *J. Biol. Chem.* **275**, 27221–27228 (2000).

276. Iwata, K., Ito, K., Fukuzaki, A., Inaki, K. & Haga, T. Dynamin and Rab5 regulate GRK2-dependent internalization of dopamine D2 receptors. *Eur. J. Biochem.* **263**, 596–602 (1999).

277. Seachrist, J. L. *et al.* Rab5 association with the angiotensin II type 1A receptor promotes Rab5 GTP binding and vesicular fusion. *J. Biol. Chem.* **277**, 679–685 (2002).

278. Murphy, J. E., Padilla, B. E., Hasdemir, B., Cottrell, G. S. & Bunnett, N. W. Endosomes: A legitimate platform for the signaling train. *Proc. Natl. Acad. Sci. U. S. A.* **106**, 17615–17622 (2009).

279. Thomsen, A. R. B., Jensen, D. D., Hicks, G. A. & Bunnett, N. W. Therapeutic Targeting of Endosomal G-Protein-Coupled Receptors. *Trends Pharmacol. Sci.* **39**, 879–891 (2018).

280. Naslavsky, N. & Caplan, S. The enigmatic endosome - Sorting the ins and outs of endocytic trafficking. *Journal of Cell Science* **131**, (2018).

281. Gruenberg, J., Griffiths, G. & Howell, K. E. Characterization of the early endosome and putative endocytic carrier vesicles in vivo and with an assay of vesicle fusion in vitro. *J. Cell Biol.* **108**, 1301–1316 (1989).

282. Dunn, K. W., McGraw, T. E. & Maxfield, F. R. Iterative fractionation of recycling receptors from lysosomally destined ligands in an early sorting endosome. *J. Cell Biol.* **109**, 3303–3314 (1989).

283. Gruenberg, J. The endocytic pathway: a mosaic of domains. *Nat. Rev. Mol. Cell Biol.* **2**, 721–730 (2001).

284. Yamashiro, D. J. & Maxfield, F. R. Acidification of morphologically distinct endosomes in mutant and wild-type Chinese hamster ovary cells. *J. Cell Biol.* **105**, 2723–2733 (1987).

285. Jovic, M., Sharma, M., Rahajeng, J. & Caplan, S. The early endosome: A busy sorting station for proteins at the crossroads. *Histology and Histopathology* **25**, 99–112 (2010).

286. Gorvel, J. P., Chavrier, P., Zerial, M. & Gruenberg, J. rab5 controls early endosome fusion in vitro. *Cell* **64**, 915–925 (1991).

287. Bucci, C. *et al.* Rab5a is a common component of the apical and basolateral endocytic machinery in polarized epithelial cells. *Proc. Natl. Acad. Sci. U. S. A.* **91**, 5061–5065 (1994).

288. Mayor, S., Presley, J. F. & Maxfield, F. R. Sorting of membrane components from endosomes and subsequent recycling to the cell surface occurs by a bulk flow process. *J. Cell Biol.* **121**, 1257–1269 (1993).

289. Van Weering, J. R. T. & Cullen, P. J. Membrane-associated cargo recycling by tubule-based endosomal sorting. *Semin. Cell Dev. Biol.* **31**, 40–47 (2014).

290. Cullen, P. J. & Steinberg, F. To degrade or not to degrade: mechanisms and significance of endocytic recycling. *Nature Reviews Molecular Cell Biology* **19**, 679–696 (2018).

291. Bright, N. A., Davis, L. J. & Luzio, J. P. Endolysosomes Are the Principal Intracellular Sites of Acid Hydrolase Activity. *Curr. Biol.* **26**, 2233–2245 (2016).

292. Ferguson, S. S. G. Evolving concepts in G protein-coupled receptor endocytosis: The role in receptor desensitization and signaling. *Pharmacol. Rev.* **53**, 1–24 (2001).

293. Sönnichsen, B., De Renzis, S., Nielsen, E., Rietdorf, J. & Zerial, M. Distinct membrane domains on endosomes in the recycling pathway visualized by multicolor imaging of Rab4, Rab5, and Rab11. *J. Cell Biol.* **149**, 901–913 (2000).

294. James, S. L. *et al.* Global, regional, and national incidence, prevalence, and years lived with disability for 354 Diseases and Injuries for 195 countries and territories, 1990-2017: A systematic analysis for the Global Burden of Disease Study 2017. *Lancet* **392**, 1789–1858 (2018).

295. National Institute of Mental Health. NIMH » Schizophrenia. *National Institutes of Health* (2016). Available at: https://www.nimh.nih.gov/health/statistics/schizophrenia.shtml. (Accessed: 21st January 2021)

296. Castañé, A. & Adell, A. *Schizophrenia*. *5-HT2A Receptors in the Central Nervous System* 191–204 (Springer International Publishing, 2018). doi:10.1007/978-3-319-70474-6_8

297. Wong, A. H. C. & Van Tol, H. H. M. Schizophrenia: From phenomenology to neurobiology. *Neurosci. Biobehav. Rev.* **27**, 269–306 (2003).

298. Rössler, W., Joachim Salize, H., Van Os, J. & Riecher-Rössler, A. Size of burden of schizophrenia and psychotic disorders. *Eur. Neuropsychopharmacol.* **15**, 399–409 (2005).

299. Fleischhacker, W. W. *Schizophrenia—Time to Commit to Policy Change*. (2014).

300. Wander, C. Schizophrenia: Opportunities to improve outcomes and reduce economic burden through managed care. *Am. J. Manag. Care* **26**, S62–S68 (2020).

301. Desai, P. R., Lawson, K. A., Barner, J. C. & Rascati, K. L. Estimating the direct and indirect costs for community-dwelling patients with schizophrenia. *J. Pharm. Heal. Serv. Res.* **4**, 187–194 (2013).

302. Miller, G. Is pharma running out of brainy ideas? *Science (80-.).* **329**, 502–504 (2010).

303. Cressey, D. Psychopharmacology in crisis. *Nature* (2011). doi:10.1038/news.2011.367

304. Greenberg, G. The Psychiatric Drug Crisis | The New Yorker. (2013). Available at:

https://www.newyorker.com/tech/annals-of-technology/the-psychiatric-drug-crisis. (Accessed: 19th October 2020)

305. O'Brien, P. L., Thomas, C. P., Hodgkin, D., Levit, K. R. & Mark, T. L. The Diminished Pipeline for Medications to Treat Mental Health and Substance Use Disorders. *Psychiatr. Serv.* **65**, 1433–1438 (2014).

306. Nicoletti, F., Bruno, V., Ngomba, R. T., Gradini, R. & Battaglia, G. Metabotropic glutamate receptors as drug targets: What's new? *Curr. Opin. Pharmacol.* **20**, 89–94 (2015).

307. Duncan, M. O. and P. Why 'big pharma' stopped searching for the next Prozac | Society | The Guardian. (2016). Available at:

https://www.theguardian.com/society/2016/jan/27/prozac-next-psychiatric-wonder-drug-research-medicine-mental-illness. (Accessed: 19 October 2020)

308. Dakić, T. Mental health burden and unmet needs for treatment: A call for justice. *Br. J. Psychiatry* **216**, 241–242 (2020).

309. Yang, A. & Tsai, S.-J. New Targets for Schizophrenia Treatment beyond the Dopamine Hypothesis. *Int. J. Mol. Sci.* **18**, 1689 (2017).

310. Meltzer, H. Y. What's atypical about atypical antipsychotic drugs? *Curr. Opin. Pharmacol.* **4**, 53–57 (2004).

311. Lieberman, J. A. *et al.* Effectiveness of Antipsychotic Drugs in Patients with Chronic Schizophrenia. *N. Engl. J. Med.* **353**, 1209–1223 (2005).

312. Lally, J., Gaughran, F., Timms, P. & Curran, S. R. Pharmacogenomics and Personalized Medicine Dovepress Treatment-resistant schizophrenia: current insights on the pharmacogenomics of antipsychotics. *Pharmgenomics. Pers. Med.* **2016**, 9–117 (2016).

313. Stępnicki, P., Kondej, M. & Kaczor, A. A. Current concepts and treatments of schizophrenia. *Molecules* **23**, (2018).

314. Stahl, S. M. Beyond the dopamine hypothesis of schizophrenia to three neural networks of psychosis: Dopamine, serotonin, and glutamate. *CNS Spectr.* **23**, 187–191 (2018).

315. Arnedo, J. *et al.* Uncovering the hidden risk architecture of the schizophrenias: Confirmation in three independent genome-wide association studies. *Am. J. Psychiatry* **172**, 139–153 (2015).

316. Allen, N. C. *et al.* Systematic meta-analyses and field synopsis of genetic association studies in schizophrenia: The SzGene database. *Nat. Genet.* **40**, 827–834 (2008).

317. Ryder, P. V. & Faundez, V. Schizophrenia: The 'BLOC' may be in the endosomes. *Sci. Signal.* **2**, 1–6 (2009).

318. Consortium, S. W. G. of the P. G. *et al.* Biological insights from 108 schizophrenia-associated genetic loci. *Nature* **511**, 421–427 (2014).

319. Hall, J. *et al.* Genetic risk for schizophrenia: Convergence on synaptic pathways involved in plasticity. *Biol. Psychiatry* **77**, 52–58 (2015).

320. Fries, G. R. *et al.* Genome-wide expression in veterans with schizophrenia further validates the immune hypothesis for schizophrenia. *Schizophr. Res.* **192**, 255–261 (2018).

321. Carpenter, W. T., Kirkpatrick, B. & Buchanan, R. W. Schizophrenia: Syndromes and diseases. *J. Psychiatr. Res.* **33**, 473–475 (1999).

322. Andreasen, N. Schizophrenia: the fundamental questions. *Brain Res. Rev.* **31**, 106–112

(2000).

323. Kambeitz, J. *et al.* Detecting Neuroimaging Biomarkers for Schizophrenia: A Meta-Analysis of Multivariate Pattern Recognition Studies. *Neuropsychopharmacology* **40**, 1742–1751 (2015).

324. Gao, S., Calhoun, V. D. & Sui, J. Machine learning in major depression: From classification to treatment outcome prediction. *CNS Neurosci. Ther.* **24**, 1037–1052 (2018).

325. Ebdrup, B. H. *et al.* Accuracy of diagnostic classification algorithms using cognitive-, electrophysiological-, and neuroanatomical data in antipsychotic-naïve schizophrenia patients. *Psychol. Med.* **49**, 2754–2763 (2019).

326. Strauss, J. Reconceptualizing schizophrenia. *Schizophr. Bull.* **40**, 97–100 (2014).

327. Thibaut, F. Schizophrenia: an example of complex genetic disease. *World J. Biol. Psychiatry* **7**, 194–197 (2006).

328. Kendler, K. S. Phenomenology of schizophrenia and the representativeness of modern diagnostic criteria. *JAMA Psychiatry* **73**, 1082–1092 (2016).

329. Cuesta, M. J. & Peralta, V. Going beyond classic descriptions to future phenomenology of schizophrenia. *JAMA Psychiatry* **73**, 1010–1012 (2016).

330. van Os, J. "Schizophrenia" does not exist. *BMJ* **352**, i375 (2016).

331. Eggers, A. E. A serotonin hypothesis of schizophrenia. *Med. Hypotheses* **80**, 791–794 (2013).

332. Marder, S. R. *et al.* Advancing drug discovery for schizophrenia. *Ann. N. Y. Acad. Sci.* **1236**, 30–43 (2011).

333. Meltzer, H. Y. & Huang, M. In vivo actions of atypical antipsychotic drug on serotonergic and dopaminergic systems. *Prog. Brain Res.* **172**, 177–197 (2008).

334. Jeffrey Conn, P., Christopoulos, A. & Lindsley, C. W. Allosteric modulators of GPCRs: A novel approach for the treatment of CNS disorders. *Nat. Rev. Drug Discov.* **8**, 41–54 (2009).

335. Lopez-Gimenez, J. F., Vilaró, M. T. & Milligan, G. Morphine desensitization, internalization, and down-regulation of the μ opioid receptor is facilitated by serotonin 5-hydroxytryptamine2A receptor coactivation. *Mol. Pharmacol.* **74**, 1278–1291 (2008).

336. Xue, L., Rovira, X., Zhao, H., Liu, J. & Pin, J.-P. major ligand-induced rearrangement of the heptahelical domain interface in a gpcr dimer. *Nat. Chem. Biol.* (2014). doi:10.1038/nchembio.1711

337. Ward, R. J., Alvarez-Curto, E. & Milligan, G. Using the Flp-In™ T-Rex™ system to regulate GPCR expression. *Methods Mol. Biol.* **746**, 21–37 (2011).

338. Wagstaff, K. M. & Jans, D. A. Protein transduction: cell penetrating peptides and their therapeutic applications. *Curr. Med. Chem.* **13**, 1371–87 (2006).

339. Arsenovic, P. T., Mayer, C. R. & Conway, D. E. SensorFRET: A Standardless Approach to Measuring Pixel-based Spectral Bleed-through and FRET Efficiency using Spectral Imaging. *Sci. Rep.* **7**, 15609 (2017).

340. Bajar, B. *et al.* A Guide to Fluorescent Protein FRET Pairs. *Sensors* **16**, 1488 (2016).

341. Chaudhry, F. A. *et al.* Glutamate transporters in glial plasma membranes: Highly differentiated localizations revealed by quantitative ultrastructural immunocytochemistry. *Neuron* **15**, 711–720 (1995).

342. Hjelle, O. P., Chaudhry, F. A. & Ottersen, O. P. Antisera to Glutathione: Characterization and Immunocytochemical Application to the Rat Cerebellum. *Eur. J. Neurosci.* **6**, 793–804 (1994).

343. Van Lookeren Campagne, M., Oestreicher, A. B., Van der Krift, T. P., Gispen, W. H. & Verkleij, A. J. Freeze-substitution and Lowicryl HM20 embedding of fixed rat brain: Suitability for immunogold ultrastructural localization of neural antigens. *J. Histochem. Cytochem.* **39**, 1267–1279 (1991).

344. A. Peters, S. L. Palay, H. Webster, deF. The Fine Structure of the Nervous System. Neurons and their Supporting Cells. 3rd edition. *J. Neuropathol. Exp. Neurol.* **50**, 282.1-282 (1991).

345. Dunn, K. W., Kamocka, M. M. & McDonald, J. H. A practical guide to evaluating colocalization in biological microscopy. *American Journal of Physiology - Cell Physiology* **300**, (2011).

346. Adler, J. & Parmryd, I. Quantifying colocalization by correlation: The Pearson correlation coefficient is superior to the Mander's overlap coefficient. *Cytom. Part A* **77A**, 733–742 (2010).

347. Ibi, D. *et al.* Antipsychotic-induced Hdac2 transcription via NF-Î° B leads to synaptic and cognitive side effects. *Nat. Neurosci.* **20**, 1247–1259 (2017).

348. Kerppola, T. K. Design and implementation of bimolecular fluorescence complementation (BiFC) assays for the visualization of protein interactions in living cells. *Nat. Protoc.* **1**, 1278–1286 (2006).

349. Kerppola, T. K. Visualization of molecular interactions by fluorescence complementation. *Nat. Rev. Mol. Cell Biol.* **7**, 449–456 (2006).

350. Murat, S. *et al.* 5-HT2A receptor-dependent phosphorylation of mGlu2 receptor at Serine 843 promotes mGlu2 receptor-operated Gi/o signaling. *Mol. Psychiatry* 1 (2018). doi:10.1038/s41380-018-0069-6

351. Delille, H. K. *et al.* Heterocomplex formation of 5-HT 2A -mGlu 2 and its relevance for cellular signaling cascades. *Neuropharmacology* **62**, 2184–2191 (2012).

352. Rankovic, Z., Brust, T. F. & Bohn, L. M. Biased agonism: An emerging paradigm in GPCR drug discovery. *Bioorganic Med. Chem. Lett.* **26**, 241–250 (2016).

353. Canals, M., Lopez-Gimenez, J. F. & Milligan, G. Cell surface delivery and structural re-organization by pharmacological chaperones of an oligomerization-defective α 1b-adrenoceptor mutant demonstrates membrane targeting of GPCR oligomers. *Biochem. J.* **417**, 161–172 (2009).

354. Lopez-Gimenez, J. F., Alvarez-Curto, E. & Milligan, G. M3 muscarinic acetylcholine receptor facilitates the endocytosis of mu opioid receptor mediated by morphine independently of the formation of heteromeric complexes. *Cell. Signal.* **35**, 208–222 (2017).

355. Devi, L. A. Heterodimerization of G-protein-coupled receptors: Pharmacology, signaling and trafficking. *Trends Pharmacol. Sci.* **22**, 532–537 (2001).

356. Milligan, G. *The role of dimerisation in the cellular trafficking of G-protein-coupled receptors*. *Current Opinion in Pharmacology* **10**, 23–29 (Elsevier, 2010).

357. Bunnett W., Cottrell G. Trafficking and Signaling of G Protein-Coupled Receptors in the Nervous System: Implications for Disease and Therapy. *CNS Neurol. Disord. - Drug Targets* **9**, 539–556 (2012).

358. Nelson, G. *et al.* Mammalian sweet taste receptors. *Cell* **106**, 381–390 (2001).

359. Zhao, G. Q. *et al.* The receptors for mammalian sweet and umami taste. *Cell* **115**, 255–266 (2003).

360. Nango, E. *et al.* Taste substance binding elicits conformational change of taste receptor T1r heterodimer extracellular domains. *Sci. Rep.* **6**, 1–8 (2016).

361. Jordan, B. A., Trapaidze, N., Gomes, I., Nivarthi, R. & Devi, L. A. Oligomerization of opioid receptors with 2-adrenergic receptors: A role in trafficking and mitogen-activated protein kinase activation. *Proc. Natl. Acad. Sci.* **98**, 343–348 (2001).

362. Hillion, J. *et al.* Coaggregation, cointernalization, and codesensitization of adenosine A2A receptors and dopamine D2 receptors. *J. Biol. Chem.* **277**, 18091–18097 (2002).

363. Schmid, C. L., Raehal, K. M., Bohn, L. M. & Lefkowitz, R. J. *Agonist-directed signaling of the serotonin 2A receptor depends on-arrestin-2 interactions in vivo*. (2008).

364. Bécamel, C. *et al.* The Serotonin 5-HT2A and 5-HT2C Receptors Interact with Specific Sets of PDZ Proteins. *J. Biol. Chem.* **279**, 20257–20266 (2004).

365. Xia, Z., Gray, J. A., Compton-Toth, B. A. & Roth, B. L. A direct interaction of PSD-95 with 5-HT2A serotonin receptors regulates receptor trafficking and signal transduction. *J. Biol. Chem.* **278**, 21901–21908 (2003).

366. Xia, Z., Hufeisen, S. J., Gray, J. A. & Roth, B. L. The PDZ-binding domain is essential for the dendritic targeting of 5-HT2A serotonin receptors in cortical pyramidal neurons in vitro. *Neuroscience* **122**, 907–920 (2003).

367. Grotewiel, M. S. & Sanders-Bush, E. Differences in agonist-independent activity of 5-HT(2A) and 5-HT(2C) receptors revealed by heterologous expression. *Naunyn. Schmiedebergs. Arch. Pharmacol.* **359**, 21–27 (1999).

368. Egan, C., Herrick-Davis, K. & Teitler, M. Creation of a constitutively activated state of the 5-HT(2A) receptor by site-directed mutagenesis: Revelation of inverse agonist activity of antagonists. in *Annals of the New York Academy of Sciences* **861**, 136–139 (1998).

369. Hamada, S. *et al.* Localization of 5-HT2A receptor in rat cerebral cortex and olfactory system revealed by immunohistochemistry using two antibodies raised in rabbit and chicken. *Mol. Brain Res.* **54**, 199–211 (1998).

370. Maeshima, T. *et al.* The cellular localization of 5-HT(2A) receptors in the spinal cord and spinal ganglia of the adult rat. *Brain Res.* **797**, 118–124 (1998).

371. Cornea-Hébert, V. *et al.* Similar ultrastructural distribution of the 5-HT2A serotonin receptor and microtubule-associated protein MAP1A in cortical dendrites of adult rat. *Neuroscience* **113**, 23–35 (2002).

372. Rodríguez, J. J., Garcia, D. R. & Pickel, V. M. Subcellular distribution of 5-hydroxytryptamine(2A) and N-methyl-D- aspartate receptors within single neurons in rat motor and limbic striatum. *J. Comp. Neurol.* **413**, 219–231 (1999).

373. Van Steenwinckel, J. *et al.* The 5-HT2A receptor is mainly expressed in nociceptive sensory neurons in rat lumbar dorsal root ganglia. *Neuroscience* **161**, 838–846 (2009).

374. Price, A. E., Sholler, D. J., Stutz, S. J., Anastasio, N. C. & Cunningham, K. A. Endogenous Serotonin 5-HT2A and 5-HT2C Receptors Associate in the Medial Prefrontal Cortex. *ACS Chem. Neurosci.* **10**, 3241–3248 (2019).

375. Griffiths, J. L. & Lovick, T. A. Co-localization of 5-HT2A-receptor- and GABA-

immunoreactivity in neurones in the periaqueductal grey matter of the rat. *Neurosci. Lett.* **326**, 151–154 (2002).

376. Wu, C. *et al. Development and Characterization of Monoclonal Antibodies Specific to the Serotonin 5-HT 2A Receptor*. *The Journal of Histochemistry & Cytochemistry* **46**, (1998).

377. Bombardi, C. Neuronal localization of 5-HT2A receptor immunoreactivity in the rat hippocampal region. *Brain Res. Bull.* **87**, 259–273 (2012).

378. Michel, M. C., Wieland, T. & Tsujimoto, G. How reliable are G-protein-coupled receptor antibodies? *Naunyn. Schmiedebergs. Arch. Pharmacol.* **379**, 385–388 (2009).

379. McDonald, A. J. & Mascagni, F. Neuronal localization of 5-HT type 2A receptor immunoreactivity in the rat basolateral amygdala. *Neuroscience* **146**, 306–320 (2007).

380. Nocjar, C., Roth, B. L. & Pehek, E. Localization of 5-HT2A receptors on dopamine cells in subnuclei of the midbrain A10 cell group. *Neuroscience* **111**, 163–176 (2002).

381. Gray, J. A. *et al. Cell-Type Specific Effects of Endocytosis Inhibitors on 5-Hydroxytryptamine2A Receptor Desensitization and Resensitization Reveal an Arrestin-, GRK2-, and GRK5-Independent Mode of Regulation in Human Embryonic Kidney 293 Cells Vol. 60, No. 5 22/936816 Pri*. **60**, (American Society for Pharmacology and Experimental Therapy, 2001).

382. Bhattacharya, A., Sankar, S. & Panicker, M. M. Differences in the C-terminus contribute to variations in trafficking between rat and human 5-HT2A receptor isoforms: Identification of a primate-specific tripeptide ASK motif that confers GRK-2 and β arrestin-2 interactions. *J. Neurochem.* **112**, 723–732 (2010).

383. Doly, S. *et al.* The 5-HT2A Receptor Is Widely Distributed in the Rat Spinal Cord and Mainly Localized at the Plasma Membrane of Postsynaptic Neurons. *J. Comp. Neurol.* **472**, 496–511 (2004).

384. Bécamel, C., Berthoux, C., Barre, A. & Marin, P. Growing Evidence for Heterogeneous Synaptic Localization of 5-HT2A Receptors. *ACS Chem. Neurosci.* **8**, 897–899 (2017).

385. Fiorica-Howells, E., Hen, R., Gingrich, J., Li, Z. & Gershon, M. D. 5-HT2A receptors: location and functional analysis in intestines of wild-type and 5-HT 2A knockout mice. *Am. J. Physiol. Liver Physiol.* **282**, G877–G893 (2002).

386. Allen, J. A., Yadav, P. N. & Roth, B. L. Insights into the regulation of 5-HT2A serotonin receptors by scaffolding proteins and kinases. *Neuropharmacology* **55**, 961–968 (2008).

387. Sorkin, A. & Von Zastrow, M. Endocytosis and signalling: Intertwining molecular networks. *Nat. Rev. Mol. Cell Biol.* **10**, 609–622 (2009).

388. Berg, K. A. *et al.* Effector Pathway-Dependent Relative Efficacy at Serotonin Type 2A and 2C Receptors: Evidence for Agonist-Directed Trafficking of Receptor Stimulus. *Mol. Pharmacol.* **54**, 94–104 (1998).

389. Abbs, B. *et al.* The 3rd Schizophrenia International Research Society Conference, 14-18 April 2012, Florence, Italy: Summaries of oral sessions. *Schizophr. Res.* **141**, 14–18 (2012).

390. Cotter, D. R., Schubert, K. O. & Föcking, M. Clathrin-Mediated-Endocytosis and Clathrin-Dependent Membrane and Protein Trafficking; Core Pathophysiological Processes in Schizophrenia and Bipolar Disorder? *Schizophr. Res.* **136**, S15–S16 (2012).

391. Schubert, K. O. *et al.* Hypothesis review: Are clathrin-mediated endocytosis and clathrin-dependent membrane and protein trafficking core pathophysiological processes in

schizophrenia and bipolar disorder. *Mol. Psychiatry* **17**, 669–681 (2012).

392. Harrison, P. J. & Weinberger, D. R. Schizophrenia genes, gene expression, and neuropathology: On the matter of their convergence. *Mol. Psychiatry* **10**, 40–68 (2005).

393. Harrison, P. J. & Law, A. J. Neuregulin 1 and Schizophrenia: Genetics, Gene Expression, and Neurobiology. *Biol. Psychiatry* **60**, 132–140 (2006).

394. Morris, D. W. *et al.* Dysbindin (DTNBP1) and the Biogenesis of Lysosome-Related Organelles Complex 1 (BLOC-1): Main and Epistatic Gene Effects Are Potential Contributors to Schizophrenia Susceptibility. *Biol. Psychiatry* **63**, 24–31 (2008).

395. Straub, R. E. *et al.* Genetic variation in the 6p22.3 Gene DTNBP1, the human ortholog of the mouse dysbindin gene, is associated with schizophrenia. *Am. J. Hum. Genet.* **71**, 337–348 (2002).

396. Weickert, C. S. *et al.* Human dysbindin (DTNBP1) gene expression in normal brain and in schizophrenic prefrontal cortex and midbrain. *Arch. Gen. Psychiatry* **61**, 544–555 (2004).

397. Nikolenko, V. N. *et al.* The mystery of claustral neural circuits and recent updates on its role in neurodegenerative pathology. *Behav. Brain Funct.* **17**, 8 (2021).

398. Wong, K. L. L., Nair, A. & Augustine, G. J. Changing the Cortical Conductor's Tempo: Neuromodulation of the Claustrum. *Front. Neural Circuits* **15**, 32 (2021).

399. Talbot, K. *et al.* Dysbindin-1 is reduced in intrinsic, glutamatergic terminals of the hippocampal formation in schizophrenia. *J. Clin. Invest.* **113**, 1353–1363 (2004).

400. Ji, Y. *et al.* Role of dysbindin in dopamine receptor trafficking and cortical GABA function. *Proc. Natl. Acad. Sci. U. S. A.* **106**, 19593–19598 (2009).

401. Iizuka, Y., Sei, Y., Weinberger, D. R. & Straub, R. E. Evidence that the BLOC-1 protein dysbindin modulates dopamine D2 receptor internalization and signaling but not D1 internalization. *J. Neurosci.* **27**, 12390–12395 (2007).

402. Numakawa, T. *et al.* Evidence of novel neuronal functions of dysbindin, a susceptibility gene for schizophrenia. *Hum. Mol. Genet.* **13**, 2699–2708 (2004).

403. Talbot, K. The sandy (sdy) mouse: A dysbindin-1 mutant relevant to schizophrenia research. *Prog. Brain Res.* **179**, 87–94 (2009).

404. McBride, H. M. *et al.* Oligomeric complexes link Rab5 effectors with NSF and drive membrane fusion via interactions between EEA1 and syntaxin 13. *Cell* **98**, 377–386 (1999).

405. Sun, W., Yan, Q., Vida, T. A. & Bean, A. J. Hrs regulates early endosome fusion by inhibiting formation of an endosomal SNARE complex. *J. Cell Biol.* **162**, 125–137 (2003).

406. Peter, A. T. J. *et al.* The BLOC-1 complex promotes endosomal maturation by recruiting the Rab5 gtpase-activating protein Msb3. *J. Cell Biol.* **201**, 97–111 (2013).

407. Hartwig, C. *et al.* Neurodevelopmental disease mechanisms, primary cilia, and endosomes converge on the BLOC-1 and BORC complexes. *Developmental Neurobiology* **78**, 311–330 (2018).

408. Marley, A. & von Zastrow, M. Dysbindin promotes the post-endocytic sorting of G protein-coupled receptors to lysosomes. *PLoS One* **5**, e9325 (2010).

409. Owen, M. J., Williams, N. M. & O'Donovan, M. C. Dysbindin-1 and schizophrenia: from genetics to neuropathology. *J. Clin. Invest.* **113**, 1255–1257 (2004).

410. Moghaddam, B. & Javitt, D. From revolution to evolution: The glutamate hypothesis of

schizophrenia and its implication for treatment. *Neuropsychopharmacology* **37**, 4–15 (2012).

411. Abdolmaleky, H. M. *et al.* Epigenetic dysregulation of HTR2A in the brain of patients with schizophrenia and bipolar disorder. *Schizophr. Res.* **129**, 183–190 (2011).

412. Holloway, T. & González-Maeso, J. Epigenetic Mechanisms of Serotonin Signaling. *ACS Chem. Neurosci.* **6**, 1099–1109 (2015).

413. Sealfon, S. C. & Olanow, C. W. Dopamine receptors: From structure to behavior. *Trends in Neurosciences* **23**, S34–S40 (2000).

414. Meltzer, H. Y. & Stahl, S. M. The dopamine hypothesis of schizophrenia: a review. *Schizophrenia Bulletin* **2**, 19–76 (1976).

415. Meltzer, H. Y. Clinical studies on the mechanism of action of clozapine: the dopamine-serotonin hypothesis of schizophrenia. *Psychopharmacology (Berl).* **99**, S18–S27 (1989).

416. Duan, J. *et al.* Translational Psychiatry Transcriptomic signatures of schizophrenia revealed by dopamine perturbation in an ex vivo model. *Transl. Psychiatry* **8**, 158 (2018).

417. Joyce, J. N. The dopamine hypothesis of schizophrenia: limbic interactions with serotonin and norepinephrine. *Psychopharmacology (Berl).* **112**, 16–34 (1993).

418. Brisch, R. *et al.* The role of dopamine in schizophrenia from a neurobiological and evolutionary perspective: Old fashioned, but still in vogue. *Frontiers in Psychiatry* **5**, (2014).

419. Alfimova, M. V., Monakhov, M. V., Abramova, L. I., Golubev, S. A. & Golimbet, V. E. Polymorphism of Serotonin Receptor Genes (5-HTR2A) and Dysbindin (DTNBP1) and Individual Components of Short-Term Verbal Memory Processes in Schizophrenia. *Neurosci. Behav. Physiol.* **40**, 934–940 (2010).

420. Hernandez, I. & Sokolov, B. P. Abnormalities in 5-HT2A receptor mRNA expression in frontal cortex of chronic elderly schizophrenics with varying histories of neuroleptic treatment. *J. Neurosci. Res.* **59**, 218–225 (2000).

421. Kasai, R. S. & Kusumi, A. Single-molecule imaging revealed dynamic GPCR dimerization. *Curr. Opin. Cell Biol.* **27**, 78–86 (2014).

422. Pellissier, L. P. *et al.* G protein activation by serotonin type 4 receptor dimers: evidence that turning on two protomers is more efficient. *J. Biol. Chem.* **286**, 9985–97 (2011).

423. Lee, S. P. *et al.* Dopamine D1 and D2 receptor Co-activation generates a novel phospholipase C-mediated calcium signal. *J. Biol. Chem.* **279**, 35671–8 (2004).

424. Toneatti, R. *et al.* Interclass GPCR heteromerization affects localization and trafficking. *Sci. Signal.* **13**, eaaw3122 (2020).

425. Jain, A., Liu, R., Xiang, Y. K. & Ha, T. Single-molecule pull-down for studying protein interactions. *Nat. Protoc.* **7**, 445–452 (2012).

426. Jain, A. *et al.* Probing cellular protein complexes using single-molecule pull-down. *Nature* **473**, 484–488 (2011).

427. Levitz, J. *et al.* Mechanism of Assembly and Cooperativity of Homomeric and Heteromeric Metabotropic Glutamate Receptors. *Neuron* **92**, 143–159 (2016).

428. Crilly, J. The history of clozapine and its emergence in the US market: A review and analysis. *History of Psychiatry* **18**, 39–60 (2007).

429. Meltzer, H. Y. *Update on Typical and Atypical Antipsychotic Drugs*. *Annual Review of*

Medicine **64**, 393–406 (2013).

430. Lieberman, J. A. *et al.* Antipsychotic drugs: Comparison in animal models of efficacy, neurotransmitter regulation, and neuroprotection. *Pharmacological Reviews* **60**, 358–403 (2008).

431. Miyamoto, S., Miyake, N., Jarskog, L. F., Fleischhacker, W. W. & Lieberman, J. A. Pharmacological treatment of schizophrenia: A critical review of the pharmacology and clinical effects of current and future therapeutic agents. *Molecular Psychiatry* **17**, 1206–1227 (2012).

432. Ellaithy, A., Younkin, J., González-Maeso, J. & Logothetis, D. E. Positive allosteric modulators of metabotropic glutamate 2 receptors in schizophrenia treatment. *Trends Neurosci.* **38**, 506–516 (2015).

433. De La Fuente Revenga, M. *et al.* Chronic clozapine treatment restrains via HDAC2 the performance of mGlu2 receptor agonism in a rodent model of antipsychotic activity. *Neuropsychopharmacology* (2018). doi:10.1038/s41386-018-0143-4

434. Kurita, M. *et al.* HDAC2 regulates atypical antipsychotic responses through the modulation of mGlu2 promoter activity. **15**, 1245–1254 (2013).

435. Kinon, B. J., Millen, B. A., Zhang, L. & McKinzie, D. L. Exploratory Analysis for a Targeted Patient Population Responsive to the Metabotropic Glutamate 2/3 Receptor Agonist Pomaglumetad Methionil in Schizophrenia. *Biol. Psychiatry* **78**, 754–762 (2015).

436. Martin, G. R., Eglen, R. M., Hamblin, M. W., Hoyer, D. & Yocca, F. The structure and signalling properties of 5-HT receptors: An endless diversity? in *Trends in Pharmacological Sciences* **19**, 2–4 (Elsevier Ltd, 1998).

437. Harvey, J. A. *Role of the serotonin 5-HT2A receptor learning*. *Learning and Memory* **10**, 355–362 (Cold Spring Harbor Laboratory Press, 2003).

438. Hu, C.-D., Grinberg, A. V. & Kerppola, T. K. Visualization of Protein Interactions in Living Cells Using Bimolecular Fluorescence Complementation (BiFC) Analysis. *Curr. Protoc. Cell Biol.* **29**, 21.3.1-21.3.21 (2005).

439. Kerppola, T. K. Complementary methods for studies of protein interactions in living cells. *Nat. Methods* **3**, 969–971 (2006).

440. Atwood, B. K., Lopez, J., Wager-Miller, J., Mackie, K. & Straiker, A. Expression of G protein-coupled receptors and related proteins in HEK293, AtT20, BV2, and N18 cell lines as revealed by microarray analysis. *BMC Genomics* **12**, 14 (2011).

VITA

Rudy Toneatti was born on June 10th, 1977 in Paris, France. He is a French citizen and spent about four years working and studying at the VCU department of Physiology and Biophysics. He received a Bachelor of Art in Philosophy at the Nice University after being graduated with a *Baccalauréat* in Math, Physics and Biology. He also obtained a Master in Social and Political Sciences at the Sorbonne University in Paris. He did a Master in Integrative Biology and completed a first internship in Paris at the *Centre du Fer à Moulin* under the supervision of Dr Marta Garcia on tracking mitochondria trafficking along genetically modified mice piriform cortex neurons. Then travelled to Richmond for completion of the second graduating internship. After a year as a research assistant in the González-Maeso's Lab, he entered the Graduate School at the VCU School of Medicine where he studied for the obtainment of a PhD in Neuroscience.

APPENDIX

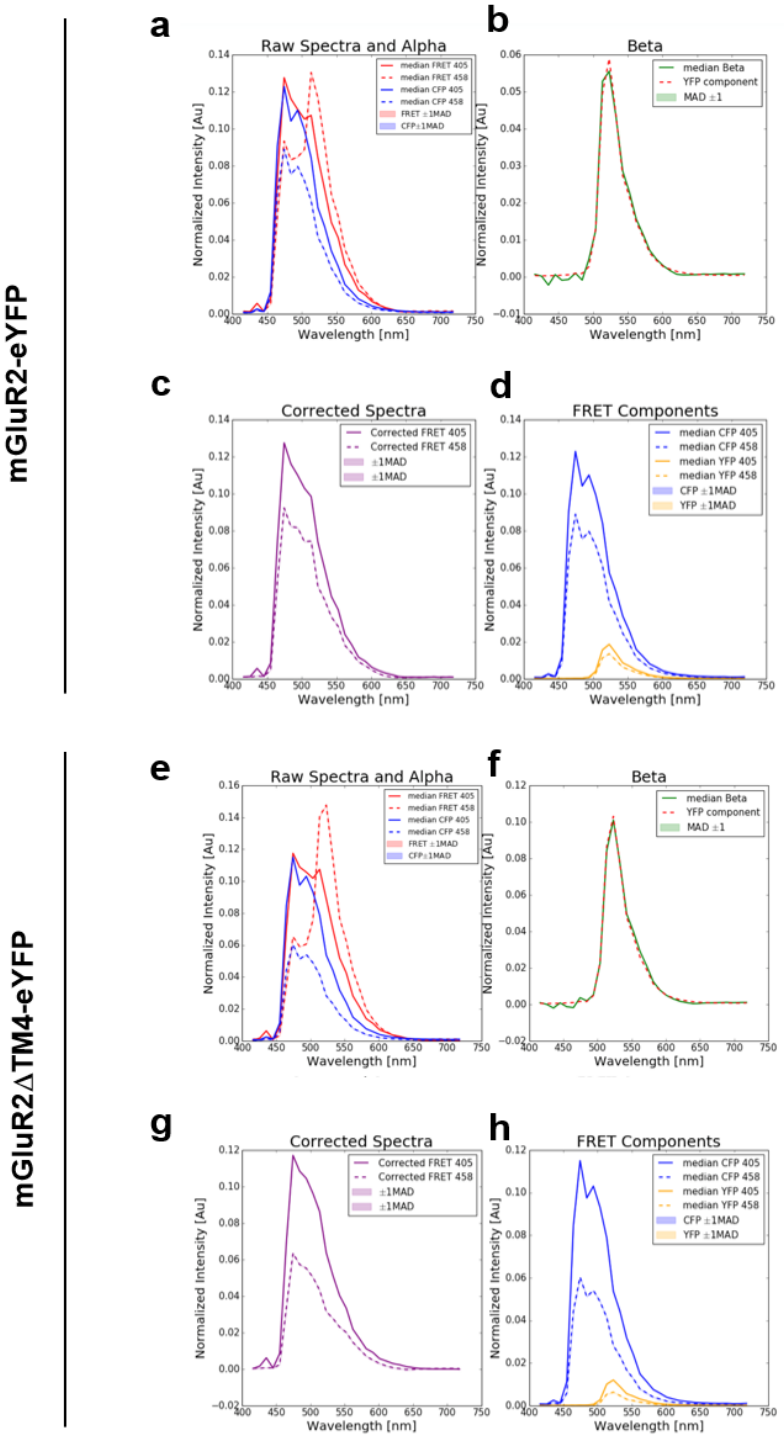

(Fig. Appendix .1)

Fig. A1. Average spectra and sensorFRET analysis for Flp-In T-REx HEK293 cells stably expressing mGluR2-eYFP or mGluR2□TM4-eYFP, and harboring 5-HT_{2A}R-eCFP at the inducible locus. (**A** and **E**) Linear unmixing of the eCFP (donor) component from the raw spectra, the ratio of which provides the alpha parameter used in the sensorFRET analysis. (**B** and **F**) Fitting of the β parameter, which is the difference between the 405 and 458 nm spectra after scaling 405 by α. (**C** and **G**) Raw spectra at both frequencies after the acceptor direct excitation component is removed using β^{339}. (**D** and **H**) Linear unmixing of the donor and acceptor from the corrected spectra, where the FRET efficiency is proportional to the ratio of acceptor magnitude to donor magnitude. It can be seen that the ratio of eYFP magnitude to eCFP magnitude is larger in the mGluR2-eYFP group (indicating a higher FRET efficiency) compared to the mGluR2ΔTM4-eYFP group.

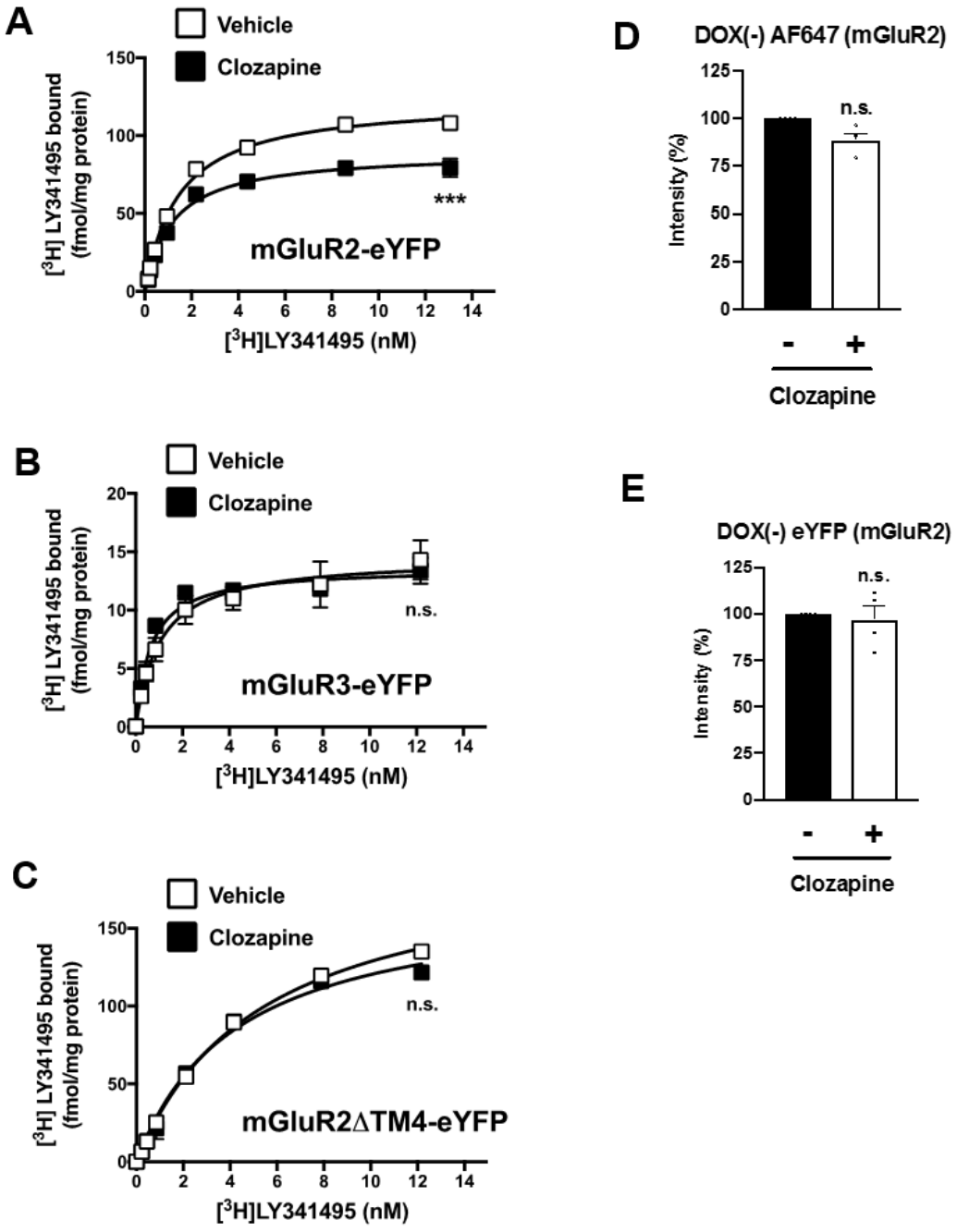

(Fig. Appendix .2)

Fig. A2. Effect of clozapine on mGluRs density. **(A** to **C)** Flp-In T-REx HEK293 cells stably expressing mGluR2-eYFP (**A**), mGluR3-eYFP (**B**) or mGluR2ΔTM4-eYFP (**C**) and harboring 5-HT_{2A}R-eCFP at the inducible locus were treated with doxycycline, exposed overnight to clozapine (10 μM), or vehicle, and harvested to perform radioligand binding assays with the mGluR2/3 antagonist [^{3}H]LY341495 (n = 4 independent groups of membrane preparations). Cell surface localization of mGluR2-eYFP with an Alexa Fluor 647 (AF647)-tagged antibody (**D**) and total mGluR2-eYFP signal (**E**) density were assessed by flow cytometry assays (n = 3 – 5 independent experiments). Data are mean ± SEM. Statistical analysis was performed using the *F* test. ***$P <$ 0.001, n.s., not significant.

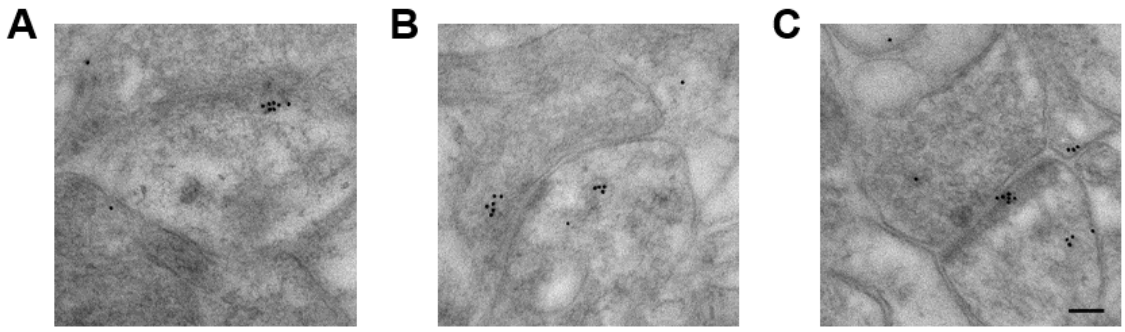

Fig. A3. Representative photomicrographs showing excitatory synapses in mouse frontal cortex scored as membrane only (**A**), intracellular only (**B**), or both (**C**) based on postsynaptic distribution. Scale bars, 100 nm.

(Fig. Appendix .3)